TECHNOLOGY, INC.

THERMOELECTRIC MATERIALS • DEVICES • SYSTEMS

HZ-083191

Evaluation of

THE CORELESS LINEAR CONDUCTION PUMP FOR THERMOELECTROMAGNETIC PUMPS

by

Robert J. Campana

Research supported by Strategic Defense Initiative/Innovative Science and Technology and managed by the Department of Energy, Idaho Operations Office

Contract DE-AC07-90ID12911

August 1991

11180 Roselle St., Suite G, San Diego, CA 92121 • Telephone (619) 535-9343 • FAX (619) 535-9350

Accession Number: 4466

Publication Date: Aug 01, 1991

Title: Evaluation of the Coreless Linear Conduction Pump for Thermoelectromagnetic Pumps

Personal Author: Campana, R.J.

Corporate Author Or Publisher: Hi-Z Technology, Inc., 11180 Roselle St., Suite G, San Diego, CA 92121
Report Number: HZ-083191

Report Prepared for: SDIO/T/SL, Washington, DC 20301-7100

Descriptors, Keywords: Coreless Linear Conduction Pump Thermoelectromagnetic Nuclear Space Power TEMP

Pages: 00100

Cataloged Date: Apr 22, 1993

Contract Number: DE-AC07-90ID12911

Document Type: HC

Number of Copies In Library: 000001

Record ID: 26727

SUMMARY

The purpose of the Coreless Linear Conduction Pump (CLCP) was to evaluate the feasibility of the CLCP as a means of building Thermoelectromagnetic Pumps (TEMPs) that are not, in themselves, temperatue limited by the Curie point of ferromagnetic cores or do not limit the temperature capability of the Nuclear Space Power Systems (NSPSs) in which they are used. A TEMP is a single component in which a thermoelectric generator (TEG) and an electromagnetic pump (EMP) are highly integrated.

The CLCP concept employs coreless linear magnets rather than circular magnets with or without ferromagnetic cores. Also in the concept, the counter-current, parallel busbars which lie on either side of the pump duct and that constitute a linear magnet carries the integrated field and armature currents to provide the magnetic field at the entrances to the magnet and the pumping section. As the current proceeds down one busbar a portion of it becomes armature current by crossing the pump duct to the other busbar while the remaining field current continues down the busbar. The partitioning of the currents happens all along the busbars and duct until it is all consumed.

The optimum partitioning factor of the total current to provide armature currents was found to be ~1/2 at each point along the pump duct and Linear Magnet (LM) length. This leads to geometric degradation of pumping capability from entrance to exit so that the upstream end of the pump produces nearly all of the pumping power. Truncation of the unproductive end leads to higher mass efficiency, but leaves the situation nearly the same as occurs without the integrated current concept and without the complications and difficulties of detailed control of the currents. The integrated current concept was abandoned in favor of separate field and armature circuits.

However, coreless magnets, including the Helmholtz and linear magnets, require substantially greater electric power for their operation which dominates the pump's power requirement. This, in turn, requires a TEG with a specific mass four to five times greater than that of the coreless pump. In fact, there is no way that such TEMPs can provide enough heat exchanger surface to provide the TEG with the heat rate needed for the TEG to meet the power demand. Thus, coreless TEMP were not found to be feasible. A pumping subsystem, that is not a TEMP, in which separate components consisting of a coreless EMP, heat exchanger, and TEG may provide the functions of a TEMP and may be feasible but too massive for NSPSs.

The substitution of ZrB_2 for Mo as the electrical conductors in the TEMPs at 1200K clearly indicated the superiority of ZrB_2 in this application. The HM-TEMP, using ZrB_2 as a conductor, was 23% lower in mass at the same pumping capacity than the same type TEMP optimized for the use of Mo conductors. However, the improvement was not sufficient to make coreless TEMPs feasible. The CLCP evaluated here is associated with a 64 kWe NSPS. For larger NSPS of interest to SDI, coreless TEMPs move still further away from feasibility.

RLW
F45

Hi-Z TECHNOLOGY, INC.

THERMOELECTRIC MATERIALS • DEVICES • SYSTEMS

3 September 1991

Mr. Richard Verga
SDIO/T/SL
Washington, DC 20301-7100

Dear Mr. Verga:

The enclosed report entitled "Evaluation of The Coreless Linear Conduction Pump for Thermoelectromagnetic Pumps", sponsored by SDIO/1ST, is hereby gtransmitted to you in accordance with the instructions contained in the associated contract (DE-AC07-90ID12911) document issued by DOE/IDO.

Sincerely yours,

Robert J. Campana

Robert J. Campana
Vice President

RJC:pgh
Enclosure

11180 Roselle St., Suite G, San Diego, CA 92121 • Telephone (619) 535-9343 • FAX (619) 535-9350

INTRODUCTION

The purpose of this program is to evaluate the Coreless Linear Conduction Pump (CLCP) concept as a potential component of a nuclear space power system that could result in significant improvement in survivability and mass reduction of such systems. The CLCP is an electromagnetic pump which, when powered by a thermoeletric power supply, can circulate the liquid metal coolant during normal operation and/or after reactor shutdown for as long as there is decay heat in the nuclear reactor to be removed. The significant factor in realization of the potential advantages is that such a pump would eliminate the current temperature limits of the Curie point of the ferromagnetic cores of the electromagnetic pumps previously used, or being developed for use, in the next or future generations of nuclear space power systems. In this project, no detailed consideration is given to the thermoelectric power source that would be ultimately integrated with the pump to form a TEMP, if the CLCP is a viable concept.

BACKGROUND

In 1967 the USA launched into orbit its first and, so far, only space power system, SNAPSHOT, employing a nuclear reactor as the primary energy source. The experimental system was designed to produce 500 W(e). It operated for only 42 days before it was inadvertently shut down. A thermoelectric electromagnetic pump (or a thermoelectromagnetic pump (TEMP)) was employed as the main pump to circulate the coolant both during normal operation and after reactor shutdown. The magnetic field in the TEMP was produced by a permanent magnet. It is not known how long the TEMP continued to circulate the coolant after shutdown.

The USA, as part of its Strategic Defense Initiative, is currently developing a new and larger (10 - 1000 kW(e)) Nulear Space Power System (NSPS) in the SP-100 Program. Its main and after-shutdown coolant circulation pumps will be TEMPs using electromagnets to produce the magnetic field.

In a previous study[1], TEMPs using permanent magnets, electromagnets, and Helmholtz coils (coreless) to produce the magnetic fields were evaluated for SP-100-type NSPSs over a range of powers from 100 kW(e) to 10 MW(e). The coreless Helmholtz coils did not perform very well in producing the magnetic field. They were excessively large and massive. Their circular nature did not fit well to the linear pumping section where the magnetic flux was needed. From this observation arose

the concept of the CLCP as described below.

THE CORELESS LINEAR PUMP CONCEPT

The basic concept of the coreless pump is shown in Figure 1. The geometry of the coreless pump has some similarities, at least at first glance, with that of rail guns. The two major current carrying busbars are similar to the rails of the guns. Current crosses from one busbar or rail to the other as it moves away from the power source. However, in the rail gun, the cross conductor (plasma) moves down the rail with time in contrast to the coreless pump where the pump cell remains in place, and liquid thrust out of the cell is replaced by liquid flowing in. Current in the linear coreless conduction pump crosses all along the busbars from one to the other.

The coreless pump concept can be described as incorporating a rectangular pump duct of height, H, width, W, and length, LT through which a conductive liquid metal (such as the alkali metals) flows and in which the pumping action is applied. Busbars, on opposite sides of the duct width, run along the length of the duct. The busbars are attached along the entire length of the duct so as to supply electric current for passage across the width of the duct and normal to the flow and pumping direction. The busbars are connected from one end of the duct to the power supply terminals, thereby requiring the current to flow in opposite directions in each busbar. With this orientation, the magnetic fluxes induced by the currents in the busbars are additive between the busbars, i.e., in the duct, and are normal to both the current and the flow. Thus, the conditions required for pumping are created. Outside the busbars, the fluxes induced by the currents in the busbars are subtractive and diminish rapidly away from the busbars.

As the current enters the positive busbar, it flows across the duct to the negative busbar. Assuming constant duct and busbar dimensions, this diminishes the density of the current continuing along the busbar before crossing the duct further along. Thus, both the flux and the pumping current fall off along the duct moving away from the power source. By tailoring the thicknesses and dimensions from end to end of the duct, it is possible to control the flux and current density crossing between busbars over the length of the pump. The width and height of the duct can be

varied along its length. Also the thicknesses, i.e., the width, of the duct walls and busbars can be varied over the length of the pump. Other adjustments are possible by selection of the materials of the wall and the busbars.

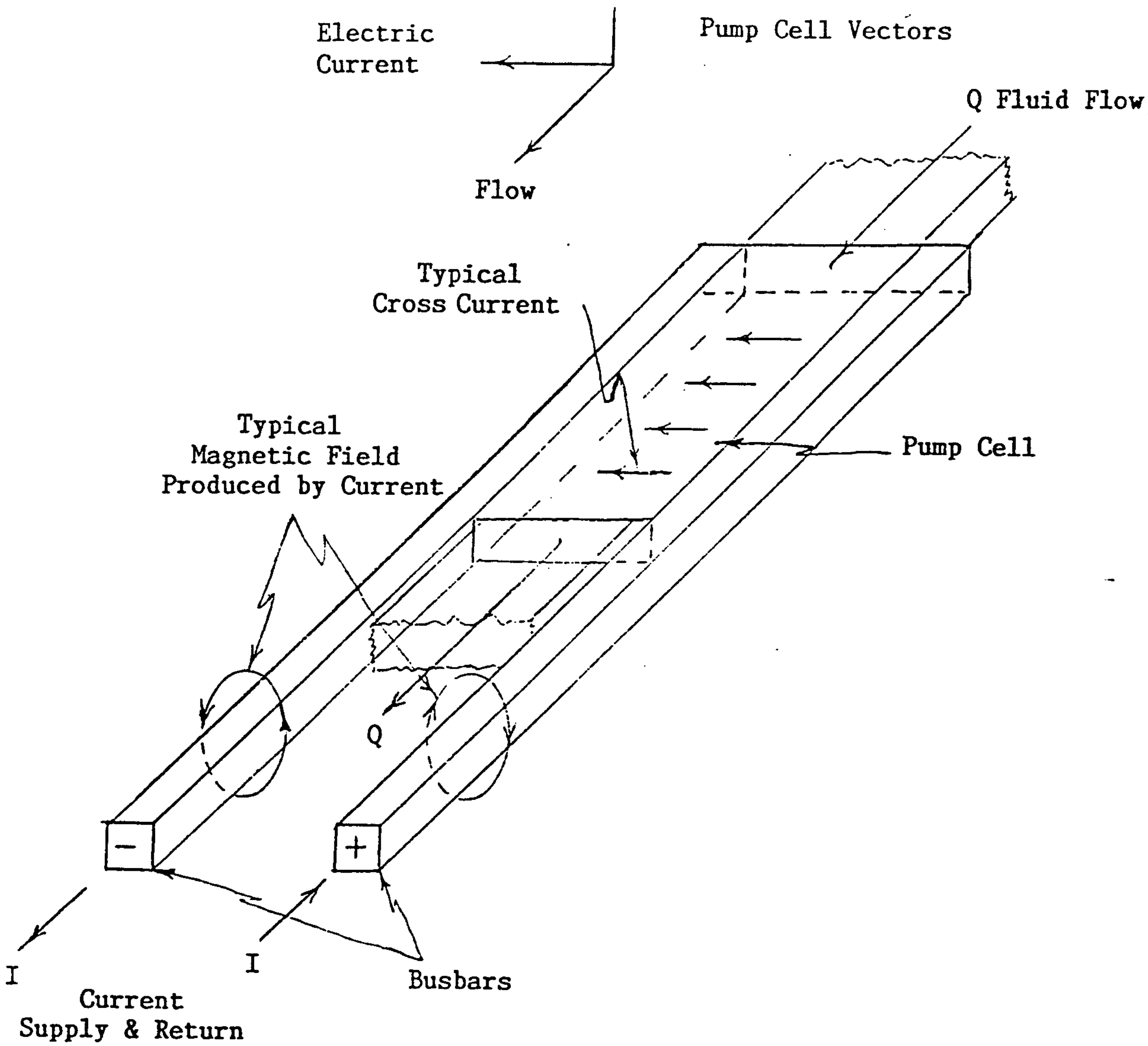

Figure 1. Coreless Linear Conduction Pump Concept

OBJECTIVES

The first major objective of the program was to establish the feasibility of Thermoelectromagnetic Pumps (TEMPs), incorporating Coreless Linear Conduction Pumps (CLCPs), for a range of NSPSs of interest to SDI.

The second major objective was to design, build, and test a CLCP to verify the concept.

There were also a number of more detailed objectives such as:

1) Identify critical issues related to TEMPs, incorporating CLCPs
2) To compare TEMPs incorporating CLCP with those incorporating EMPs, using permanent magnets, electromagnets, or Helmholtz magnets
3) Identify the temperature limiting items of CLCP-TEMPs
4) Determine the comparable survivability of CLCP-TEMPs
5) Identify the busbar and duct materials to use in CLCP-TEMPs above 1300K
+6) Determine if CLCP masses are more than those of cored EMPs of the same size
7) Determine if ZrB_2 as a conductor material is a potential alternative to Mo

TASKS

The original statement of work contained five tasks. Tasks 3 and 4 were deleted and Task 6 was added by amendment of the contract when the results of the design and analyses indicated that testing was not warranted. Nevertheless, some work was done on the deleted tasks prior to their deletion, and it is reported below.

The statement of work for each task is presented below immediately followed by a description of the work done, a statement of results, a discussion of its significance, and any decisions made in consequence.

An M2 thermoelectromagnetic pump (TEMP) specification was initially selected as a pump that would be used on the smallest nuclear space power system (NSPS) of interest to SDI. This specification is one of a family of TEMP specifications developed in a previous TEMP study[1] and defines one of three 4 psi - 100 gpm TEMPs that would be needed in a 64 kWe NSPS using Li as coolant, Nb-1Zr containment, Na heat-pipe radiators and SiGe thermoelectric generators (TEGs). At this size, any superiority of the CLCP TEMP will be most evident since experience has shown[1] that integration of a thermoelectric generator and an electromagnetic pump (EMP) into TEMP becomes harder for larger NSPSs.

Task 1. Using design parameters of operating temperatures, pump flowrate, delivered head and materials (chosen to optimize energy and mass efficiencies), a verification Coreless Linear Conduction Pump will be designed for use in thermoelectric electromatic pumps for space power systems

1.1 Helmholtz Magnet TEMP Revisited

In a previous work[1], a TEMP using Helmholtz rings (coreless) to produce the magnetic field was studied. The unsatisfactory results obtained led to the linear coreless magnet concept. It was decided to revisit the Helmholtz TEMP (HM-TEMP) to establish a basis for comparison of the relative merits of the two coreless concepts. Additional analysis was required since the previous work on the HM-TEMP was incomplete. Also, analytical expressions have been developed to evaluate the effects of circular conductors and/or coils whose cross-section is large enough to be significant in determining the magnetic fields produced, and their distributions. Such expressions have not been developed, or are unknown, for the parallel counter-current (PCC) magnets to be used in the CLCP.

The effects of size for the parallel-counter-current (PCC) flux generators or linear magnets (LMs) is evaluated in Task 6 below. The inclusion of the large conductor effects in the Helmholtz model thus provides an easy way of evaluating these effects for comparison with the same effects in the PCC magnets. Finally, the Helmholtz analytical, or design, model with its circular geometry also provides a basis for assessing the relative merits of Mo and of Zr diboride as the electrical conductors. The HM-TEMP analytical, or design models (HMM2EMP2 and HMM2TEG2), are presented in Appendices A and B.

1.2 Mass Optimization of TEMP Using the HMM2EMP2 Model

The HMM2EMP2 model was developed for a 4 psi - 100 gpm EMP. It also estimates the total mass of the TEMP assuming a g/W(e) derived from previous analyses or from an earlier analysis of the TEG for this particular TEMP. The mass of the TEG is estimated by multiplying the W(e) needed by the EMP by the TEG g/W(e). A multivariate optimization was carried out where the criterion was the lowest possible mass estimated (EMASS) for the TEMP, which includes both the EMP and the TEG. The optimization variables were H, the height of the pump duct, LT, the length of the pumping section, B, the axial-magnetic-flux density in the

pump duct, and ETA, the length of one side of the cross-section of the Helmholtz conductor/coil. A typical optimization curve is shown in Figure T1.1, where the estimated TEMP mass is plotted against the square cross-section dimension of the coil. The results of the optimization is an estimate of the HM-TEMP mass of 217 kg of which the mass of the TEG is 180 kg or 83% of the total. That leaves 37 kg for the EMP of which the Helmholtz coils are 30 kg. It is obvious that the estimated TEMP mass is only as good as the specific mass (45 g/W) that was assumed for this iteration of the EMP/TEG analysis cycle. When the EMP is electrically, thermally, and hydraulically matched to the TEG, EMP mass usually increases. The g/W(e) of the EMP derived from this analysis, along with the power and voltage requirements of the EMP, must be matched in the optimization of the TEMP using the HMM2TEG2 Model.

In fact, it was found that TEG could not be matched to the HMM2EMP2 in the highly integrated configuration that was applicable with permanent magnet- (PM) and electro magnet- (EM) TEMPs. In order to get enough heat transfer surface to supply the heat rate needed to produce the required power, the length and height of the pumping section had to be increased significantly. This, in turn, degraded the efficiency of the EMP and required still more power to be generated by the TEG. The system was obviously divergent with no practical solution attainable without changing the configuration. The solution is to make the TEG a separate component with its own heat exchanger. However, the power and mass of the TEG could be estimated from experience with the specific masses of TEGs that have been designed for space power applications. Table T1.1 is a comparison of three types of TEMPs to provide some perspective of the merits of the HM-TEMP and of the LM-TEMPs to be developed in the remainder of this report. The data for the permanent- and electro- magnet TEMPs (PMM2 and EMM2) were taken from[1], while that for the Helmholtz magnet TEMP (HMM2) was developed as described above.

It is obvious that TEG becomes increasingly the dominant mass of the TEMPs as the power required to produce the magnetic field increases. It is also known that the TEG's waste heat radiator is the dominant mass of the TEG. If the coreless EMP and TEG can be operated at higher temperatures than the TEMPs based on ferromagnetic materials, then they may become competitive in mass per delivered pumping power as well. The Curie point, the temperature at which materials lose their ferromagnetic properties, is about 1175K for most of the high-temperature magnet

materials, such as Alnico V and Hyperco 20. If a coreless TEMP could be operated at 200K higher temperature, i.e., ~1375K, then the radiator could be reduced in mass by a factor (1375/1175)^4, or 1.875. Assuming the radiator mass to be 50% of the 180 kg of the HMM2 TEMP, or 190 kg, 90/1.875 would be its lowered radiator mass, or 48 kg, and the HMM2 TEMP would still be 169 kg. A substantial improvement, but still not competitive unless there are other indirect benefits of the higher temperature capability. The case for the linear magnet (LM) will be made later in this report.

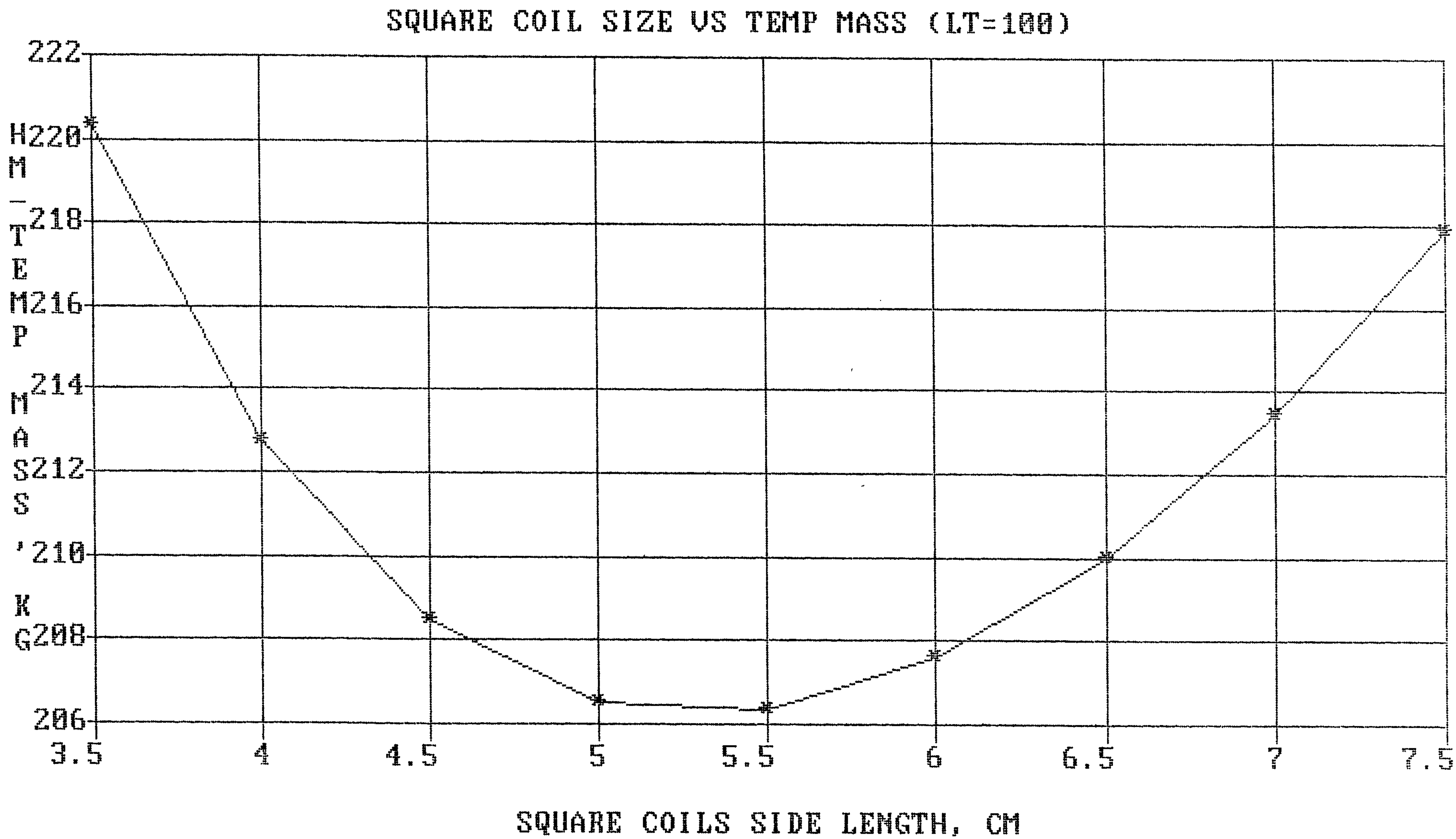

Figure T1.1. Typical Optimization of EMP Model

Table T1.1

Comparison of Three Types of TEMPs

		PMM2	EMM2	HMM2
TEMP Mass	(kg)	27.3	70.2	217
TEG Mass	(kg)	14.4	43.4	180
TEG/TEMP Mass	(%)	52.7	61.8	83
Hydraulic Power Delivered	(We)	174	174	174
EMP Efficiency	(%)	33.9	19.5	10.2
Total TEMP Power	(We)	513	1286	4045
Terminal Voltage of TEG/EMP	(mV)	106	280	317
Optimum Magnetic Flux Density	(mT)	78	77	40
Specific Mass of TEG	(g/We)	28	33.8	45
Specific Mass of EMP	(g/We)	25.1	20.8	9.15

1.3 The Coreless Linear Conduction Pump (CLCP)

An analytical model was developed for the Coreless Linear Conduction Pump (CLCP), which is presented in Appendix C and is named LMM2EMP2. LMM2 designates a linear magnet and an M2 pump specification, i.e., a pump delivering 100 gpm at a head of 4 psi. The EMP2 means simply the electromagnetic pump; analytical model, version 2. When coupled with the LMM2TEG2, a complete CLCP-TEMP analytical model is created.

The principal items in the development of the CLCP are the parallel, counter-current conductors that constitute the magnet which develops the magnetic field to interact with the armature current in the pump duct to produce the pumping action. This item is called the linear magnet, LM, throughout this document. Throughout the analysis, SI units are used exclusively. Only the pump specification (gpm and psi) is stated in non-SI units. However, in the models, the specifications were converted to SI units for all subsequent use.

The use of vector analysis was considered, as is frequently done in magnetic field analysis. However, the size and directions of the vectors must be accounted for separately in the computer modeling. Thus, vector analysis did not seem to provide any advantage in the computer model over computing the magnitude in the usual manner and

using a geometrical analysis to provide the directional aspects. Therefore, the latter methodology seemed more natural for computer use, and thus, it has been used here.

1.4 Optimum Magnetic Flux Density in EM Conduction Pumps

The pressure delivered by the pump to the external hydraulic circuit is given by the following equation:

$$PO=C1*B*I-C2*B^2*Q-C3*B^2*Q-C4*Q^2 \qquad \text{Eqn. 1}$$

where PO = Pressure delivered to the external hydraulic circuit (Pa)

B = Magnetic field density (Tesla) normal to the fluid and the armature current flow directions

I = Electric armature current (A)

Q = Volumetric flow rate of the fluid pumped (m^3/s)

Cx = Coefficents relating to fixed parameters (temperatures, materials, and pumping section dimensions) defined by the detailed terms of the equation and subscripts x=1 through 4--identifying the coefficient of each term.

The terms on the right side of Eqn. 1 are, respectively:

Term 1 - the total pressure rise developed in the pump

Term 2 - loss of pressure from the braking effect developed by the counter-current across the duct, resulting from the counter or back EMF generated by the fluid flowing across the magnetic field

Term 3 - pressure loss from eddy current and fringe end effects that develop near the entrance and exit to the pumping section

Term 4 - Internal pressure loss from friction and from contraction and expansion in the nozzle and diffuser at the ends of the pumping section.

Taking the derivative of Eqn. 1 with respect to B and setting it equal to zero, the optimum value of B is found to be:

$$B(opt) = I/Q*C1/(2*(C2+C3)) \qquad \text{Eqn. 2}$$

Thus, the optimum magnetic flux density is seen to be proportional to the ratio of the armature current to the flow rate where the

proportionality coefficient is the constant ratio of C1 to 2*(C2+C3). Unfortunately, this optimum cannot be achieved in TEMPs which are optimized for the minimum mass per unit of pumping power. Minimum mass is reached by reducing the power that must be provided by the TEG, since the specific power (g/We) to be supplied by the TEG is greater than the specific power (g/We) demanded by the EMP. While the power needed by a permanent magnet (PM) TEMP is only the armature load, in electromagnet (EM) TEMPs, HM, and LM TEMPs, the magnet must be powered in addition to the armature power. Consequently, the optimum magnetic flux density and maximum EMP efficiencies are not realized.

1.4.3 <u>Partitioning of Current for Armature and Linear Magnet Use</u>

When considering CLCP, the amount of current available will be limited. This raises the question of how the current should be partitioned between the armature current, IA, and the field current, IF, in the pump as a whole and everywhere along the pumping section length. The pressure rise developed by the pump is:

$$PO = B*IA*W/(W*H) = B/H*IA$$

Now if we let IA = I*f where I is the total pump current and f is the fraction of I that is armature current, then

$$PO = B/H*f*I \quad \text{but} \quad B = MuO*(1-f)*I/(pi*d)$$

where (1-f) = the fraction of I that is IF, the field current.

Then,

$$PO = MuO/(PI*d*H)*I*f*(1-f) = CF1*(f-f^2) \qquad \text{Eqn. 3}$$

Differentiating Eqn. 3, setting the result equal to zero and solving for f produces the result:

$$d(PO)/df = CF*(1-2*f) = 0$$

therefore: f = 1/2

Thus, as far as developing the highest possible head in the pump from a given supply of current, IA = IF. Of course, adding the other terms to the equation for the delivered head and flow rate specified, i.e., Eqn. 1, the result is modified as shown here

$$f = (CF1+2*(CF2+CF3))/(2*(CF1+CF2+CF3)) \qquad \text{Eqn. } 4$$

where CF1, CF2, and CF3 are the coefficients of the first three terms on the right side of Eqn. 1, respectively. The more complete equation, 4, for the optimum partition of the current is greater than 1/2 but probably not very much. This being the case, then previous relationship for B(opt), Eqn. 2, which provides maximum pumping efficiency, cannot be simultaneously attained by this arrangement. It should be noted that an electrically parallel arrangement between the armature and the field circuits is inherent in the counter current arrangement.

In the CLCP concept, part of the field current would later (further down the pumping section) be converted to armature current until it was all consumed. With the partitioning fraction of the total current close to 1/2, half of the field current would go to armature current and the other half to residual magnetic field current for each subsequent partition. In a preliminary analysis of how the current would be distributed, the CLCP was divided into 5 serially-connected pumping cells to be supplied by common armature and field current busbars that also consisted of a linear magnet. When power was supplied to the entrance end of five pump cells, and the current partitioned half-and-half to the armature and field currents, that left half the current for the second cell, 1/4th for the 3rd cell, 1/8th for the 4th cell, and 1/16th for the 5th cell. But the pumping forces, or pressure developed, are proportional to the product of the armature and field currents, or, since IA=IF in each cell, the square of the current to each cell. Thus, the following proportional pumping powers and ratios would be produced in the five cells:

		Proportional Pumping Power	Pumping Power Ratio
1st cell $(1/2)^2$	=	1/4	1
2nd cell $(1/4)^2$	=	1/16	1/4
3rd cell $(1/8)^2$	=	1/64	1/16
4th cell $(1/16)^2$	=	1/256	1/64
5th cell $(1/32)^2$	=	1/1024	1/256

in a decreasing geometric progression.

Thus the optimum partitioning indicated that nearly all the pumping would be provided by the first one or two cells, but the mass of the other cells would be undiminished, or nearly so. It is obviously more effective to eliminate the last 3 or 4 cells under this partitioning. The optimum partition was abandoned and smaller partitioning fractions considered. But if the partition fraction were made still smaller, then the progression would be less steep and more cells would be needed. But ultimately, the end-most cells would be relatively very unproductive and would be eliminated. After cell truncation, the last cell would pump a significant fraction of the first cell. Why, then, integrate the currents in the first place? The whole idea of using the current twice--first to provide the magnetic field and then to become armature current--did not seem to make much sense, or provide much gain, if any, over separate armature and field circuits. In addition, it was found that as voltage between the two counter-current busbars dropped theoretically to zero at the pump exit, the voltage to drive the current across the duct was competing with the back EMF generated by the fluid flowing through the magnetic field. For this reason, some end cells had to be cut off but not the busbars so that the voltage at the last cell was sufficient to overcome the back EMF. For these reasons, and the elimination of the complexities in controlling and partitioning the currents, the integrated armature and field current concept was eliminated in favor of separate armature and field circuits. What remained was a simpler concept with the basic essence of the CLCP; namely, an EMP with a linear magnet.

1.4.1 <u>The Infinite Linear Magnet</u>

There is a magnetic field associated with every electric current such that, according to the right hand rule, there is a circular magnetic field force encircling a conductor as the direction taken by the fingers of the right hand grasping the conductor with its thumb pointing in the direction of conventional current flow. The field is a vector quantity which is perpendicular to both the current and a normal radial vector from the conductor to a point of interest (see Figure T1. 2).

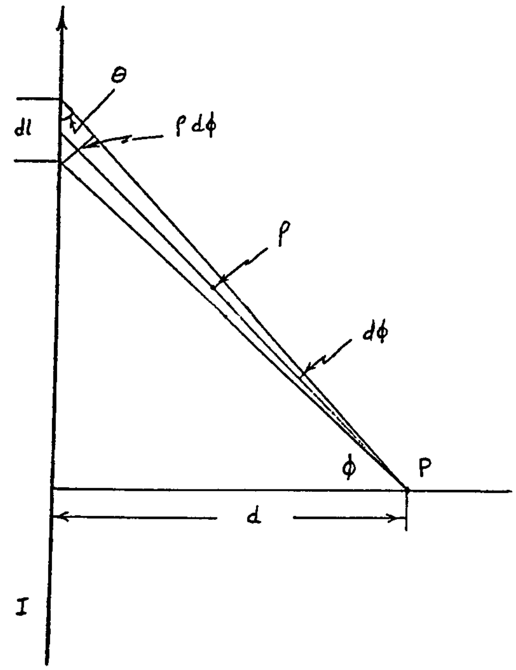

Figure T1.2. Ampere's Law as Applied to a Long Straight Conductor

The magnetic field, density B, associated with a current-carrying conductor of negligible cross-section and infinite length is given by Ampere's Law[2,3] as

$$dH = I*dL*\sin(phi)/(4*pi*d^2)$$

where H = magnetic field intensity (A/m)

I = current (A)

dL = differential length of conductor (m)

phi = angle made with dl when viewed from the point of interest in the field

and d = distance from dL to the point of interest (m)

If we integrate the above equation from minus infinity to + infinity, the result is that

$$H = I/(4*pi*d)*\int_{-\pi/2}^{\pi/2} \cos(phi)d(phi))$$

Since the integral is exactly 2,

$$H = I/2*pi*d \qquad (A/m)$$

Then the magnetic flux density is B = muo*mur*H

where B = magnetic flux density (T)
muo = absolute permeability (V-s/A-m) or (T-m/A)
mur = relative permeability
muo = 4*pi*10^-7.

Since mur = 1 for vacuum and air and $\simeq$1 for all but ferromagnetic materials,

$$B = muo*I/(2*pi*d) \quad (T) \qquad \text{Eqn. 5}$$

For two infinite parallel counter-current conductors, separated by a distance 2*d, the flux density at the mid-separation point, d is 2*B or

$$B(mid\text{-}point) = muo*I/(pi*d)$$

and if d is the separation distance between conductors

$$B(mid\text{-}point) = 2*muo*I/(pi*d)$$

1.4.2 <u>The Finite Linear Magnet</u>

For a finite (in length) straight current conductor (see Figure T1.3), the magnetic field intensity at a point, P, separated from the conductor by d meters is given by the Biot-Savart Law[4],

$$H = I/(4*pi*d)*[\sin(b1)+\sin(b2)]$$

where b1 = angle between a line from P to one end of the conductor and the normal from the conductor to P, or
b1 = atan (L1/d)
and b2 = angle between a line from P to the other end of the conductor and the normal from P to the conductor, or
b2 = atan(L2/d) where L1 and L2 are the lengths of conductor in each direction from the point of interest

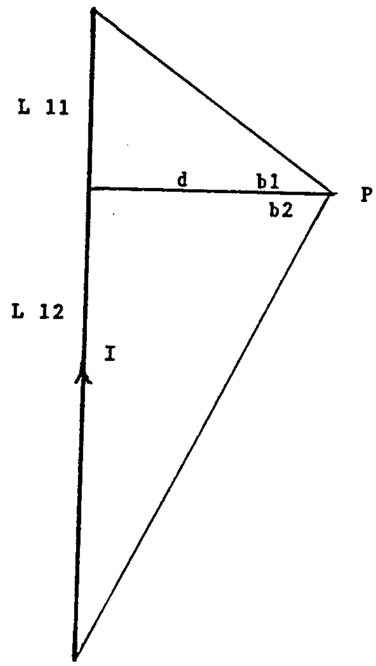

Figure T1.3. Biot-Savart Law Diagram

For a pair of finite counter-current conductors of the same length and ends not displaced from one another, the magnetic intensity at the mid-point between the conductors will be just twice that of a single conductor. If w (for width) is the length of the line between conductors, then at any point, P, between conductors, the magnetic intensity will be the sum of the contributions from each of the two conductors. At any point, P, between the conductors, the distance from the first conductor is, say fw*w, where fw is simply a fraction of w, then the distance from the second conductor will be (1-fw)*w. Then

$$H = [1/(fw*w)+1/((1-fw)*w)]*I/4*pi*[\sin(b1)+\sin(b2)]$$

The magnetic flux density, B, is then simply muo*H. The above equation is the basis for the linear magnet (LM) and was written into the LMM2EMP2 model program.

Using the LMM2EMP2 LM model, a typical magnetic field distribution between the magnetic field busbars was calculated as shown in Figure T1.4 at the mid-length of the magnet. It is seen that the field is strongest near the conductors and is minimum at the mid-point between the busbars. In Figure T1.5, the magnetic field distribution along the pump duct between the busbars is shown. The busbars coincide in length

with the pumping section. The field is seen to be strong in the pumping section, which extends from 0.2 to 0.8 of the total length. Upstream and downstream of the pumping region, the field is seen to fall off rapidly.

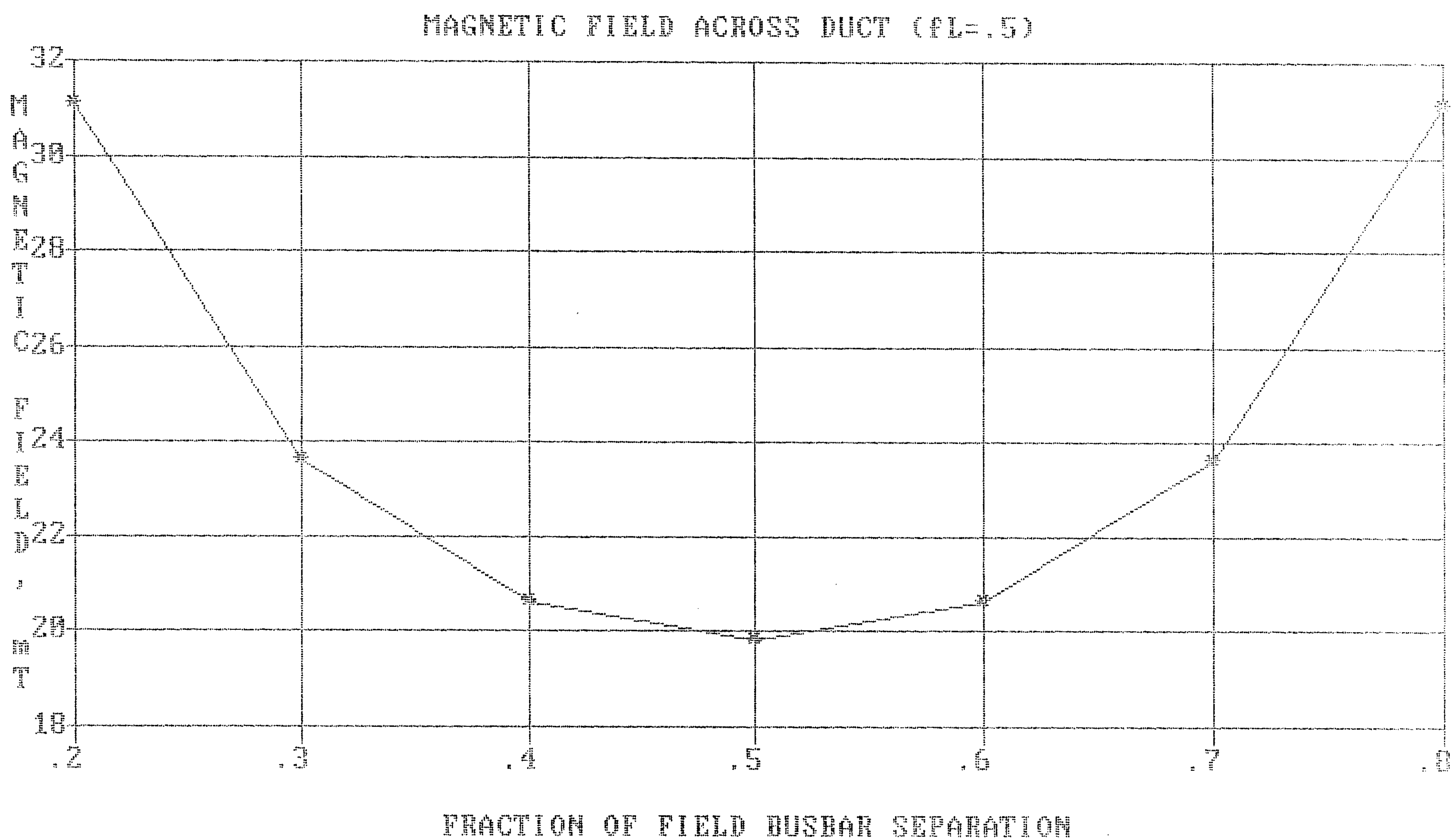

Figure T1.4. Magnetic Flux Density Distribution Across the Pump Duct

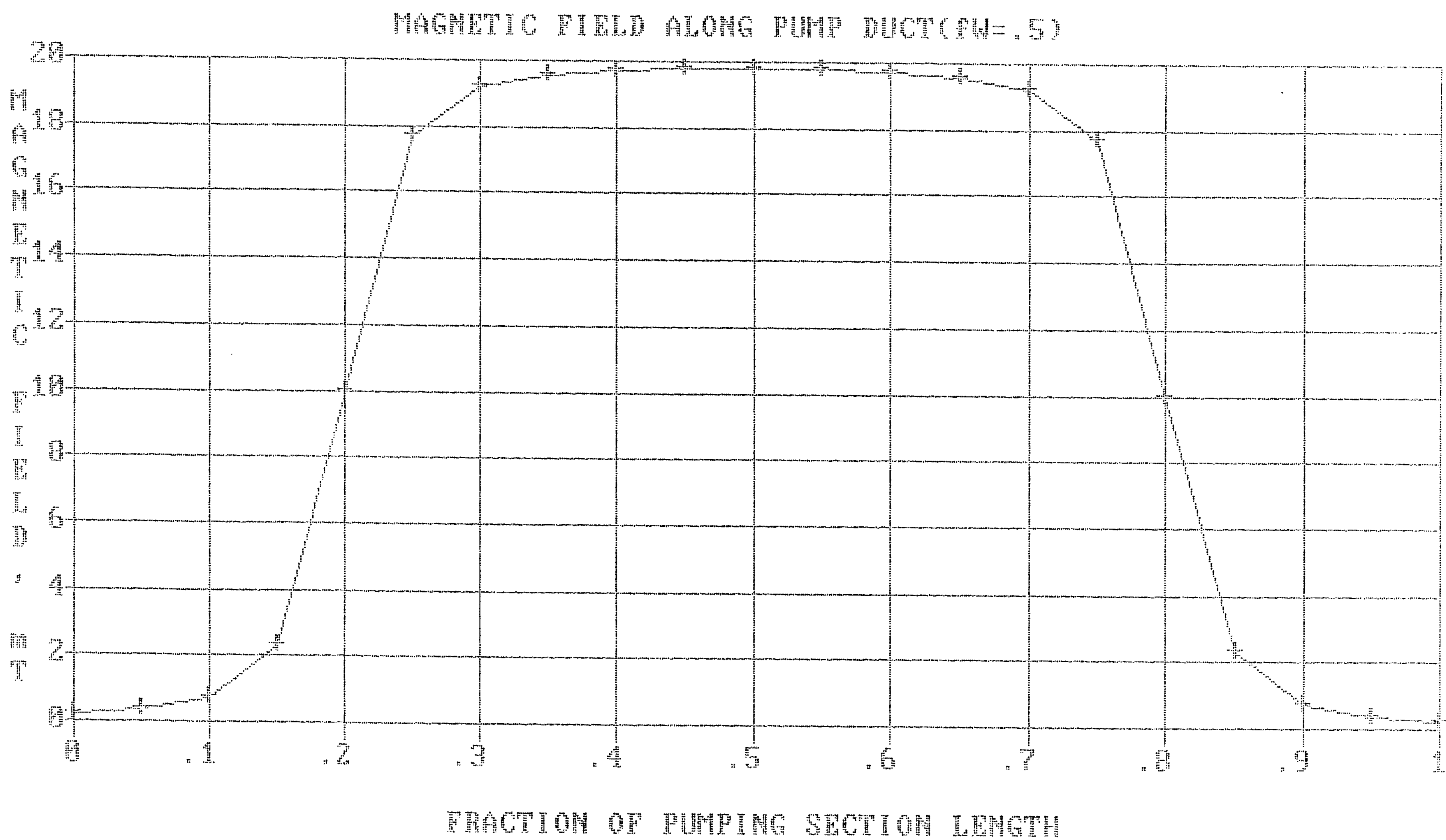

Figure T1.5. Magnetic Flux Density Distribution Across the Pump Duct

In the pumping section, only the axial magnetic flux density is effective in developing useful pumping action. The magnetic flux on the line between the conductors is theoretically all axial flux. However, parts of the pump duct lie above and below the theoretical line, and the busbars are not point current conductors. Thus, it is necessary to consider second order effects which may be important. The magnetic intensity above the line between the conductors will be considered in the next paragraph. The effects of busbar size will be considered in Task 6.

Above and below the line connecting the centers of the busbars (the busbar line), the points along the perpendicular bisector of the busbar line are by definition always equidistant from the busbars. Thus the magnetic intensity is twice that of one busbar. However, since the magnetic vectors are normal to the radial vectors from the busbars to the point of interest, P, they are not axial but have equal opposing non-axial components that cancel each other. Their axial component is, however, twice that of one busbar. The components are shown in Figure T1.6 to be the total flux times the cos(atan(2*h/w)), and the distance from each busbar is d=(h^2+(w/2)^2)^(1/2). The distribution of the total and axial magnetic flux density as calculated by the LMM2EMP2 model is shown in Figure T1.7.

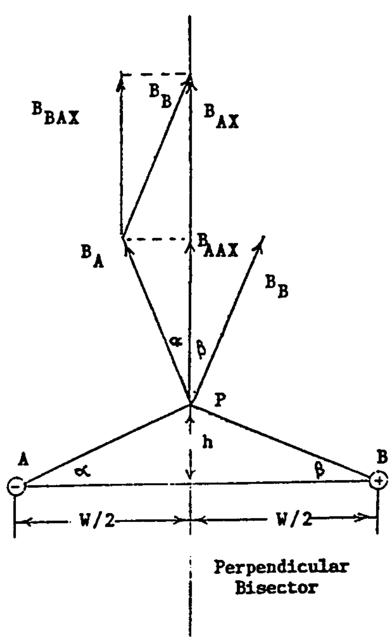

Figure T1.6. Vector Diagram of B_{BX} On The Bisector

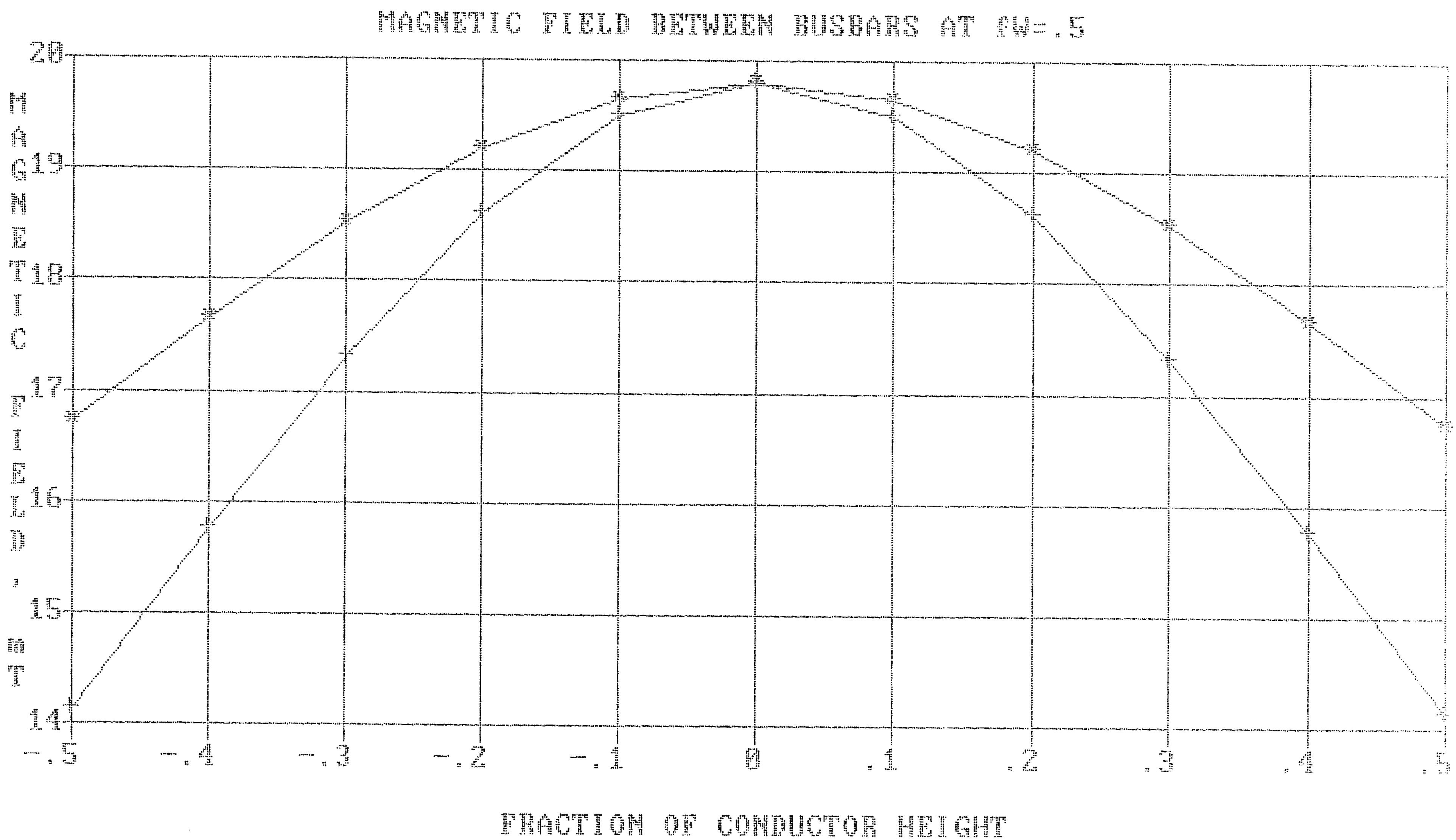

Figure T1.7. Axial Magnetic Flux Density vs Height

When the point of interest is not on perpendicular bisector of the busbar line, then contributions of each of the busbars to the magnetic intensity must be calculated separately and vectors summed, as shown in Figure T1.8. Thus, in general,

d=(h^2+(fw*w)^2)^(1/2) and d′=(h^2+((1-fw)*w)^2)^(1/2)

H1 = I/4*pi*d*[sin(b1)+sin(b2)]*cos(atan(h/(fw*w))) Eqn. 10

H2 = I/4*pi*d′*[sin(b1)+sin(b2)]*cos(atan(h/((1-fw)*w))) Eqn. 11

and B_{AX} = muo*H = muo*(H1 + H2)

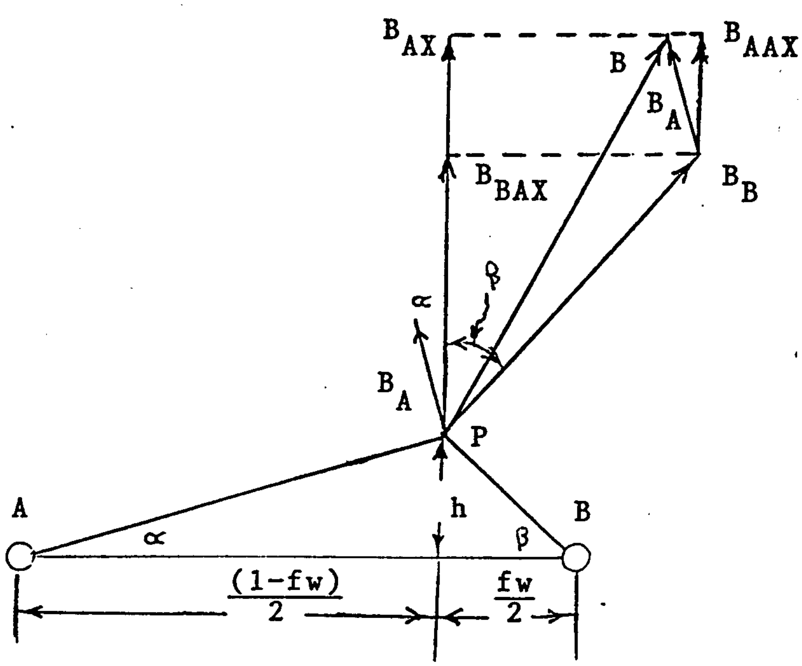

Figure T1.8. General Vector Diagram of B_{AX} Between Busbars

1.4.4 <u>Linear Magnet (LM) TEMP</u>

An analytical model of the LM-TEMP was developed for comparing this concept with permanent magnet, electromagnet, and Helmholtz magnet TEMPs. The LM-TEMP model is essentially the same model as the HM-TEMP except for the substitution of the LM model for the HM model. The LM-TEMP model is shown in Appendix C and is named LMM2EMP2.TK.

The basic configuration of the LM-TEMP is shown in Figure T1.9 and is similar to those used for evaluating the cored-magnet and HM-TEMPs.

The EMP consists of a double pass arrangement where fluid is being pumped in opposite directions, as, for example, to and from a heat source. There are two LMs, one just above and outside the upper pump duct, and the other directly just below the lower pump duct.

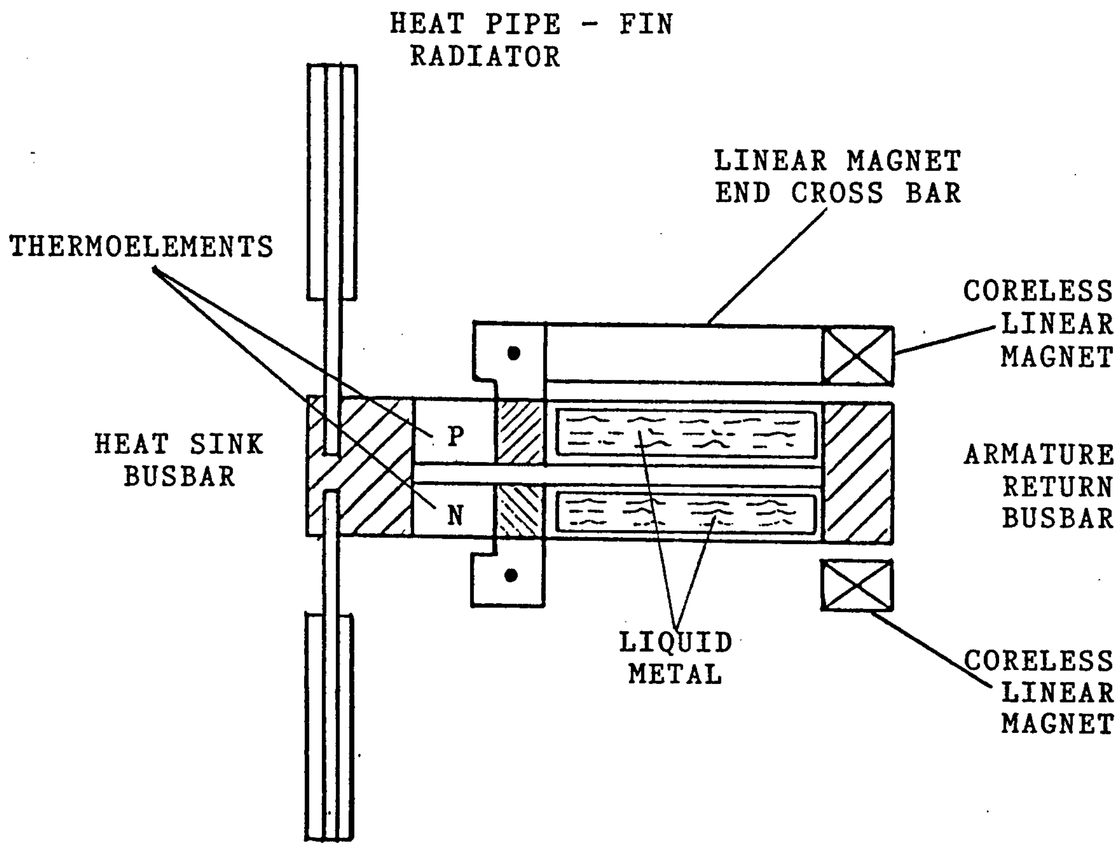

Figure T1.9. Basic Configuration of LM-TEMP

The counter-current busbars in each magnet carry current in the same direction on the same side of the stacked pump ducts, but with cross-bars at opposite ends of the main busbars. Field current enters the top magnet at one end of a busbar and the bottom magnet at the opposite end of the busbar on other side of the duct. Opposing flow of current in the two ducts provides self-compensation of the magnetic end effects that would occur if no compensation were provided.

The LM model used for the evaluation uses the average method described above in Section 6.3.3. While this model is not as accurate as the "Differential Busbar Model", it is good enough for preliminary comparisons, and much easier to use. In fact, the difference in axial flux calculated by the two methods is less, the smaller the conductors

are. The conductors in the optimized TEMP calculation are $\lesssim 36$ cm^2 in cross-sectional area, and most of them are less than 20 cm^2. The differences in the two methods are thus <17 and 11%, respectively, derived from Figure T6.7.

Some of the results of the calculations are shown in Table T1.1. The results are similar to those obtained from the HM. The power required by coreless pumps of a given pumping capacity is much greater than required by the cored pumps, i.e., the permanent and electromagnet pumps. Large currents are required to produce very modest magnetic flux densities. Whether the required current is provided as a single Amp-turn or many Amp-turns, the total current must be the same. Thus, the power required can only be reduced by the use of lower resistivity materials and smaller structures (which can only be achieved by the use of lower resistivity materials). When more than one amp-turn is used, electrical insulation between turns is required. Some dilution of the current density by the insulation is unavoidable, resulting in the need for more amp-turns per unit of magnetic flux at the point or region of interest. The use of insulation at very high temperatures introduces additional problems which would have to be addressed.

The magnet power is critical. Every Watt of electrical power required must be supplied by the thermoelectric generator. It has been found that in the coreless magnet TEMPs, the magnet power dominates the power required by the EMP. This, in turn, means that the TEG mass to supply the power will be predominately that needed by the LM.

The larger the TEG becomes, the greater the thermal energy it must be provided from the liquid stream being pumped. In attempting to integrate the TEG with the EMP, as was done with the cored TEMPs, it was found that heat exchanger requirements distorted the EMP, thereby reducing its efficiency. The loss of efficiency is evidenced by both armature current and magnet current increases. The result is an even larger TEG is required, etc. That is, the TEMP design diverges, blows up, or there is no solution. A configuration change is required which separates the design into a thermoelectric generator component with its own heat exchanger and an electromagnetic pump without a heat exchanger. It is no longer a TEMP.

Table T1.2

Comparison of TEMPs Based on Coreless

Helmholtz and Linear Magnets

PARAMETERS		HM	LM
Axial Magnetic Flux	(mT)	40	24
Mass of Magnets	(kg)	30.8	19.6
Mass of EMP	(kg)	33.5	21.3
Mass of TEG	(kg)	227	199
Estimated TEMP Mass	(kg)	262	220
Power Output of Pump	(Wh)	174	174
Hydraulic/Electric Efficiency	(%)	9.0	7.7
Power Input to EMP	(We)	1935	2165
Power Input to Magnets	(We)	3159	2261
Power Output of TEG	(We)	5093	4426
Terminal Voltage of EMP	(mV)	123	148
Terminal Voltage of Magnets	(mV)	251	570
Number of Pump Cells or Passes		2	2
Number of Magnets		2	2
Specific Mass of EMP	(g/We)	6.97	4.8
Specific Mass of TEG	(g/We)	44.5	45
Armature Current	(kA)	15.7	15.3
Field Current	(kA)	6.3	1.9

1.4.5 The Feasibility of Coreless TEMPs

Both the coreless HM and LM TEMPs are not feasible except perhaps in very small pumps that are of no interest to SDI. While coreless EMPs are feasible as separate components, they may even be practical and useful in SDI NSPSs. When they are integrated into a single component (a TEMP) where they must provide heat-exchanger surface and perhaps current, voltage, and flow compromises with the TEG, they have been found not to be feasible. The hoped-for advantages of the coreless TEMPs (elimination of the Curie point loss of ferromagnetism and its derivative benefits) may yet be availabe to SDI with a pumping system employing coreless EMPs, heat exchangers, and TEGs as separate components working together to provide all the functions of TEMPs. The investigation of such systems appears to have merit.

No analysis of larger coreless LM TEMPs for larger NSPSs was undertaken as originally planned since magnet power requirements will be more than proportionately larger because the volumes to be magnetized are larger, and the magnets themselves will be further removed from the location where the field must act. This effect was observed in the previous study[1] even with the PM and EM TEMPs. Thus, the larger the coreless TEMP required, the further from feasibility it will be.

Task 2. <u>Based on the results of Task 1, a Coreless Linear Conduction Pump will be fabricated in such a manner that it can be tested in existing test facilities. A test plan will be generated.</u>

2.1 Design of the Test Pump.

Initially it was confidently thought that the test pump could be designed to fit the available existing loop with minor modifications. This did not turn out to be the case.

An analytical model of the VCLCP was developed to design the test device as shown in Appendix E. The minimum pump performance that could be acccomodated by the loop was thought to be 5 psi of delivered head at 5 gallons per minute. Attempts to design the test pump resulted in very high magnet currents at very low voltages. Test pump performance was reduced until a pump of .2 psi and 1 gpm was reached requiring currents of 12 to 30 kA at voltages $\leq$1 V. This would have resulted in severe instrumentation and heat removal problems requiring significant cost and time to solve. Later, it became obvious that such a test would not provide any credible data for the CLCP. Construction and testing of the VCLCP was deleleted from the program.

The electrical network schematic for an analytical model of the verification CLCP is shown in Figure T2.1. The electrical network was developed to control the partitioning of the armature and field currents along the length of the pumping section. The network model is shown in Appendix F. This model was subsequently incorporated into the overall VCLCP design model. After the decision to completely separate armature and field currents, the model was not needed.

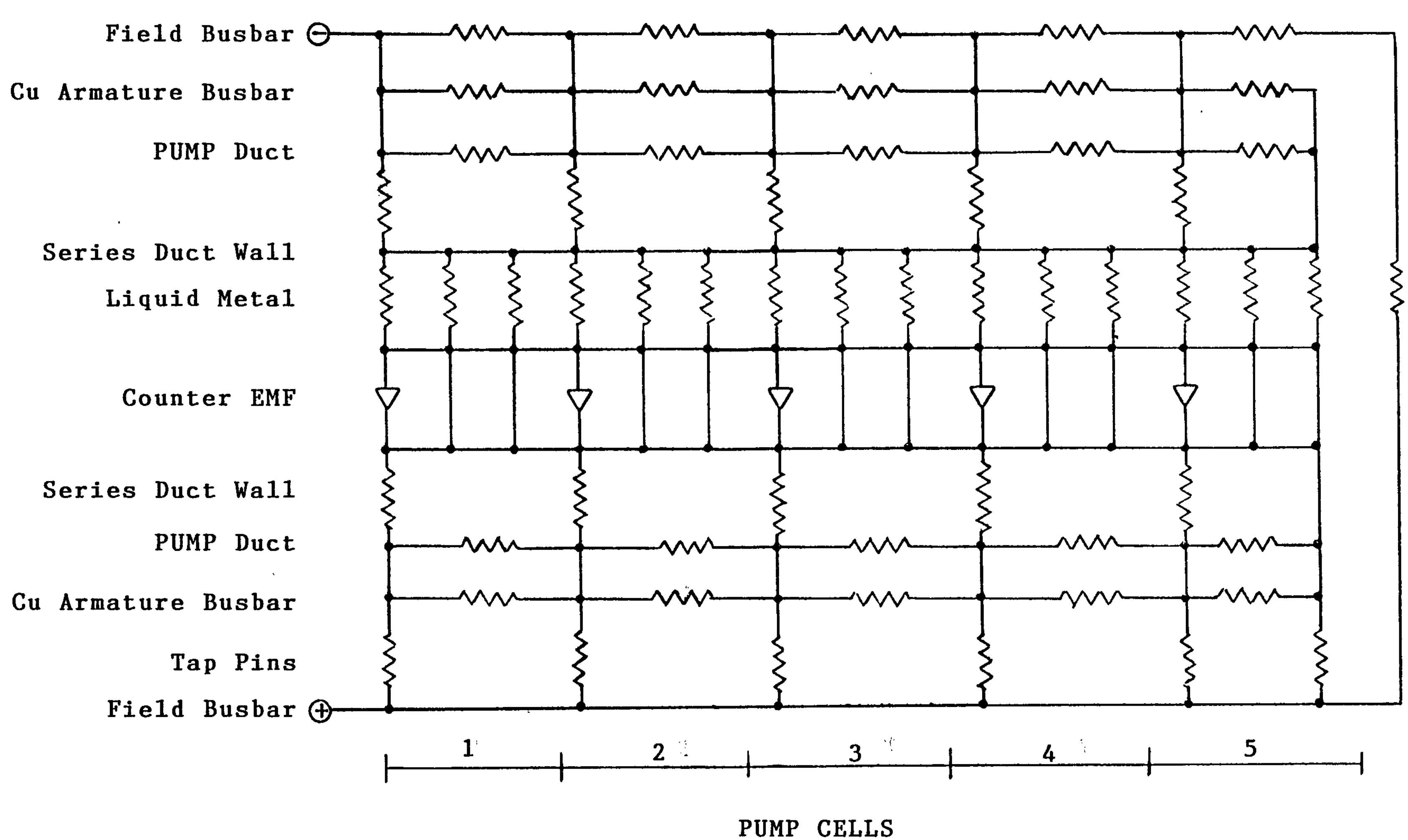

Figure T2.1. Preliminary VCLCP Electrical Network

NaK-78, the near eutectic alloy of Na and K, was selected as the liquid metal to be pumped by the VCLCP. Its physical properties were taken from the literature[5,6] and the data as a function of temperature over the range of interest was fitted by polynomial equations that could be readily used in the design model. Plots of the data, the fit of the polynomial equations and the polynomial coefficients are given in a series of figures and computer output that comprises Appendix G. The resulting polynomial equations were incorporated into the VCLCP design and analysis model. A similar set of equations was developed for NaK-56 alloy before the NaK-78 alloy was selected.

The design of the VCLCP never progressed to the point where stress analysis was appropriate and a LM cooling system design was required.

2.2 Fabrication of the VCLCP

The most critical item in the construction of the VCLCP was believed (based on the history of fabrication dc EMPs) to be the attachment of the armature current eletrodes to the pumping section wall. For the test pump to operate at relatively low temperature, 304L stainless steel and Cu were selected for the pumping section and eletrodes respectively. This suggested that commercial fabrication of these materials for kitchenware might be applied. An order was placed with Texas Instruments' (TI) Foil Division for sheets of SS rolled and bonded together with Cu to form a finished foil of SS clad on Cu with layers of 20 and 99 mils respectively. This was the thickest layer of Cu that TI felt they could fabricate. Additional Cu would have been electroplated onto the electrodes as required. Figure T2.2 is a photomicrograph of the bonded region of the foil and was used to verify the thicknesses. Figure T2.3 is a photograph of a fabrication test specimen made from the foil by first removing Cu from selected areas by precision machining and lapping, bending the SS to the pumping section cross-section configuration and then seam welding. No further fabrication testing was conducted after the decision was made to forego building and testing of the pump.

Some electrical insulation fabrication tests were started but immediately abandoned upon the decision to forego construction.

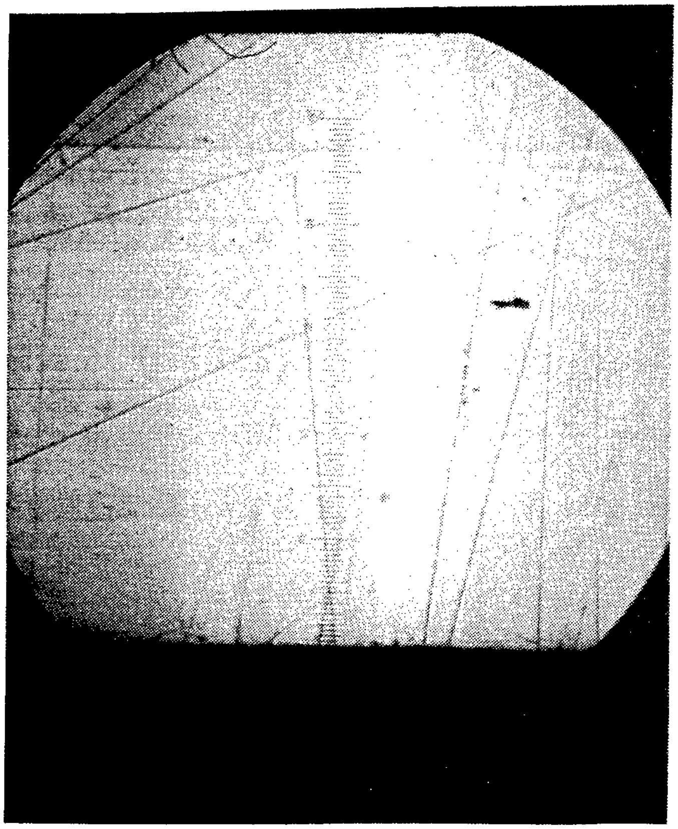

Photomicrograph of the cross-section of SS Clad Cu sheet. The dark band at the top is 304L Stainless Steel, and the lower thickness is pure Cu.

The optically measured thickness agreed with the results of a caliper measured total thickness and measurement of the thickness fractions with a ruler from which the layer thicknesses were calculated. A number of scratches are apparent after light polishing that were not polished out to avoid off-flatness aberrations.

Figure T2.2. Photomicrograph of SS Clad Cu Sheet

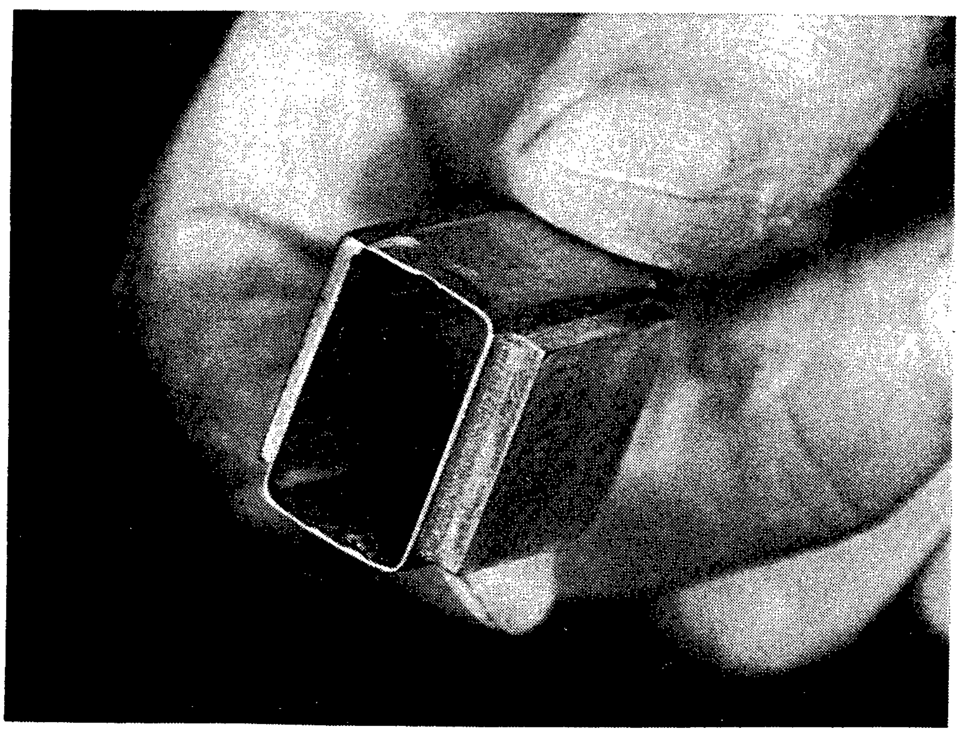

Figure T2.3. Fabrication Test Specimen of Pumping Section of VCLCP

Task 3. Existing test loops will be modified and instrumented to accommodate the Coreless Pump, and to collect the necessary test data (current voltage, flowrates, pressure, and magnetic flux).

3.1 The NaK Cart Loop at ETEC

The NaK Cart Loop, Figure T3.1, at Energy Technology Engineering Center (ETEC) was selected for testing the VCLCP. However, the results of Tasks 1 and 2 did not support testing. Modifications to the facility, instrumentation, power supply and heat sink could have been made, but their cost was beyond the scope of this program. This task was deleted by contract modification. However there are a few activities that were accomplished that are reported below.

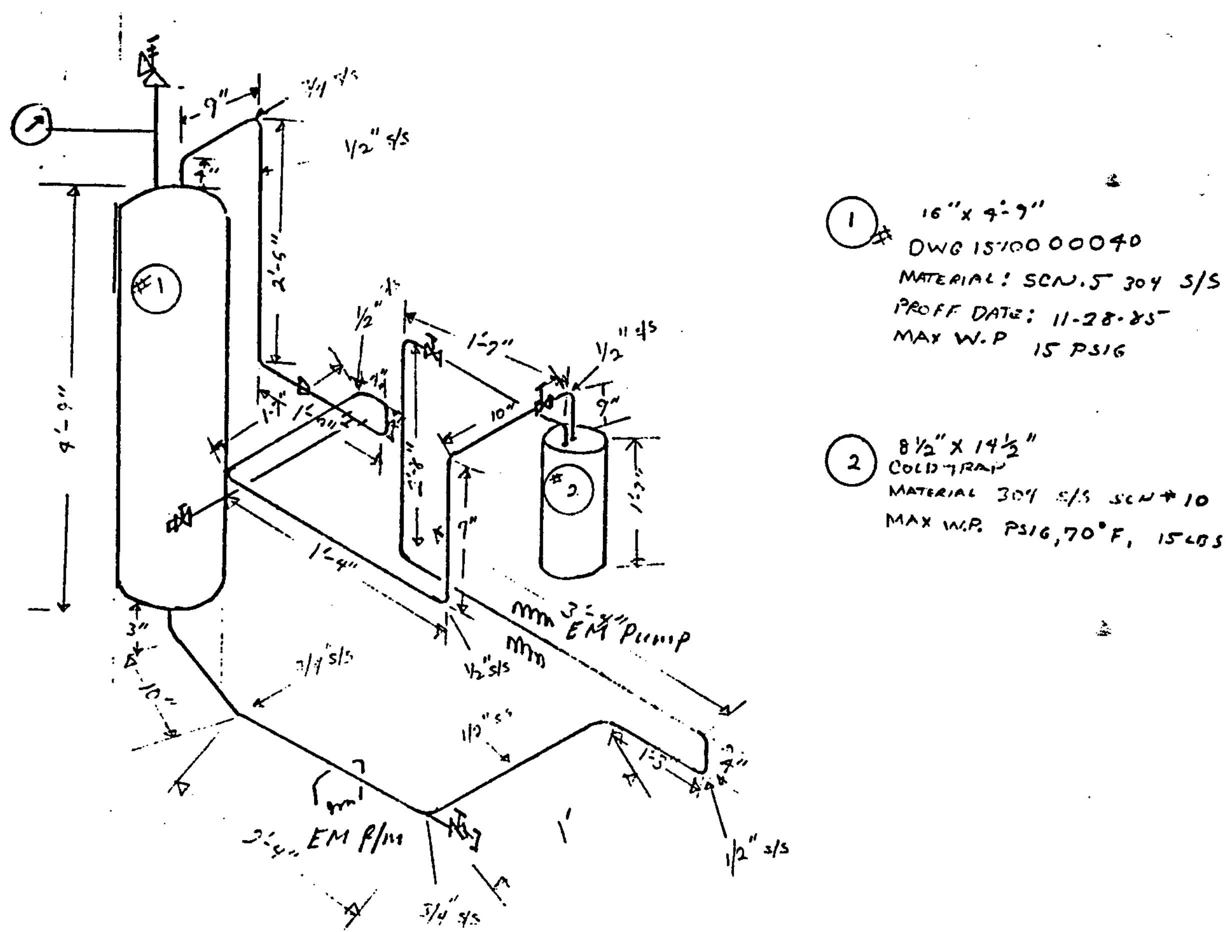

Figure T3.1. ETEC NaK Cart Loop Schematic

An analysis was made of the pressure losses to be expected in the NaK Cart Loop using the schematic sketch provided by ETEC. The equivalent velocity head loss of all of the components in the flow path were determined as shown in Table T3.1. The losses in the NaK resevoir tank and the oxygen filter were shown to be uncertain or excessive relative to the low delivery pressure to be developed by the test pump. The solutions agreed to by ETEC and Hi-Z were modifications to the loop piping to (1) eliminate the static head rise in the resevoir by returning the NaK to the bottom of the tank instead of the top and (2) installing valves and piping to by-pass the filter during testing.

Table T3.1

Velocity Head Losses

Quantity	Element	Velocity Head Coefficient, K
2	45° El-3/4"	0.45
1	Tee (3/4"-1/2"-3/4") - Side exit	5.0
2	Valves 1/2" (fully open)	1.15
1	Flowmeter	0.
1	EM Pump (nozzle & diffuser)	0.08
1	Reservoir (expansion & contraction)	1.5
1	Cold Trap (mechanical filter)	10
1	90° El (1/2" x 3/4")	0.94
1	90° El 3/4"	0.9
1	Tee (1/2") (straight through)	1.8
1	3/4" Tubing (54" total length)	2.52
1	1/2" Tubing (241" total length)	16.87
		41.21

Loop pressure drop is estimated to be ~7×10^{-2} Pa at 2 gpm flowrate

Static head of reservoir entrance is ~10^{4} Pa

(There is a free surface in the reservoir where cover gas pressure may be applied)

Static head (half-full reservoir) $\simeq 5 \times 10^{3}$ Pa

ETEC indicated that the existing EM flowmeter had never been calibrated for such low flow as would be occuring in the VCLCP tests. Mapping of the magnetic flux distribution and calibration of the flow meter would have been required.

The existing pressure gage (pitot-tube type) in the NaK Cart Loop had a range that was not compatible with the pressure head to be developed by the VCLCP. A remotely operated differential liquid-metal manonmeter would have been required.

3.2 Magnetic Flux Measurement

Measurement of the magnetic flux and its distribution can be difficult. Measurement on the installed pump would be non-existent to severely limited and of limited usefulness. Measurements outside of the loop can only confirm that the stray flux is low and very local. The areas of interest are in the pumping section and near the ends of the pumping section. Measurements at these locations have to be outside of the loop and at reduced power. Two methods are possible: one uses ac power to the magnet with induction coils that measure the flux induced voltage. The sensivity is low at the low frequency of the power supply. The directional aspects are difficult to measure without an elaborate three dimensional positioning system.

A second method uses a Hall Effect (HE) sensor. Such sensors are commercially available. Complete HE flux meters are also available commercially but can be expensive. Some preliminary tests were made at Hi-Z using a HE sensor sample given by the Siemens Co. A simple instrument was made using a standard circuit. The small size (<3 mm) of the sensor was a considerable advantage over the size of an effective induction coil. (It could easily be fit into the pumping section duct). However, the HE device was little better in directional aspects than the induction coils. Either ac or dc magnet power can be used with HE method. Some measurements were made of the magnetic flux and its vertical distribution between two parallel counter-current Cu busbars. Using a welding machine power supply both ac and dc measurements were made successfully and correlated well with the analytical model. However, the power supply was limited in capacity to ~350A. The HE method was selected but no further work on it was conducted.

Power Supply

A power supply capable of supplying ≤24 kA current at ≤1 Vdc was indicated by the design analysis. ETEC could supply 50 kA, at 10 Vdc by a rectified 3ϕ source without a filter. The details had not been worked out at the time the test was cancelled, but long heavy Cu cables were foreseen in which the voltage would be dropped to the user's requirement and parasitic power in the cable would be dissipated by forced air cooling, if necessary. To get to 1V, about 90% of power would be wasted, or about 450 of 500 kW. The remaining power, 25-50 kW, would be consumed in the VCLCP. That could not be accomplished without a local water heat sink. That power supply was to power the VCLCP, which would produce an output of less than 1/2 W of hydraulic power! Incredible! This is not what was envisioned in our proposal which said "In parallel with analyses, a low-cost proof-of-principle coreless pump will be designed and tested in a small, low-cost test loop".

Task 4. Tests will be performed, and the data will be analyzed to verify the design.

This task was deleted by program contract modification. See Task 3 above.

Task 5. A final report will be written, covering the design, and test results, and will specifically address the feasibility of the coreless pump in thermoelectric magnetic pumps. Based on the results, a Phase II proposal may be developed which would include the development of a prototype thermoelectric magnetic pump.

This report is the product of Task 5.

Task 6. The use of ZrB_2 as magnetic-field conductors and busbars will be assumed and the affect of its use on CLCP feasibility will be analyzed and compared with the normal use of Mo at 1200 K or higher for these purposes. The effects of large cross-section current conductors on magnetic flux generation will be analyzed.

6.1 Comparison of ZrB_2 & Mo as High Temperature Conductors in LM Magnets

6.1.1 High Temperature Conductor Materials

At the high temperatures of space power systems, the choice of electrical and thermal conductors is limited. Without going to such exotic concepts as canned liquid metals, Mo is a frequent choice and is the likely choice for the TEMPs. However, Hi-Z Technology, Inc. (Hi-Z) is currently in the SBIR Phase II development of ZrB_2, zirconium diboride, which is comparable in electrical resistivity to Mo at 1000K and can be used up to 2000K. The program is funded by SDIO and managed by The Defense Nuclear Agency (DNA). Zirconium diboride's advantage is its density which is only 6 Mg/m^3 compared to 10.1 of Mo. Based on the obvious potential for lower mass conductors using zirconium diboride, its use in coreless TEMPs was analyzed to determine if lower pump masses would result and if it would contribute to coreless pump feasibility. The following analysis was conducted.

This analysis was carried out using the HMM2EMP2 analytical model of the Helmholtz electromagnetic pump which would deliver 100 gpm of Li coolant at a head 4 psi (See Appendix A). The masses of the Helmholtz conductor rings made of Mo and ZrB_2 were compared while all remaining pertinent variables were adjusted so as to optimize the TEMP design with respect to the total TEMP mass, i.e., including TEG mass as described in Section 1.2 above. The results of the optimization analyses are shown in Table T6.1.

The analytical result reflects the difference in their conductivities per unit mass. The conductivity per unit mass of ZrB_2 and Mo are 4.35×10^3 and 3.54×10^3 $cm^2/g.Ohm$, respectively. Thus, the conductivity per unit mass of ZrB_2 is 23% greater than that of Mo at 1200K. The results show the estimated mass of the HM-TEMP optimized for the use of ZrB_2 is 22% less than that when optimized for Mo use. Similar differences appear in the power output and mass of the TEG. The superiority of ZrB_2 with respect to the Mo is clear. At higher temperatures, the situation would seem to favor Mo because of its lower coefficient of resistivity compared to ZrB_2, as shown in the equations below. However, there appears to be some confusion in the accuracy of these equations or the data sources from which they were derived. This

Table T6.1

Comparison of HM-TEMPs

Using Mo versus ZrB_2 Conductors

PARAMETERS		Conductors: Mo	Conductors: ZrB_2
Axial Magnetic Flux	(mT)	40	24
Mass of Magnets	(kg)	30.8	12.0
Mass of EMP	(kg)	33.5	14.3
Mass of TEG	(kg)	227	190
Estimated TEMP Mass	(kg)	262	204
Power Output of Pump	(Wh)	174	174
Hydraulic/Electric Efficiency	(%)	9.0	6.8
Power Input to EMP	(We)	1935	2570
Power Input to Magnets	(We)	3159	1690
Power Output of TEG	(We)	5093	4260
Terminal Voltage of EMP	(mV)	123	393
Terminal Voltage of Magnets	(mV)	251	244
Number of Pump Cells or Passes		2	2
Number of Magnets		2	2
Specific Mass of EMP	(g/We)	6.97	3.4
Specific Mass of TEG	(g/We)	44.5	45
Armature Current	(kA)	15.7	6.5
Field Current	(kA)	6.3	3.5

is being pursued under the referenced ZrB_2 development program noted above in this section.

$$RhoZrB = -5.710+0.0357*T \text{ micro-Ohm-cm}$$ [8]

$$RhoMo = -0.183+0.0321*T \text{ micro-Ohm-cm}$$ [8]

6.1.2 The Electric Resistivity of Molybdenum Versus Temperature

The electrical resistivity of molybdenum (Mo) was seen to be critically important in the design comparison with ZrB_2, zirconium diboride, as the conductors. Resistivity data from various sources lead to some confusion. An additional attempt has been made using well-

documented Mo data[7]. The data are from one of the oldest and largest commercial suppliers, and was reviewed and selected to be used in a highly regarded materials handbook of recent publication. It is regarded to be as well-founded as one can expect at this writing. Several points were taken from the published graph of the full temperature range presented. These data were fit with a fourth order polynomial to derive the following set of coefficients for the equation. The original data points were then plotted as shown in Figure T6.1, with the curve (solid line) calculated from the equation. The fit appears to be excellent.

RHOMo=A+B*T+C*T^2+D*T^3+E*T^4 (microOhm-cm)

where A = -8.144267
B = +0.21863752
C = -6.88*10^-10
D = +2.3868*10^-8
E = -5.28*10^-12
and T = Temperture K)

$RHOZrB_2$=-5.71+0.0357*T (microOhm-cm)

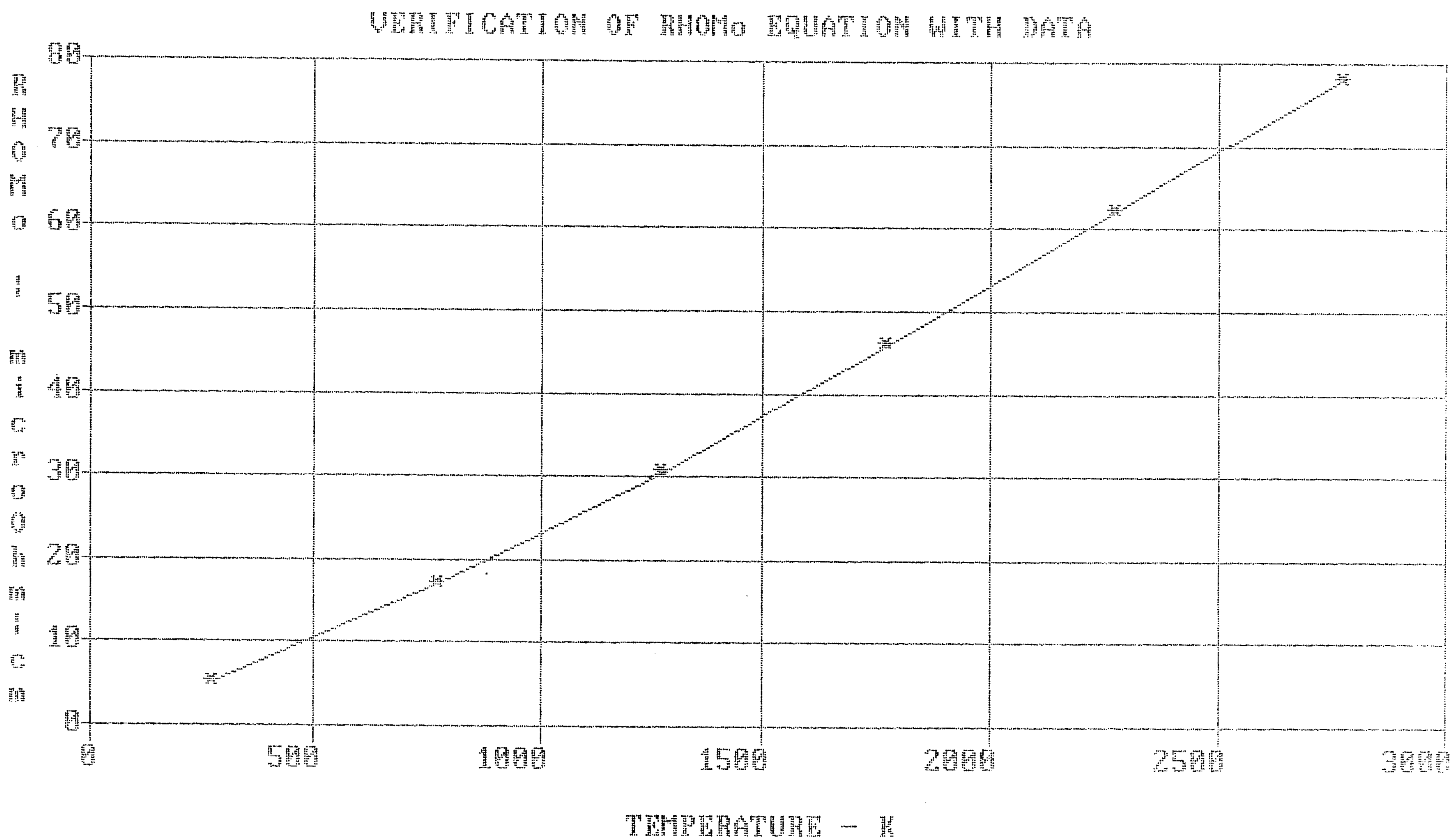

Figure T6.1. Verification of Mo Resistivity Equation

Zirconium diboride is actively under development as a conductor material, including aerospace applications[8]. Its electrical resistivity, among other properties, is somewhat in a state of flux. However, the resistivity curve given above is regarded as a reasonable working model until the work in progress is completed in 1992.

A comparison of the electrial resistivities of Mo and ZrB_2 over a temperature range of 300 to 1500K is shown in Figure T6.2. At room temperature, the resistivities are essentially equal but Mo, at least initially, has a smaller slope. Mo's resistivity is 35% lower at 1200K, and the curves are still diverging.

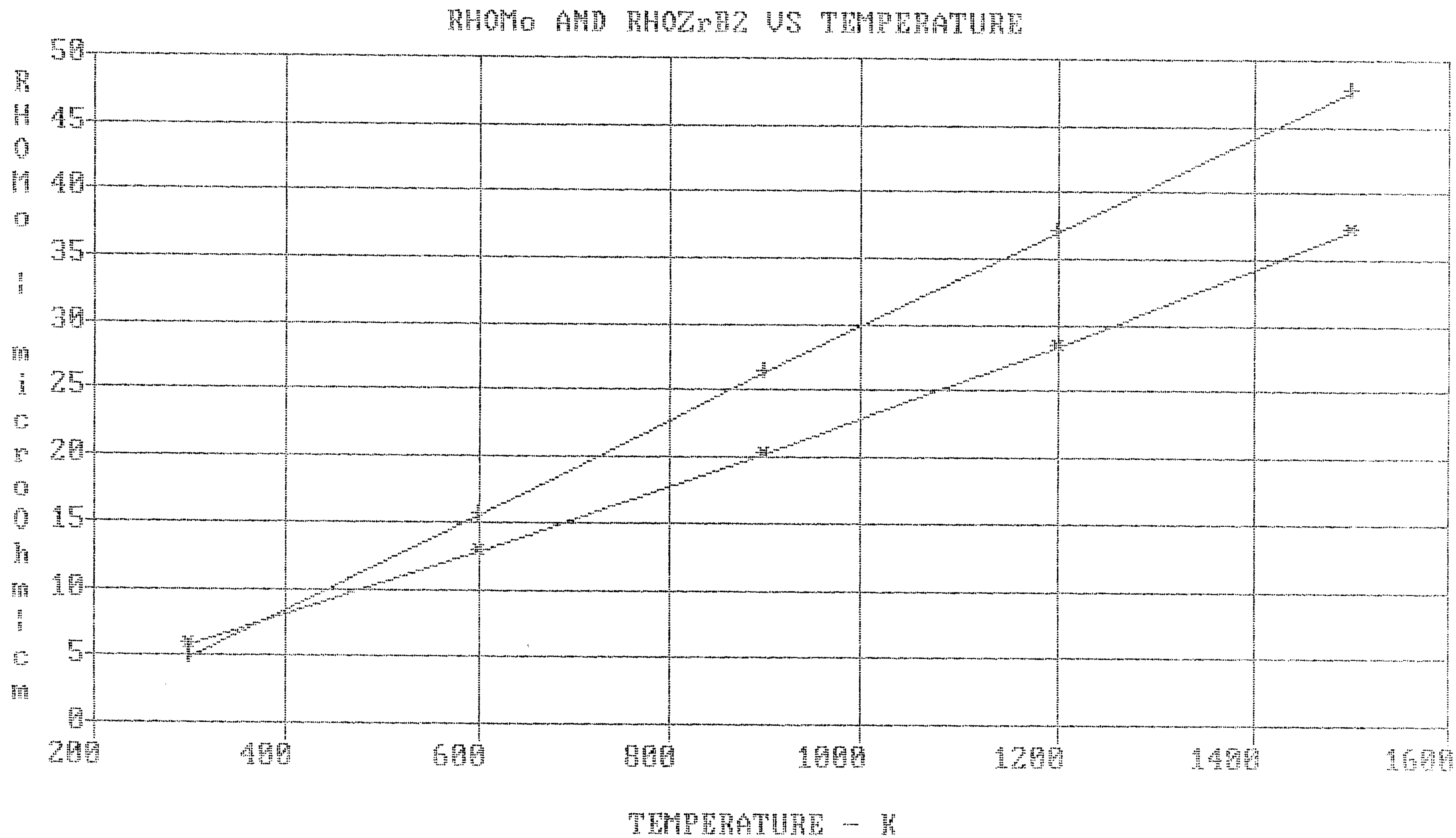

Figure T6.2. Resistivity-Temperature Curves of Mo and ZrB_2

6.2 Effect of Conductor Size on Magnetic Field Calculation in HM

In calculating the magnetic field produced by an electric current flowing in conductors, it is generally assumed that the cross-sectional area of the conductors is negligible and thus two amp-turns will produce twice the field strength of one amp-turn. However, when the conductors or the number of amp-turns gets very large, the total conductor can grow to a size where its dimensions can no longer be neglected. For circular conductors, such as the Helmholtz conductors, analytical expressions for the magnetic flux have been developed to take into account the size of the conductors[9]. Such an expression is contained in HMM2EMP2 for conductors of square cross-sections. However, such an expression for PCC conductors is unknown or, at least, not readily available. It was thus of interest to use the Helmholtz coil model to determine if it would be an important effect in generating magnetic fields for coreless TEMPS.

The analysis was conducted using the HMM2EMP2 program (See Appendix A) and decoupling the magnetic flux section from the rest of the program by replacing B, the axial magnetic flux density generated in the pump duct, by BT, the test magnetic flux density, which is unrelated to the pumping equations. This is done by "quoting-out", that is, by placing a quotation mark at the beginning of any equation that causes it to be ignored. So the Bs were quoted-out and BT inserted for the coil flux.

The coil current was divided by the coil cross-sectional area to yield a current density that could then be held constant. Keeping the current density constant, increasing the cross-sectional area, is equivalent to raising the current or the number of amp-turns of the conductors and vice-versa. If there were no effect of the conductor size, the flux would increase in proportion to the the cross-sectional area. Otherwise, the increase would be less than proportional. Thus by comparing the two cases, the effectiveness or efficiency of the conductors can be established. The result of such an analysis is shown in Figure T6.3. The magnetic flux is shown to rise in proportion to the cross-sectional area along the upper curve when the size of the conductors is ignored, and to fall along the lower curve when size and shape are considered. The efficiency of the conductors is seen to decrease as the size grows. These results were obtained when the effective radius of 8 cm. The effect of size becomes less as the radius

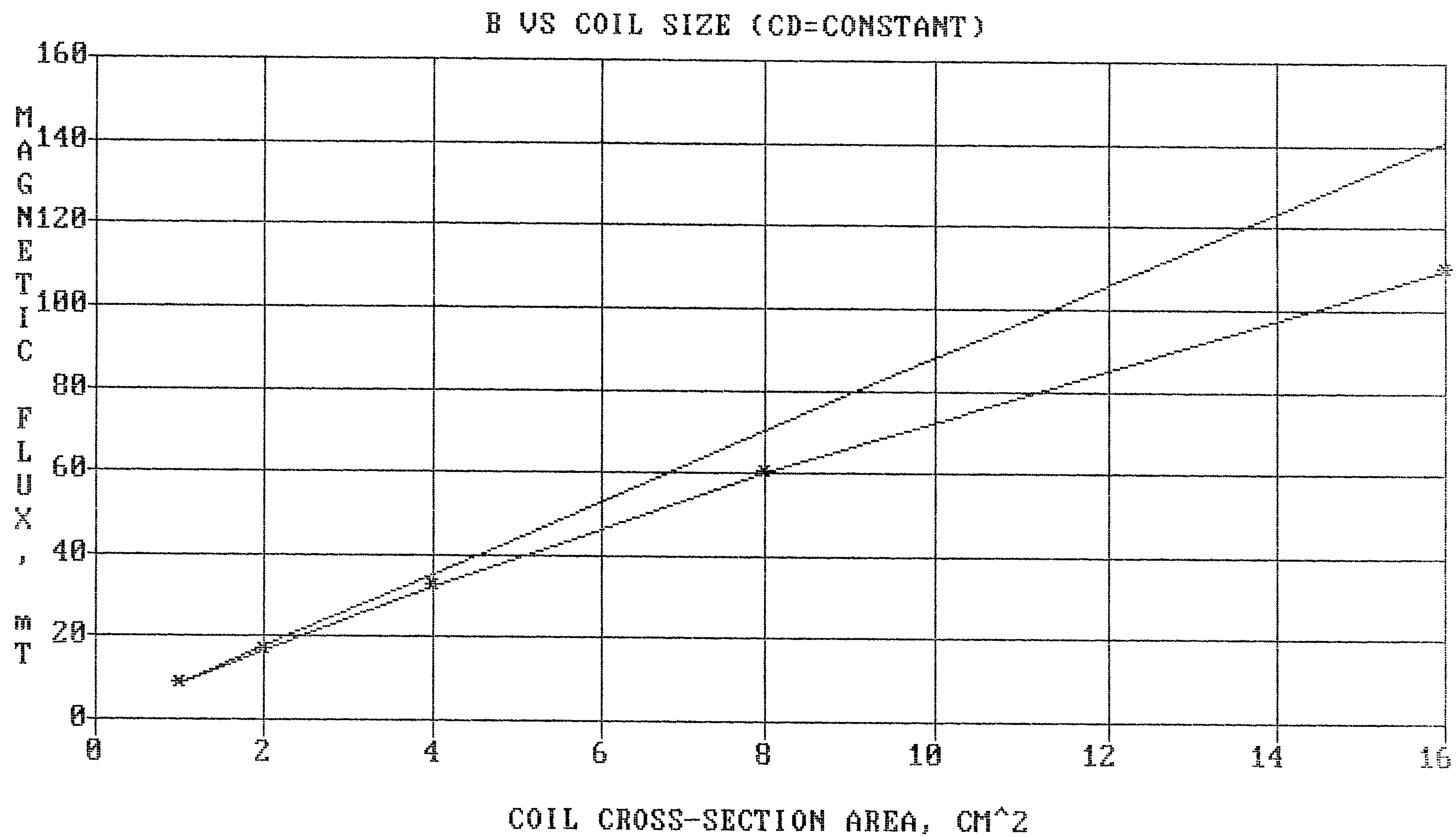

Figure T6.3. HM Flux vs Conductor Size

increases, but becomes very sensitive to coil size as the radius decreases. It is clear that the size of the conductors carrying the magnetic-field-producing current cannot be neglected in coreless TEMPs. The effects of the conductors size is considered next for the LM.

6.3 The Effect of Conductor Size on Magnetic Field in LM

Analysis in previous paragraphs of the effect of the size of the cross-sectional area on the efficiency of magnetic field production showed that dimensions of the conductors may be important in the design of coreless electromagnetic pumps. While analytical expressions are available for such effects in circular coils, there is no readily available data for counter-current conductors such as those of interest here. Thus, the following method was developed using superposition and adapting analytical techniques available in the literature.

The approach is to subdivide square busbar cross-sections into 25 smaller squares so that a 5 by 5 array of square conductors or minibusbars make up the total busbar of each of two matched counter-current busbars used to generate the magnetic field for an electromagnetic pump. The contribution of each minibusbar-pair to the magnetic flux density at a given location will be determined. The total magnetic intensity, or flux density, may be obtained by adding the individual contributions asserting that superposition applies for this purpose. It is assumed that the cross-sectional current density will be constant for each minibusbar per case, but may be different from case to case.

The equations 6 and 7 developed in Section 1.4.2 above were applied here. Only instead of obtaining the axial magnetic flux density at various distances, P, from a busbar pair, we now calculated the axial magnetic flux density at a point contributed to by busbar pairs located at several distances from the point, P. The equations are the same, only our orientation in applying them changed.

The cross-sectional area of each of a pair of parallel, large counter-current busbars comprising a LM are divided into a five-by-five matrix of square bars (minibusbars) as shown in Figure T6.4. Equipotential electric field lines are circles passing through the busbar locations like those shown as dotted lines in Figure T6.5. The magnetic field vector at any point P on one of those circles will be directed toward the center of its circle. The centers of these equipotential circles lie on the perpendicular bisector of the busbar lines and grow

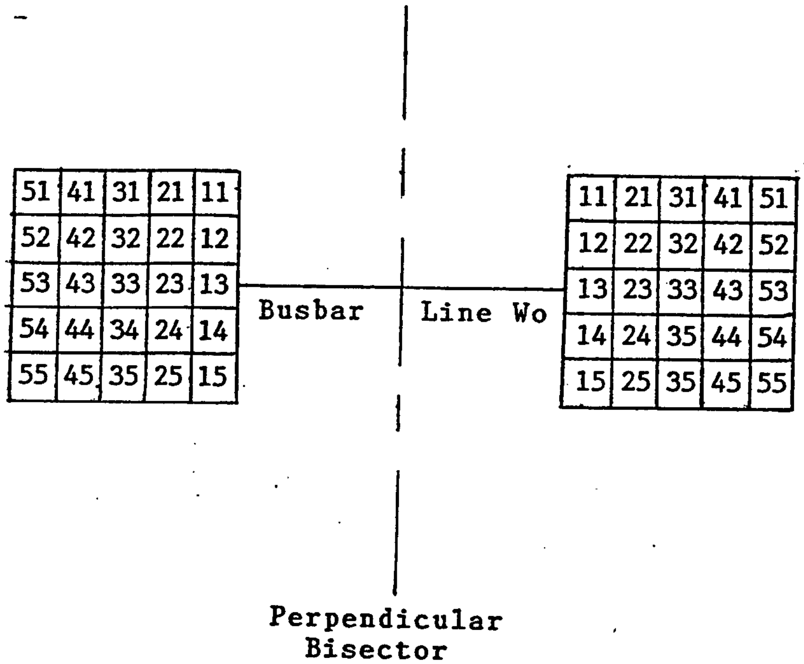

Figure T6.4. Minibusbars Matrix of a Large Conductor

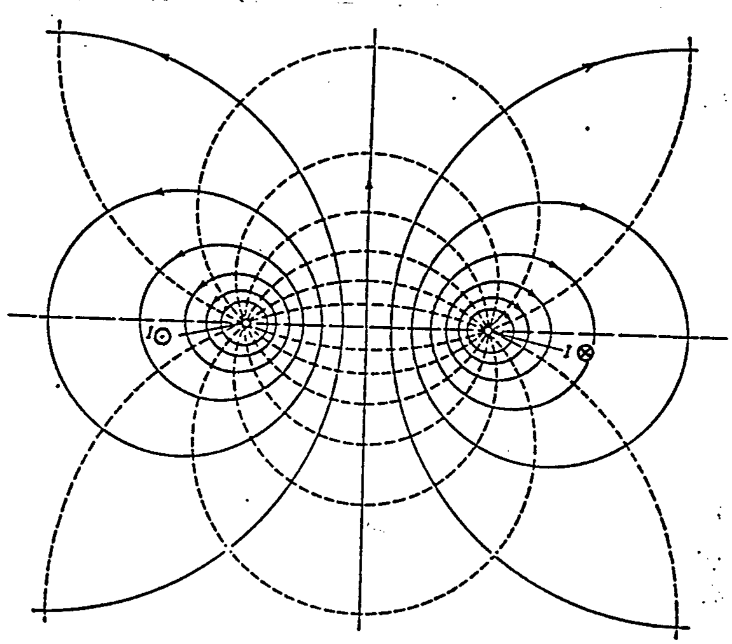

Figure T6.5. Equipotential Electric Field Circles and Magnetic Flux Density Lines about a Linear Magnet

larger in radius as they fall more to one side or the other of the busbar line. Lines of magnetic flux must cross the equipotential lines normally. The magnetic flux lines are also circles whose centers may be found as follows. First, draw a radial vector from the center of the equipotential circle to any point, P, on its circumference. Then a line drawn tangent to the circle at P (and perpendicular to the radial vector) will intersect the extension of the busbar line at the center of the magnetic-flux-line circle. From this geometrical information, the direction aspects of the magnetic flux may be developed.

6.3.1 P On or Off the Minibusbar Line

Now consider the busbar pair labeled 11-11 in Figure T6.4 and a point of interest, P, at the mid-point between the minibusbar pair 31-31. Equations 6 and 7 developed in Section 1.4.2, The Finite Linear Magnet, for the general case of P locations are used to calculate contributions of the minibusbar pairs to the axial magnetic flux at P, the point of interest, and then to sum the contributions for the total axial magnetic flux.

Equations for the 25 minibusbar contributions were incorporated into the MAGFLDDT.TK computer program, Appendix D. Equations for one of the five vertical minibusbar pairs as a group in which the distance from the busbar to point of interest were related as fractions of the overall busbar height, eta. Within this column, the busbar line width, w, was constant but was written as wo + 2*(nf+1/2)*eta/5 where eta is the length of one side of the overall square busbar cross-section, wo is the busbar line width (center-to-center) of the innermost minibusbar pairs, and nf is the column number (i.e., 0-4). Thus there are five sets of indexed equations, one for each of five busbar pairs in a column.

It was then necessary to generate four more sets of the column sets properly indexed, so there is one column set for each of the five columns, and 5 minibusbars per column (layer). The effects of finite busbars were then evaluated below.

6.2.2 Comparison Between Point and Finite Busbar Calculations

A comparison of the flux calculated assuming point conductors with busbars of significant dimensions was conducted similar to the one done for the Helmholtz coils, as shown in Section 6.3 above. A typical result is shown in Figure T6.6. All of the current in the point conductors was assumed to flow in straight, parallel counter-current

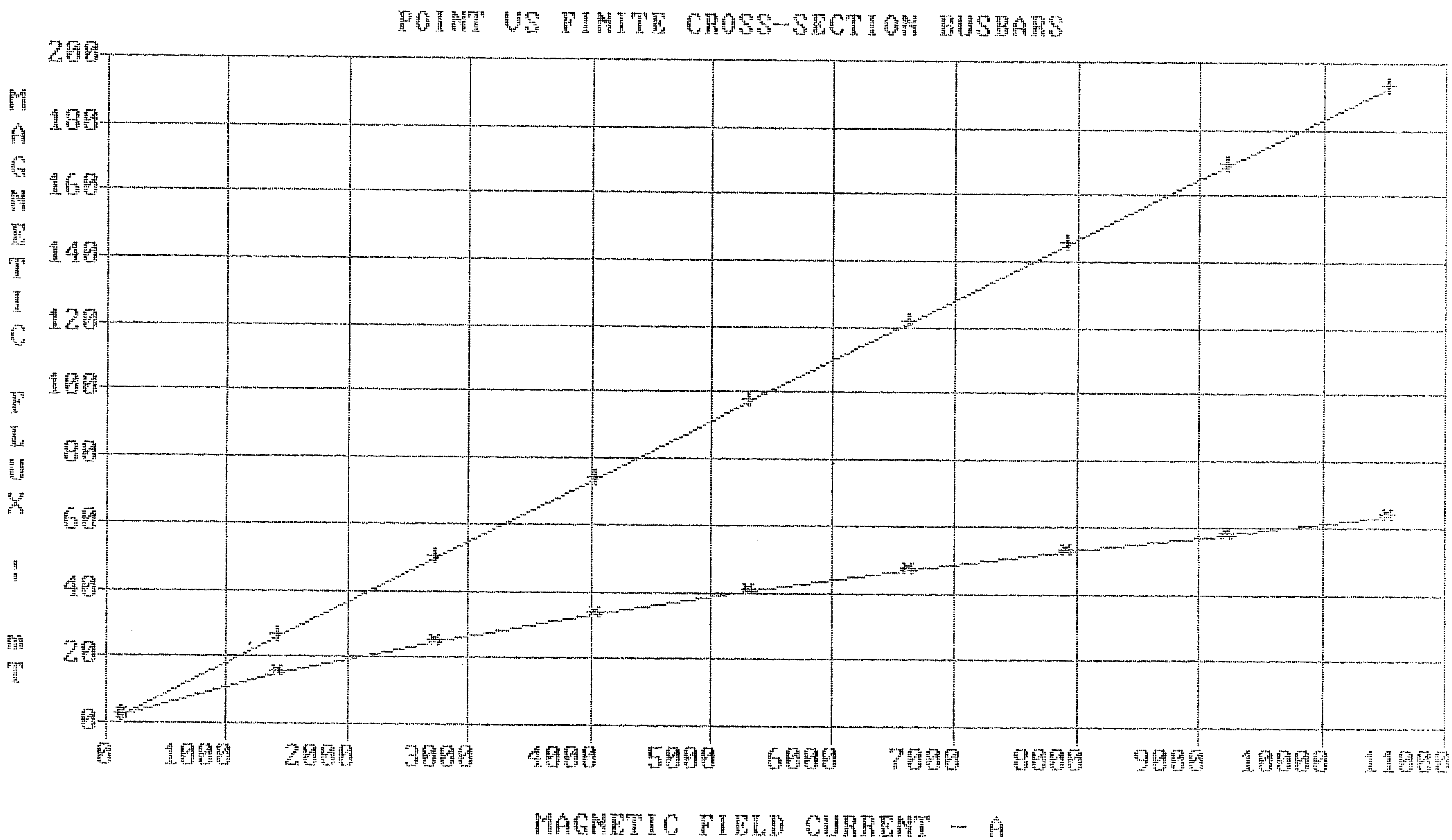

Figure T6.6. B of LM by Point and Finite Conductor Methods

conductors of negligible cross-section separated by a constant busbar line of 4.2 cm while the current was increased as shown. The calculated flux at the mid-point between the busbars then increases in a straight line, as shown by the upper curve. The lower curve shows the axial magnetic flux density at the same point as calculated by summing the contributions of the twenty-five minibusbars pairs. In the latter calculation the total current, which is the same as that used for the point busbars, was distributed among the minibusbars as described above. The current density of 130 A/cm^2 was used and, as the cross-section was increased, the total current increased. The equations take into account the changing distances and vector relationships as documented above. The lower curve shows the dramatic reduction that can occur as a result of the busbar size. Unfortunately, the lower curve represents the real world and becomes a significant factor in the potential performance of the Coreless Linear Conduction Pump concept.

6.3.3 Average Busbar Line Length Versus Differential Busbar Calculation

Another common method of calculating the magnetic flux is to assume all the current is flowing in point conductors located at the center of the cross-section of finite busbars. The busbar line length is then a mean, or average, value of some kind. The vertical distribution of the current is ignored. Figure T6.7 shows a comparison of the common method with the differential method of MAGFLDDT.TK. As the cross- section area of the busbars increase, the busbar line length in the common method increases as well as in the differential method, as discribed above. In Figure T6.7, the upper curve is axial flux density calculated by the differential method as used in MAGFLDDT.TK, and the lower curve is the result using the common method. At relatively small cross-sections, the difference is not large; but at larger sizes, the difference is not negligible being ~21 % at 81 cm^2 as shown here. Apparently in the Helmholtz coil analytical expression there an effective radius (analagous to half the busbar line length as used here) is used, which is different from the mean radius.

6.3.4 Layer or Column Effectiveness

Another valuable result of the differential analysis using MAGFLDDT.TK is shown in Figure T6.8. The contribution of each of the five columns or layers from the inside pairs to the outside pairs is shown both in terms of the axial magnetic flux density produced and the

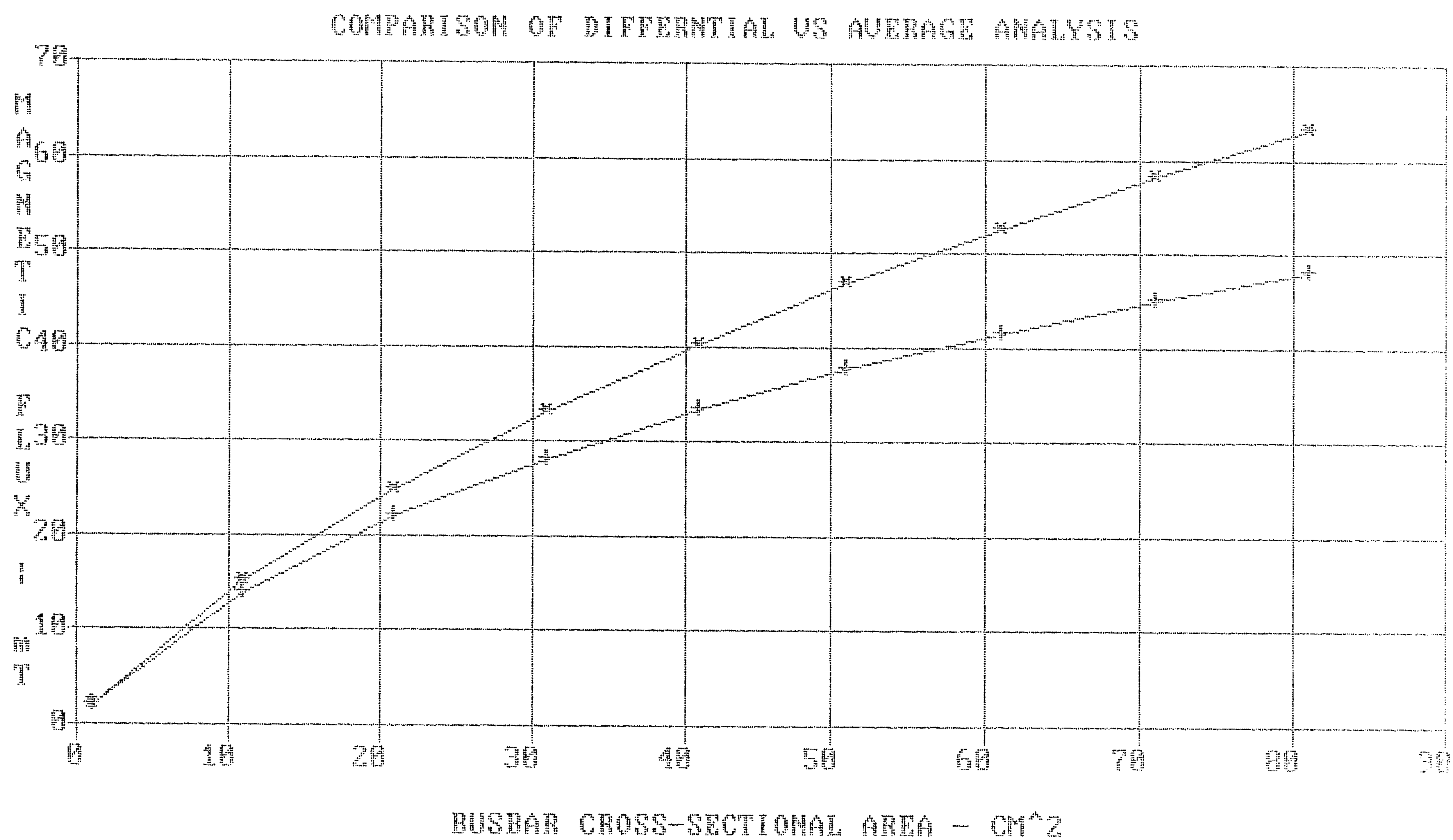

Figure T6.7. B of LM by Average and Differential Methods

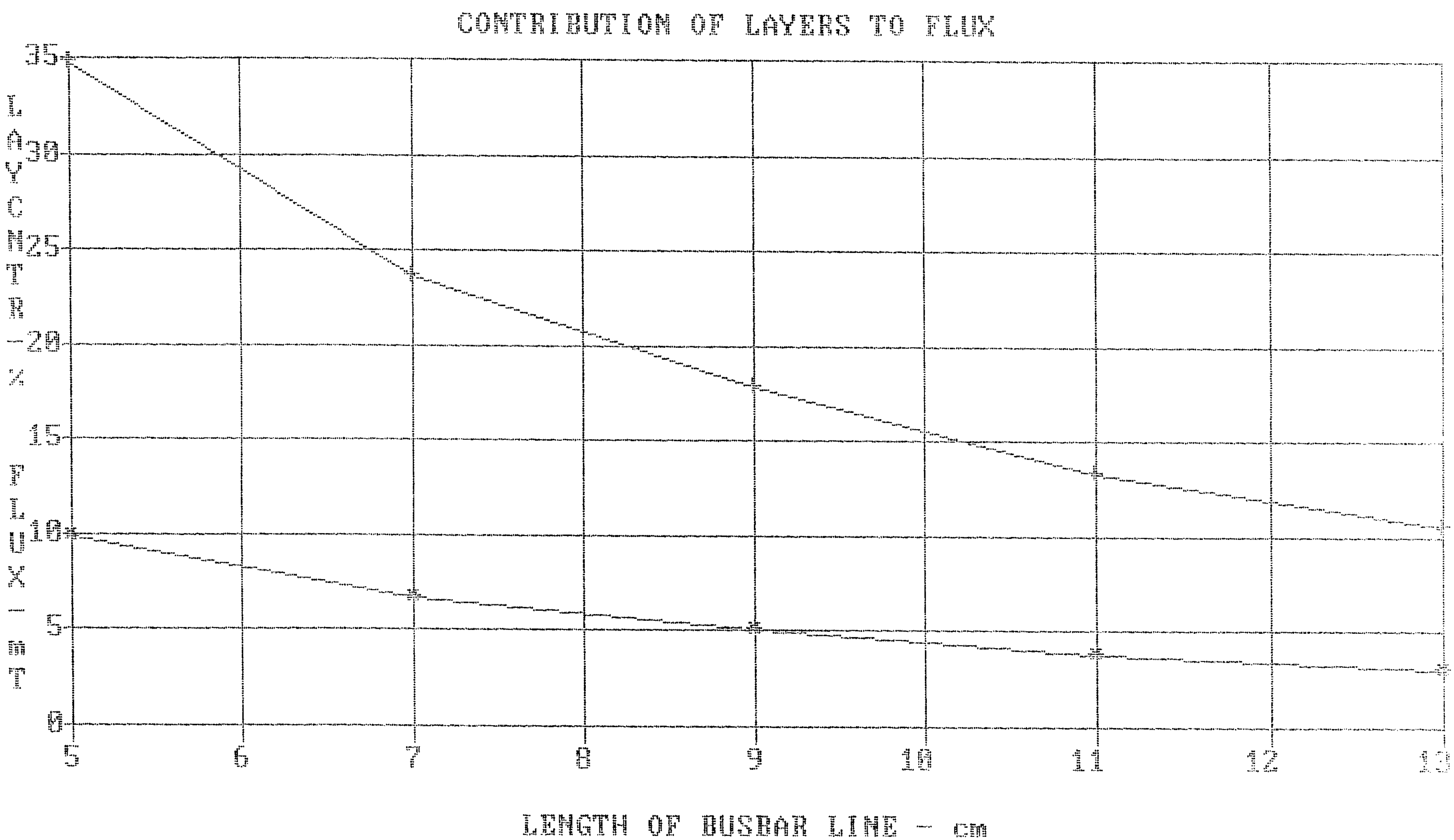

Figure T6.8. Contributions of Minibusbar Columns to B_{AX}

percentage of the flux produced by each column or layer. The upper curve shows the percentage contributed by each layer or column at the points (+) indicating their busbar line lengths. The inner column produces more than three times as much as the outer column. Since each column contains the same amount of material and mass (weight), it will be more efficient to remove the two outer columns and use a rectangular cross-sectional busbar rather than a square, if possible. This is easily accommodated in MAGFLDDT.TK by going to a 3 X 5 matrix by removing the unwanted equations. This is done in the rule sheet of MAGFLDDT.TK by simply "quoting" them out (See Appendix D). This would allow them to simply be reinstated if it was later desired to use the square matrix again.

6.3.5 Effectiveness of Vertical Distribution of Minibusbars

The effectiveness of the vertical distribution or rows of the mini-busbars that make up the overall busbar magnet is shown in Figure T6.4. It was generated by first assuming a point of interest midway between the busbar pairs and at the top busbar pair level. The contribution of each of the busbar levels to the total magnetic flux at the point of interest was then calculated. The point of interest was then shifted down to the second level, and the calculations of all the contributions from the other busbar levels repeated. And so on until five points of interest at all five busbar levels were calculated.

The results are shown in Figure T6.9 and in more detail in Table T6.2. It is seen in Figure T6.9 that the axial magnetic flux varies only slightly over the range. The same result can be seen in Table T6.2 for all the other columns in the matrix. The variation is ~1 % or less.

This result appears to justify the neglect of the vertical portion of the busbar in the common practice approach to calculating the magnetic flux discussed above in Section T6.3.4. However, when the point of interest exceeds the height of the busbars, the vertical distribution of the minibusbars can no longer be ignored.

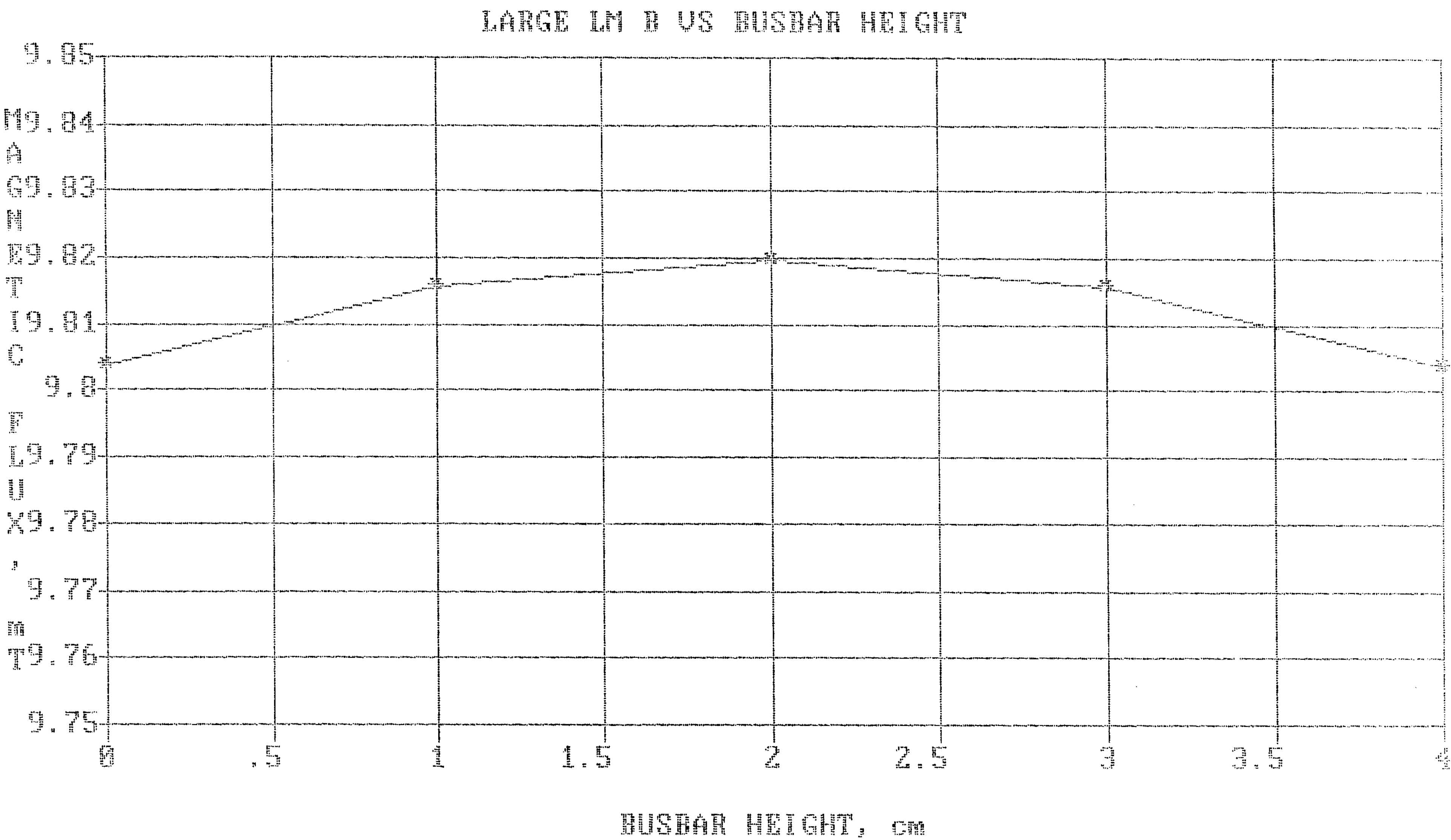

Figure T6.9. Contributions of Minibusbar Rows to B_{AX}

Table T6.2.
Axial Flux of Layers vs Height

NF1	0	1	2	3	4
NF2	1	0	1	2	3
NF3	2	1	0	1	2
NF4	3	2	1	0	1
NF5	4	3	2	1	0
fH11	0	1	2	3	4
fH12	1	0	1	2	3
fH13	2	1	0	1	2
fH14	3	2	1	0	1
fH15	4	3	2	1	0
HFFAX11	1.96548872	1.96470284	1.96234897	1.95843835	1.95298959
HFFAX12	1.96470284	1.96548872	1.96470284	1.96234897	1.95843835
HFFAX13	1.96234897	1.96470284	1.96548872	1.96470284	1.96234897
HFFAX14	1.95843835	1.96234897	1.96470284	1.96548872	1.96470284
HFFAX15	1.95298959	1.95843835	1.96234897	1.96470284	1.96548872
HFFAX1	9.80396847	9.81568173	9.81959235	9.81568173	9.80396847
ETA	5	5	5	5	5
CD	130	130	130	130	130
Wo	4	4	4	4	4

RESULTS

The analysis established that LM-TEMPs and HM-TEMPs (i.e., TEMPs incorporating coreless pumps) are not feasible for NSPS of 64 kWe and larger. Thus, the first major objective was not achieved. The second major objective of building and testing a verification pump, and most of the detailed objectives, depend on the establishment of feasibility and thus became moot. Consequently, Tasks 3 and 4 concern with the test loop modifications and the verification test program were deleted and Task 6 pertaining to the use of ZrB_2 conductors and calculation of magnetic flux produced from large busbar and their effect on feasibility was added. The use of ZrB_2 conductors did result in better performance, but not enough better to make the coreless magnet TEMPs feasible.

The loss of feasibility of the TEMPs results from the large power demand of the coreless magnets which must be supplied by the TEG. There is not enough heat transfer surface in the optimized EMPs to supply the TEG. Heat-fluxes required are too high by two orders of magnitude. The specific power of the TEGs was assumed to be 45 g/We, an optimistic number based on TEGs built for use in space applications. (This is equivalent to a specific weight of 10 We/lb.)

The heat exchanger problems grow worse when the compromises required to match EMP and TEG electrical, thermal, and hydraulic circuits. The EMPs demand even more power; the TEGs get larger and require more heat flow thus moving the TEMPs further away from feasibility.

The normal, or average, busbar analytical method was found to be adequate for this feasibility study, but the "differential method" or something better, would be needed for detailed design and performance. The sizes of the conductors found in the LM magnets were not so large the errors of <20% in the flux were never exceeded.

The LM-TEMPs were found to be better than HM-TEMPs. The LM mass was, itself, also less than the HM mass.

The ZrB_2 conductors produced lower mass in the otpimized LM-TEMPs compared to the HM-TEMPs, but not low enough to make these TEMPs feasible. The electrical resistivity of ZrB_2 used in the analyses was based on state-of-the-art data, which is quite different from handbook values. Still lower resistivity of ZrB_2 is expected to result from ongoing support by SDI in another program[8].

Double-pass, self-compensated LM-TEMPs were found to be about a factor of 4 less massive than single-pass uncompensated LM-TEMPs.

The lack of feasibility of the CLCP-TEMP was sufficient reason to delete the verification pump test work from the tasks defined. However, both the cost and time to conduct the program would have been grossly exceeded because of unforeseen pump construction and instrumentation and power supply problems which developed.

ESTIMATE OF FEASIBILITY

The concept of CLCP is technically feasible, while the TEMPs based on the CLCPs are not feasible.

ESTIMATE OF ECONOMIC FEASIBILITY

The economic feasibility of the CLCP is a moot consideration since the CLCP-based TEMPs are not feasible.

REFERENCES

(1) Campana, R.J., J.C. Bass, N.B. Elsner, and T. Ciarlariello, "Thermoelectromagnetic Pump Development Study", May 1988 (USAF Contract F33615-87-C-2751, WPAFB-ASD), Electro Technology Corporation Report ETC-88-1.

(2) Bleaney, B.I., and B.Bleaney, Electricity and Magnetism, 3rd Ed., Oxford Univ. Press 1976.

(3) Boeker, Henry G., An Approach to Science, McGraw-Hill, New York 1959.

(4) Suydam, Vernon Andrew, Fundamentals of Electricity and Electromagneticism, D. VanNostrand Co., Inc., New York 1940.

(5) Bomelburg, et al., "Physical Properties of Liquid Metals", O.J. Foust (Ed), Na-NaK Engineering Handbook, Vol. 1, Liquid Metal Eng. Center, Gordon Breach Sci. Pub. Inc., New York 1972.

(6) Lyons, R.H., et al., Liquid Metal Handbook, Na-NaK Supplement, USAEC and Dept. of Navy, 3rd Edition (1955).

(7) Metals Handbook, Ninth Edition; Vol. 2, Properties and Selection: Non-Ferrous Alloys and Pure Metals. Am. Soc. for Metals, Pg. 7721 Rare Metals, Fig. 65, Temp. Dependence of Mo from 0-2700°C.

(8) Elsner, N.B., J.H. Norman, C.L. Beckel, and V.M. Kenkre, "Electrical Conductors for 1000-2000 K Operation", APL-AFWAL, WPAFB, Contract F33615-88C-2902, Hi-Z Technology, Inc. Report Hi-Z 4300-88, April 1989.

(9) Dwight, H.B., Electric Coils and Conductors, McGraw-Hill, New York (1945).

APPENDICES

APPENDIX A

HELMHOLTZ MAGNET EMP DESIGN AND ANALYSIS MODEL
HMM2EMP2.TK

L	VLCOP	251.12174	mV	Terminal voltage of parallel coils
	VT	374.22061	mV	Voltage of EMP + HM
L	EEH	8.9928881	%	Electrical to hydraulic efficiency
	POH	174.00631	W	Output power (hydraulic)
	VOLND	388.9114	cm^3	Volume of nozzle and diffuser
	VOLNDI	128.13048	cm^3	Volume of nozzle
	VOLNDO	260.78092	cm^3	Volume of diffuser
	S	306.20446	cm^2	Surface area of nozzle and diffuser
	R2		mm	Equivalent radius of throat area
	SELECTW	1		1=(D-W) & 0=(D-H) EQNS used for LNDs
	LNDI	67.991482	mm	Length of nozzle
	LNDO	138.38144	mm	Length of diffuser
	LND	206.37293	mm	Length of nozzle and of diffuser
1200	TL		K	Temperature of fluid
	TWC	727	C	Temperature of the walls
	MND	.26252216	kg	Mass of nozzles and diffusers
	ML	.50946919	kg	Mass of fluid
	MT	.10897914	kg	Mass of pump throat
	MB	3.7705728	kg	Mass of busbar
L	MASS	35.487131	kg	Total mass of EMP
1	TI		mm	Thickness of therm. & elect insulation
L	MTEG	226.67485	kg	Estimated Mass of TEG
L	EMASS	262.16198	kg	Estimate total TEMP mass
44.5	SPMTEG		g/W	Specific mass of the TEG
	SRATIO	192.7467		
	VAR			EMASS
136.01373	DPTVAR		kg	
	SPMEMP	6.9667072	g/W	Specific mass of EMP as calc. here
				MATERIALS PROPERTIES
295	TRM		K	Room temperature
	TWK	1000	K	Temperaure of wall material
	DENRTW	8.5734271	Mg/m^3	RT density of wall material
	DENW	8.4286	Mg/m^3	Density of wall material
	RHOW	44.292631	uOhm-cm	Resistivity of throat wall material
	RHOL	40.531	uOhm-cm	Resistivity of pumped fluid
	MU	.2729	cp	Viscosity of fluid
	DENL	.4618	Mg/m^3	Density of fluid
	DENRTL	.5272515	Mg/m^3	RT density of fluid
	RHOB	31.99	uOhm-cm	Resistivity of busbar
	DENSB	5.89152	Mg/m^3	Density of busbar
7.3	DENM		Mg/m^3	Density of PM material
	RHOMo	20.138	uOhm-cm	Resistivity of Mo
	DENMo	10.1234	Mg/m^3	Density of Mo
	KMo	1.1157822	W/cm-K	Thermal conductivity of Mo
	DENZrB	5.89152	Mg/m^3	Density of zirconium diboride
	RHOZrB	31.99	uOhm-cm	Resistivity of zirconium diboride
				HM1 HELMHOLTZ MAGNET DESIGN
				06/12/91 1730
	SCO	15.5	cm	Separation magnet coils center lines
	Z		cm	Axial displacement to pt of interest
	Z1	5.65	cm	Z to center of nearest pump cell
	Z2	9.85	cm	Z to center of 2nd pump cell
	RM	8.5	cm	Mean coil radius
	RE	8.7401961	cm	Equivalent radius of coils

		C		-	Separation factor, coils to duct CL
		C1	1.5469374	-	Separation factor, coil 1 to duct CL
		C2	.88732955	-	Separation factor, coil 2 to duct CL
		Hm		Oe	Magnetic field intensity
		HOC1	267.80434	Oe	Magnetic field intensity from coil 1
		HOC2	132.19566	Oe	Magnetic field intensity from coil 2
		HOC	400	Oe	Magnetic field intensity both coils
LG	6289.5481	ICO		A	Coil current
L	40	B		mT	Magnetic flux density
		BT		mT	
L	7	ETA		cm	Radial width of turn cross-section
		SR		cm	Slant radius
	1	MMU		-	Ratio of B/Hm in the coil flux field
		RHOCO	31.99	uOhm-cm	Resistivity of coil material
L		DENCO	5.89152	Mg/m^3	Density of the coil material
		RCO	3.9927E-5	Ohm	Resistance of one coil
		LCO	61.157075	cm	Length of each coil and lead
		ACO	49	cm^2	Cross-sectional area of the coils
		CD	128.35812	A/cm^2	Current density in coils
		RCOP	3.9927E-5	Ohm	Resistance of parallel connected coils
		RCOS		Ohm	Resistance of series connected coils
		PCOS		W	Power input to series coils
		PCOP	3158.8845	W	Power input to parallel coils
		VLCOS		Volt	Terminal voltage of series coils
	2	NCELL		-	Single or Double Pass Pump
		RI	5	cm	Inside coil radius
		RO	12	cm	Outside coil radius
		VCO	2616.9467	cm^3	Volume of coil
L		MCO	30.835587	kg	Mass of the coils
		R1		cm	Slant radius to variable location
		R	0	cm	Variable radius position
		R12			Slant radius opposite from R1
		k		-	Modulus of the elliptical integrals
		X		deg	Angle associated with k
		Y1		-	Ellitical integral of 1st kind
		Y2		-	Ellitical integral of 2nd kind
	0	fR		-	Frational value of RE
		RFL1		-	1ST TERM OF RFLUX
		RFL2			2ND TERM OF RFLUX
		RFLUX			Radial magnetic flux normalized (0,C)
		RFLUX2			Radial magnetic flux normalized (0,C)
		RFLUX3			Radial magnetic flux normalized (0,C)
		RFLUX4			Radial magnetic flux normalized (0,C)
		RFLUX5			Radial magnetic flux normalized (0,C)
		MMB			

```
MMMMMMMMMMMMMMMMMMMM RULE SHEET MMMMMMMMMMMMMMMMMMMMMMMMMMMMMMMMMMMMMMMMMMMMMM
S RuleDDDDDDDDDDDDDDDDDDDDDDDDDDDDDDDDDDDDDDDDDDDDDDDDDDDDDDDDDDDDDDDDDDDDDDDD
  "HELMHOLTZ MAGNET EMP DESIGN   07-01-91 1600

* DPDV=M1*B*IT
* DPMB=M2*B^2*Q
* DPMF=M3*B^2*Q
* DPHY=(DPT+DPNAD)
* TDPDL=DPDV-DPMB-DPMF-DPHY
* CEMF=B*W*Q/AF
* IC=CEMF/(RB+RL)
* IL=IT*RB/(RB+RL)
* AF=W*H
* RL=RHOL*10^-8*W/(H*LT)
* RB=RF*RW/(RF+RW)
* RF=FX*2.6*RHOL*10^-8/H
* RW=RHOW*10^-8*(W+2*TW)/(TW*2*LT)
* QE=15850*Q
* M1=RB/(RB+RL)*1/H
* M2=1/(RB+RL)*1/H^2
* M3=1/(H^2*RF)
* M4=1
* NRE=DENL*V*4*RH/(MU*10^-6)
* RH=W*H/(2*(W+H))
* V=Q/AF
* DPCV=DENL*VMAX^2/2
* f=.043/NRE^.2                              "For 5000<NRE<200000
* HYHD=DENL*V^2/2
* DPT=f*LT/(4*RH)*HYHD
* DPNAD=(CN+(1-E)*(1-AR^2))*HYHD
* AR=4*W*H/(PI()*D^2)
* RTW=RHOW*10^-8*2*TW/(H*LT)
* PIE=VL*IT
* PIT=PIE+PCOP
* BMIN=IT/Q*M1/(2*(M2+M3))
  "B=BMIN
* EEH=POH/PIE*100
* MT=NCELL*2*(H+W)*TW*LT*DENRTW
* ML=NCELL*(H*W*LT+VOLND)*DENRTL
  "ML=2*(H*W*LT+4*VOLND)*DENRTL
* S=PI()*(H^2+W^2)^(1/2)*(LNDI/COS(PI()/12)+LNDO/COS(PI()/24))
  "S=(PI()*D+(W+H))*(LNDI+LNDO)/2
  "S=PI()*(D/2+R2)*(LND^2+(D/2-R2)^2)^(1/2)
* SELECTW=STEP(H,W)
* (1-SELECTW)*LNDI=(D-H)/(2*TAN(PI()/12))*(1-SELECTW)
* (1-SELECTW)*LNDO=(D-H)/(2*TAN(PI()/24))*(1-SELECTW)
* SELECTW*LNDI=(D-W)/(2*TAN(PI()/12))*SELECTW
* SELECTW*LNDO=(D-W)/(2*TAN(PI()/24))*SELECTW
* LND=LNDI+LNDO
  "LND=(D/2-R2)/TAN(PI()/12)
* MND=NCELL*S*TW*DENRTW
  "MND=4*S*TW*DENRTW
* VOLNDI=(PI()*D^2/4+(W*H))*LNDI/2
* VOLNDO=(PI()*D^2/4+(W*H))*LNDO/2
* VOLND=VOLNDI+VOLNDO
  "VOLND=PI()*LND/3*((D/2)^2+D/2*R2+R2^2)
  "R2=(W^2+H^2)^(1/2)/2
```

```
  "MATERIALS PROPERTIES

* TWC=TL-273
* TWK=TL
* DENW=8.6304-1.895E-4*TWK-1.23E-8*TWK^2
* DENRTW=8.6304-1.895E-4*TRM-1.23E-8*TRM^2
* RHOW=16.337+4.224E-2*TWC-4.922E-6*TWC^2-3.941E-10*TWC^3 "For Nb-Zr in uOhm-cm

* RHOL=13.735+2.9256*10^-2*TL-2.46*10^-6*TL^2           "For Li in micro-Ohm-cm
* DENL=.5593-1.133E-4*TL+1.58E-8*TL^2                   "For Li in Mg/m^3
* DENRTL=.5593-1.133E-4*TRM+1.58E-8*TRM^2               "For Li in Mg/m^3
* MU=1.8739-4.667E-3*TL+4.933E-6*TL^2-1.867E-9*TL^3     "For Li in centipoise
* RHOMo=(-0.183+2.0321E-2*TL)                           "For Mo in uOhm-m
  "RHOMo=-3.174+.03171*TL                                "For Mo in uOhm-cm
* DENMo=10.2698-1.056E-4*TL-4.08E-8*TL^2                "For Mo in Mg/m^3
* KMo=(0.3602-1.142E-4*TL+2.050E-8*TL^2)*4.1868         "For Mo in W/cm-K

  "RHOL=36.768-1.6212E-2*TL+7.1741E-5*TL^2             "For NaK in micro-Ohm-cm
  "DENL=.9390-2.426E-4*TL                              "For NaK in Mg/m^3
  "DENRML=.9390-2.426E-4*TRML                          "For NaK in Mg/m^3
  "MU=1.1914-2.7431E-3*TL+2.5463E-6*TL^2-8.492E-10*TL^3    NaK in Mg/m^3

* DENZrB=6.08*.969                             "For ZrB2 in Mg/cm^3
* RHOZrB=-3.71+.0357*TL                        "For ZrB2 in uOhm-cm

  "SINGLE-PASS PUMP SECTION

  "DPDL=DPDLE                             "SP
  "VLL=IT*RB/(RB+RL)*RL                   "SP
  "VLW=IT*RB/(RB+RL)*RTW                  "SP
  "VL=VLL+VLW+CEMF+VBS                    "SP
  "POH=DPDL*Q                             "SP
  "LB=H/2+TI+3/2*TB+W                     "SP
  "MB=(LB-TB/2+H/2)*TB*LT*DENSB           "SP


  "DOUBLE-PASS PUMP SECTION

* DPDL=DPDLE/NCELL                        "DP
* VLL=NCELL*IT*RB/(RB+RL)*RL              "DP
* VLW=NCELL*IT*RB/(RB+RL)*RTW             "DP
* VL=VLL+VLW+VC+VBS                       "DP
* VT=VL+VLCOP
* VC=NCELL*CEMF                           "DP
* POH=NCELL*DPDL*Q                        "DP
  "LB=TB+TI+H                             "DP Backside busbar only
  "AB=LT*TB                               "DP Backside busbar only
* LB=LT/2                  "DP Backside connections to series electromagnet
* AB=2*H*TB                "DP Backside connections to series electromagnet
* RHOB=RHOZrB
* RBS=RHOB*10^-8*LB/AB
* VBS=IT*RBS
* DENSB=DENZrB
* MB=2*LB*AB*DENSB                        "DP
* MASS=MCO+MB+MT+ML+MND
* EMASS=MTEG+MASS
* MTEG=SPMTEG*PIT
* SRATIO=100*EMASS/DPTVAR
```

```
* SPMEMP=MASS/PIT

  "HM1 - HELMHOLTZ MAGNET DESIGN

* RM=(LT+ETA)/2
* R1^2=(RE+R)^2+Z^2
* R12^2=(RE-R)^2+Z^2
* k^2=1-(R12/R1)^2
* X=180/PI()*ASIN(k)
* Y1=RELATE1(X)
* Y2=RELATE2(X)
* Z1=H/2+TI+TW+ETA/2
* Z2=1.5*H+2*TI+3*TW+ETA/2
* RE=RM*(1+ETA^2/(24*RM^2))
* C1=RE/Z1
* C2=RE/Z2
* SCO=Z1+Z2
  "Hm=2*PI()*1000*ICO*RE^2/(10*SR^3)
* HOC1=2*PI()*ICO/10*C1^3/(RE*(C1^2+1)^1.5)*10^-2
* HOC2=2*PI()*ICO/10*C2^3/(RE*(C2^2+1)^1.5)*10^-2
  "SR=(RE^2+Z^2)^0.5
  "B=2*MMU*Hm
* HOC=HOC1+HOC2
* B=MMU*HOC/10^4 "1Oe/4*pi()*10^-3 Oe/(A/m)*4*pi()*10^-7 T-m/A*10^3 mT/T =.1 mT
  "BT=MMU*HOC/10^4  "1Oe/4*pi()*10^-3 Oe/(A/m)*4*pi()*10^-7 T-m/A*10^3 mT/T =.1
* RHOCO=RHOZrB
* RCO=RHOCO*10^-8*LCO/ACO
* RI=LT/2
* RO=RI+ETA
* VCO=PI()*(RO^2-RI^2)*ETA
* DENCO=DENZrB
* MCO=NCELL*VCO*DENCO
* ACO=ETA^2
* CD=ICO/ACO
  "RCOS=2*RCO
* RCOP=RCO
  "VLCOS=1000*ICO*RCOS
* VLCOP=ICO*RCOP
* PCOS=ICO^2*RCOS
* PCOP=2*ICO^2*RCOP
  "MCO=ACO*LCO*2*DENCO
* LCO=2*PI()*RM+SCO/2
  "Z=RE/C
* R=fR*RE
  "S=2*Z
* RFL1=(C^2+1)^1.5/(PI()*C^2*(C^2*(1+fR)^2+1)^.5)
* RFL2=2*C^2*(1-fR)*Y2/(C^2*(1-fR)^2+1)+Y1-Y2
  "RFLUX=RFL1*RFL2
  "RFLUX2=RFL1*RFL2
  "RFLUX3=RFL1*RFL2
  "RFLUX4=RFL1*RFL2
* RFLUX5=RFL1*RFL2
```

APPENDIX B

HELMHOLTZ MAGNET TEG
HMM2TEG2.TK

MMMMMMMMMMMMMMMMMMMMM VARIABLE SHEET MMMMMMMMMMMMMMMMMMMMMMMMMMMMMMMMMMMMMMMMMMMMMM

St	InputDDDD	NameDDD	OutputDDD	UnitDDDDD	CommentDDDDDDDDDDDDDDDDDDDDDDDDDDDDDD
					HMM2TEG2 - THERMOELECTRIC GEN. DESIGN
					SI-GE + GAP MATERIALS 26kB
					5/13/88 2140
					Tcc-72,L-81, DT1-175
					HEAT EXCHANGER DESIGN
		HR	15.945295	kW	Heat transport rate by fluid
		m	2.8009404	kg/s	Fluid mass flowrate
		DELTAT1	1.4158034	K	Temperature drop inlet to oulet
		V	6.6958047	m/s	Velocity of fluid flow
		NRE	361831	-	Reynolds number
		DH	30.615945	mm	Hydraulic diameter
	942.25393	AF		mm^2	Cross-sectional area in flow stream
		PER	123.1063	mm	Perimeter of flow duct
	28.553149	H		mm	Height of flow duct
		W	33	mm	Width of flow duct
	230	LT		mm	Duct length
		HYHD	9951.9616	Pa	Hydraulic head
		FF	.00355678	-	Friction factor
		Q	6.3091483	Litre/s	Volumetric flowrate
	100	QE		gpm	Volumetric flowrate
		QHX	15.945295	kW	Heat transfer rate fluid to wall
		HX	6.2589593	W/cm^2-K	Heat transfer coefficient
		AFHX	131.34449	cm^2	Heat transfer area
		PEN	5948.7223	-	Peclet number
		NUN	31.150438	-	Nusselt number
		PRN	.01644061	-	Prandlt number
		WDELTAT	8.6714692	K	Temperature drop across duct wall
		TWI	1208.6715	K	Temperature of inside of wall
		TWO	1200	K	Temperature of outside of wall
		HFLX	121.40057	W/cm^2	Heat flux through wall
		FDELTAT	19.396287	K	Temperature drop across fluid film
	.5	tDW		mm	Thickness of duct wall
	.7	CONDW		W/cm-K	Thermal conductivity of wall material
					MATERIALS PROPERTIES
		DTLQ	29.483559	K	Temperature of fluid
	1228.6	TFL		K	Temperature of fluid
		COND	.61515654	W/cm-K	Thermal conductivity of fluid
		MU	.25152306	cp	Viscosity of fluid
		DENL	.44394906	Mg/m^3	Density of fluid
		Cp	.96056449	cal/g-K	Heat capacity of fluid
		RHOMo	11.581969	uOhm-cm	Resistivity of Mo
		DENMo	10.194986	Mg/m^3	Density of Mo
		CONDMo	1.2602791	W/cm-K	Thermal conductivity of Mo
					THERMOELECTRIC CONVERTER DESIGN
	5.67E-12	SIG		W/cm^2-K^	Boltzmann constant
	256	Te		K	Effective temperature near Earth
	.00053045	S		V/K	Couple Seebeck Coef.
	.05799219	K		W/cm-K	Couple thermal conductivity
	.00529696	RHO		Ohm-cm	Couple resistivity

	RHOcc	1.1582E-5	Ohm-cm	Resistivity of cold "
0	Rhc		Ohm	Resistance of hot connector
	Rcc	6.1146E-5	Ohm	Resistance of cold connector
	Qte	19.398138	W	Thermoelectric source heat rate
	Qbp	1.3656913	W	Bypass heat in leg insulation
	Qs	20.763829	W	Couple Source Heat Rate
	Qrj	19.080411	W	Couple reject heat rate
	Qst	15945.295	W	Total input heat
	Qr	14652.538	W	Heat to be rejected by radiator
0	Ts		K	Heat Source Temperature
0	Thc		K	Temperature of hot connector
1200	Th		K	Hot Junction Temperature
	Tm	922.5	K	Mean temperature across couples
645	Tc		K	Cold junction temperature
L	Tcc	578.95621	K	Temperature of cold connector
	Tci		K	Temperature " " insulator
0	Tcp		K	Temperature " compression pad
	Thp	557.53268	K	Temperature of heat pipe
	ET	.08741286		Theoretical conversion efficiency
	EA	.08136901		Actual " "
	Mo	1.3583095		Max. Efficiency load matching factor
	IG	23.567306	A/cm	Current gradient
10	I		A	Electric current in Thermoelements
.15017817	L		cm	TE element length
	A	.06372309	cm^2	TE " cross-sectional area
1	NS			No. of series-connected couples
L	NP	767.93618		No. of parallel circuits
	NT	767.93618		Total number of couples
	Vc	.16956467	V	Couple load voltage
	Vcc	.00061146	V	Cold connector deltaV
L	VL	.16956467	V	Generator or module terminal voltage
	P	1.6895322	W	Couple output power
L	PO	1297.4529	W	Module output power
	Act	131.34449	cm^2	Total area covered by thermocouples
1	AR			Area ratio heat source/thermocouples
0	Khi		W/cm-K	Conductivity of hot insulator
0	Khc		W/cm-K	Conductivity of hot connector
.0035	Kli		W/cm-K	Conductivity of leg insulator
	Kcc	1.2602791	W/cm-K	Conductivity " cold connector
0	Kci		W/cm-K	Conductivity of cold insulator
0	Kcp		W/cm-K	Conductivity " compression pad
0	Khpj		W/cm-K	Conductivity of heat pipe joint
.7	Khp		W/cm-K	Conductivity " " " wall
	Ac	.17103568	cm^2	Area of couple for heat conduction
	Ahc	.13754356	cm^2	Hot connector heat conduction area
	Aj		cm^2	" " joint area
0	Lhi		cm	Thickness of hot insulator
.6	b		cm	Thickness of hot and connector
	Lcc	.72855315	cm	Length of cold connector or busbar
.02	Lli		cm	Thickness of leg insulator
0	Lci		cm	Thickness " cold insulator
0	Lcp		cm	Length of compression pad
.1	tI		cm	Thickness of insulation between ducts
0	Lj		cm	Thickness of joint
0	Lhpw		cm	Thickness of heat pipe wall
.3	F			Factor of 1D/2D correction
.1	Fbp			Bypass heat allowance factor
	ME	.05585247	kg	Mass of thermoelements

	MC	.50522957	kg	" " cold connector - radiator blk
	MHLC		g	Not applicable
	MLI	.01256764	kg	" " leg insulation
	MR	57.929759	kg	Mass of radiator
	MCB	.39258017	kg	Mass of clamping blocks
L	TM	58.895989	kg	Total Mass of TEG
	SPPO	45.393548	g/W	Specific Power
3.8	DE		g/cm^3	Density of thermoelements
	DC	10.194986	g/cm^3	" " connectors
4	DI		g/cm^3	" " hot/cold side insulators
2.5	DLI		g/cm^3	" " leg insulation
2.7	DCB		Mg/m^3	" " clamping block
	dCB	1.2	cm	Thickness of clamping block
	Acb	131.34449	cm^2	Area of clamping block
	RG	1.6256E-5	Ohm	Resistance of the module
	IM	7679.3618	A	Total module current
	VOC	.29439975	Volt	Open circuit voltage
	WM	1332.9178	W	Power dissipated in module
	VLP	.57596744		Fraction of VOC disssipated in module
	WP	2.4758E-5		Fraction of power disssipated in module
	IP	.00130219		
	EAP			

WASTE-HEAT RADIATOR DESIGN
RECTANGULAR RADIATOR FIN DESIGN

	dL	2.6	cm	Differiential slab length
	f1	.2	-	fractional length of slab 1
	f2	.4	-	fractional length of slab 2
	f3	.6	-	fractional length of slab 3
	f4	.8	-	fractional length of slab 4
	f5	1	-	fractional length of slab 5
	L1	2.6	cm	Length of slab 1
	L2	5.2	cm	Length of slab 2
	L3	7.8	cm	Length of slab 3
	L4	10.4	cm	Length of slab 4
	L5	13	cm	Length of slab 5
	Q1	3228.5254	W	Heat entering slab 1
	Q2	2377.0369	W	Heat entering slab 2
	Q3	1631.9696	W	Heat entering slab 3
	Q4	996.75833	W	Heat entering slab 4
	Q5	461.21832	W	Heat entering slab 5
	Qr1	851.4885	W	Heat radiated from slab 1
	Qr2	745.06729	W	Heat radiated from slab 2
	Qr3	635.21124	W	Heat radiated from slab 3
	Qr4	535.54001	W	Heat radiated from slab 4
	Qr5	461.21832	W	Heat radiated from slab 5
.9	e1		-	emissivity of radiator surface
	Ar1	2152.4425	cm^2	Radiation area of slab 1
	Ar2	2152.4425	cm^2	Radiation area of slab 2
	Ar3	2152.4425	cm^2	Radiation area of slab 3
	Ar4	2152.4425	cm^2	Radiation area of slab 4
	Ar5	2152.4425	cm^2	Radiation area of slab 5
	Tf	557.35534	K	Root temperature of fin
	T1	534.82298	K	Mean temperature of slab 1
	T2	518.23328	K	Mean temperature of slab 2
	T3	499.25034	K	Mean temperature of slab 3
	T4	479.92665	K	Mean temperature of slab 4

L

	T5	463.83209	K	Mean temperature of slab 5
	DT1	45.064734	K	Temperature drop across slab 1
	DT2	33.1794	K	Temperature drop across slab 2
	DT3	37.965875	K	Temperature drop across slab 3
	DT4	38.647373	K	Temperature drop across slab 4
	DT5	32.189125	K	Temperature drop across slab 5
1.5	Kf		W/cm-K	Thermal conductivity of fin material
	Wf	827.86252	cm	Width of fin
13	Lf		cm	Lenght of fin
.3	tf		mm	Unit thickness of fin
2.7	DR		g/cm^3	Density of fin material
13	N1		-	No. of unit layers in slab 1
5	N2		-	No. of unit layers in slab 2
3	N3		-	No. of unit layers in slab 3
1.8	N4		-	No. of unit layers in slab 4
1	N5		-	No. of unit layers in slab 5
	FEFF	6.3755991	-	Fin effectiveness
	CT	3228.5254	W	Radiated heat from slabs
	RT	5063.8776	W	Radiated heat at fin root temperature
	MF	18.83225	kg	Mass of fins
	Nf	2.2692308	-	No. of fins in radiator
				HEAT PIPE MASS
	SHP	2622.3354	cm^2	Surface area of heat pipe surface
1	DHP		cm	Inner diameter of heat pipes
	LHP	834.71527	cm	Length of pipe
	HPLDR	834.71527	-	Heat pipe length/diameter ratio
	MP	1.1151601	kg	Mass of pipe wall
	MW	15.602895	kg	Mass of pipe wick
	MFL	.5113554	kg	Mass of fluid
	MHP	17.229411	kg	Mass of heat pipes
	MHPT	39.09751	kg	Total mass of heat pipes
.5	tP		mm	Thickness of pipe wall
8.5	DENP		g/cm^3	Density of pipe wall
	LE	6.8527559	cm	Length of evaporator section
1	tW		mm	Thickness of wick
8.5	DENW		g/cm^3	Density of wick material
	AE	48.853288	cm^2	Heat pipe evaporator area
	AC	5901.8308	cm^2	Heat pipe condenser area
.3	fV		-	Excess volume factor
.5	DENHPL		g/cm^3	Density of heat pipe fluid
.3	fPOR		-	Porosity factor of wick
	HPEVFX	299.92942	W/cm^2	Evaporator wall heat flux

```
MMMMMMMMMMMMMMMMMMMMMM RULE SHEET MMMMMMMMMMMMMMMMMMMMMMMMMMMMMMMMMMMMMMMMMMMMMMMM
S RuleDDDDDDDDDDDDDDDDDDDDDDDDDDDDDDDDDDDDDDDDDDDDDDDDDDDDDDDDDDDDDDDDDDDDDDDD
  "THERMOELECTROMAGNETIC PUMP TEG DESIGN              2/22/88   1415
                                                     "Revised 5/17/88
  "HEAT EXCHANGER DESIGN

* HR=m*1000*Cp*4.186*DELTAT1
* m=DENL*AF*V*1000
* NRE=DENL*V*DH/MU*1000000
* DH=4*AF/PER
* AF=W*H
* PER=2*(W+H)
* HYHD=DENL*1000*V^2/2
* FF=.046/NRE^.2                        "For 5000<NRE<200000
* Q=AF*V*1000
* QE=15.85*Q
* QHX=HX*AFHX*FDELTAT
* HX=NUN*COND/DH*100
* PEN=PRN*NRE
* NUN=5+.025*PEN^.8
  "NUN=.023*NRE^0.8*PRN^0.4
* PRN=Cp*4.186*MU/(100*COND)
* HR=QHX
* HFLX=QHX/AFHX
* AFHX=2*LT*H
* WDELTAT=HFLX*tDW/(CONDW*100)
* WDELTAT=TWI-TWO
* HR=Qst
* DTLQ=WDELTAT+FDELTAT+DELTAT1

  "MATERIALS PROPERTIES

* MU=.00142*100*EXP(702.4/TFL)                             "For Li in cp
* COND=.2725+2.789E-4*TFL                                  "For Li in W/cm-K
* DENL=.5593-1.133E-4*TFL+1.58E-8*TFL^2                    "For Li in Mg/m^3
* Cp=1.1816-4.429E-4*TFL+3.035E-7*TFL^2-7.28E-11*TFL^3     "For Li in cal/g-K
* RHOMo=-0.183+2.0321E-2*Tcc                               "For Mo in Mg/m^3
* DENMo=10.2698-1.056E-4*Tcc-4.08E-8*Tcc^2                 "For Mo in Mg/m^3
* CONDMo=(0.3602-1.141E-4*Tcc+2.05E-8*Tcc^2)*4.1868        "For Mo in W/cm-K

  "TEG MODULE DESIGN
* Th=TWO
  "Qs=Khi*Ac*(Ts-Thc)/Lhi
  "Qs=Khc*Ahc*(Thc-Th)/b
* Ac=2*(A+4*Lli*(A^(1/2)+Lli))
* Ahc=2*A+A^(1/2)*2*Lli
* ET=(Th-Tc)/Th*(Mo-1)/(Mo+Tc/Th)
* Z=S^2/(RHO*K)
* Mo=(1+Z*Tm)^(1/2)
* Tm=(Th+Tc)/2
* Qte=S*Th*I+K*(Th-Tc)/(L/A)-I^2*RHO*(L/A)/2-I^2*Rhc
* Qs=Qte+Qbp
* EA=P/Qs
* Rhc=F*RHOhc*(2*A^(1/2)+Lli+b)/(A^(1/2)*b)
* Qbp=Fbp*K*A*(Th-Tc)/L
* IG=I*L/A
* IG=S*(Th-Tc)/(RHO*(Mo+1))
* Vc=S*(Th-Tc)*(Mo/(1+Mo))
```

```
* P=(S*(Th-Tc)/(1+Mo))^2*Mo/(RHO*L/A)-I^2*Rcc
* Qrj=Qs*(1-EA)+I^2*Rcc
* RHOcc=RHOMo*10^-6
* Rcc=RHOcc*Lcc/(LT*b)
* Lcc=b+tI+H
  "Rcc=F*RHOcc*(2*A^(1/2)+Lli+b)/(A^(1/2)*b)
* Vcc=I*Rcc
  "Rcc=Rhc/RHOhc*RHOcc
* Kcc=CONDMo
* Qrj=Kcc*Ahc*(Tc-Tcc)/b
* Qr=Qrj*NT
  "Qrj=Kcp*Ahc*(Tci-Tcp)/Lcp
* Qr=Khp*AE*(Tcc-Thp)/tP
* Qr=Khp*AC*(Thp-Tf)/tP
  "Qr=Khp*Ahp*(Thp-Tf)/Lhpw
* VL=NS*Vc
* NT=PO/P
* NP=NT/NS
* Qst=Qs*NT
* Act=Ac*NT
* AR=Act/AFHX/10000
* RG=NS*RHO*L/A/NP
* IM=NS*S*(Th-Tc)/(RG*(1+Mo))
* VOC=NS*S*(Th-Tc)
* WM=(VOC/2)^2/RG
* VLP=VL/VOC
* WP=W/WM
* IP=I/IM
                              "MASSES
* ME=(DE*(2*A*L)/1000)*NT                                "TE Elements
  "MC=NT*DC*2*(2*A^(1/2)+Lli)*(A^(1/2)*b)                "Connectors
* DC=DENMo
  "MC=NT*DC*(2*A^(1/2)+Lli+tI)*(A^(1/2)*b)/1000"Pump connector - radiator blk
* MC=(2*H+3*tI+4*tDW)*b*LT*DC
* MLI=(2*DLI*L*(4*Lli*(A^(1/2)+Lli)))*NT/1000          "Leg Insulation
* MCB=DCB/10^3*(Acb*dCB*10^4-Nf*PI()*DHP^2/4*LE)                "Clamping Blocks
* dCB=1.2*DHP
* Acb=2*H*LT*AR
  "TM=NT*(ME+MC+MHCI+MLI+MCB)+MR+MRHP                  "Total Mass of TEG
* TM=ME+MC+MLI+MR+MCB                                     "Total Mass of TEG
* SPPO=TM/PO

  "WASTE HEAT RADIATOR DESIGN
  "RECTANGULAR RADIATOR FIN DESIGN

* Nf=2*(LT*10^2+Lf/2)/(2*Lf)
* HPEVFX=Qr/AE
* HPLDR=LHP/DHP
* LE=(2*H*10^2*AR)*1.2

* dL=Lf/5
* f1=L1/Lf
* f2=L2/Lf
* f3=L3/Lf
* f4=L4/Lf
* f5=1
* L1=dL
* L2=2*dL
```

```
* L3=3*dL
* L4=4*dL
* L5=Lf
* Q1=Qr1+Q2
* Q2=Qr2+Q3
* Q3=Qr3+Q4
* Q4=Qr4+Q5
* Q5=Qr5
* Qr1=SIG*e1*Ar1*(T1^4-Te^4)
* Qr2=SIG*e1*Ar2*(T2^4-Te^4)
* Qr3=SIG*e1*Ar3*(T3^4-Te^4)
* Qr4=SIG*e1*Ar4*(T4^4-Te^4)
* Qr5=SIG*e1*Ar5*(T5^4-Te^4)
* Ar1=Wf*dL
* Ar2=Wf*dL
* Ar3=Wf*dL
* Ar4=Wf*dL
* Ar5=Wf*dL
* T1=(2*Tf-DT1)/2
* T2=(2*T1-DT2)/2
* T3=(2*T2-DT3)/2
* T4=(2*T3-DT4)/2
* T5=(2*T4-DT5)/2
* DT1=Q1*dL/(Kf*Wf*N2*tf)
* DT2=Q2*dL/(Kf*Wf*N2*tf)
* DT3=Q3*dL/(Kf*Wf*N3*tf)
* DT4=Q4*dL/(Kf*Wf*N4*tf)
* DT5=Q5*dL/(Kf*Wf*N5*tf)
* FEFF=10*CT/RT
* CT=Qr1+Qr2+Qr3+Qr4+Qr5
* RT=SIG*e1*Wf*Lf*(Tf^4-Te^4)
* MF=Wf*dL*tf*(N1+N2+N3+N4+N5)*DR*2*Nf/1000
* Nf=Qr/(2*Q1)
* MR=MF+MHPT

  "HEAT PIPE MASS

* SHP=PI()*DHP*LHP
* MHPT=MHP*Nf/1000
* MHP=MP+MW+MFL
* MP=(SHP+PI()*DHP^2/2)*tP*DENP
* LHP=Wf+LE
* MW=SHP*tW*(1-fPOR)*DENW
* MFL=SHP*tW*DENHPL*fPOR*(1+fV)
* AE=PI()*DHP*LE*Nf
* AC=PI()*DHP*Wf*Nf
```

MMMMMMMMMMMMMMMMMMMMM UNIT SHEET MMMMMMMMMMMMMMMMMMMMMMMMMMMMMMMMMMMMMMMMMMMMMMMMM

FromDDDDD	ToDDDDDDD	Multiply ByDD	Add OffsetDDD
m	mm	1000	
m^3/s	Litre/s	1000	
m^2	mm^2	1000000	
kW	W	1000	
Mg/s	kg/s	1000	
N	kg-m/s^2		
cp	Pa-s	.001	
cal/g-K	W-s/g-K	4.186	
W/cm^2-K	W/m^2-K	10000	
W/cm^2	W/m^2	10000	
kg	g	1000	
cm	mm	10	
m^2	mm^2	1000000	
m^2	cm^2	10000	
Mg	kg	1000	
hg	kg	10	
V	dV	10	
kg/W	g/W	1000	

APPENDIX C

LINEAR MAGNET EMP
LMM2EMP.TK

MMMMMMMMMMMMMMMMMMMMM VARIABLE SHEET MMMMMMMMMMMMMMMMMMMMMMMMMMMMMMMMMMMMMMMMMMMMMMMM

St	InputDDDD	NameDDD	OutputDDD	UnitDDDDD	CommentDDDDDDDDDDDDDDDDDDDDDDDDDDDDDDDD
					FILE: LMM2EMP2.TK - 34.5 kB
					CORELESS LINEAR CONDUCTION PUMP
					DESIGN AND PERFORMANCE PROGRAM
					07-24-91
L	4	DPDLE		psi	Delivered pressure from cell
L	100	QE		gpm	Volumetric flowrate
		DPDL	13.79	kPa	Delivered pressure from cell
		TDPDL		kPa	Trial DPDL
		Q	6.3091483	litre/s	Volumetric flowrate
		DPDV	16.883366	kPa	Differential pressure rise developed
		DPMB	.26159966	kPa	Pressure loss from magnetic braking
		DPMF	.13640714	kPa	Pressure loss from magnetic fringe
		DPHY	2.6953594	kPa	Pressure loss from fluid friction
		DPT	.43080041	Pa	Pressure loss in throat flow
		DPNAD	2.264559	Pa	Pressure loss in nozzle and diffuser
L	24	B		mT	Magnetic flux noraml to Q and I
		BMIN	509.03751	mT	Optimum magnetic flux
LG	15.324931	IT		kA	Total pump current
		IL	14.144309	kA	Electric current in fluid
L		H	20.106383	mm	Inside height of throat duct
L	47	W		mm	Inside width of throat duct
L	400	LT		mm	Length of throat
		V	6.6763474	m/s	Velocity of liquid in throat
		VMAX	6.6958047	m/s	Velocity limited by cavitation
		M1	45.903868	1/m	First term coefficient
		M2	71985324	1/Ohm-m^2	Second term coefficient
		M3	37535646	1/Ohm-m^2	Third term coefficient
		M4	1	-	Fourth term coefficient
L	945	AF		mm^2	Throat cross-sectional flow area
		IC	.21915929	kA	Counter current from CEMF
		RB	3.1715E-5	Ohm	Electrical resistance bypassing fluid
		RL	2.6473E-6	Ohm	Electrical resistance across W
		RF	.0000659	Ohm	Resistance of fringe path
L	1.125	FX		_	Empirical factor from MSA calcs
	.5	TW		mm	Thickness of throat walls
		NRE	556074.9	-	Reynolds Number in the throat
		RH	7.041059	mm	Hydraulic radius in the throat
	10000	DPCV		Pa	Pressure margin for cavitation limit
		f	.003051	-	Fluid friction factor in throat
		HYHD	9941.9664	Pa	Hydraulic velocity head in throat
	.05	CN		-	Discharge coefficient of nozzles
	.8	E		-	Diffuser recovery coefficient
	.33333333	AR		-	Area ratio throat to pipe
		D	60.080231	mm	Diameter of circuit piping
		RTW	6.335E-8	Ohm	Resistance of throat wall at busbar
		RW	.00006114	Ohm	Resistance of throat walls
L		PIE	2261.4391	W	Input power to EMP (electrical)
		VC	15.06184	mVolt	Counter EMF of fluid moving across B
		CEMF	7.5309198	mVolt	Counter EMF of fluid moving across B
		VLL	74.887951	mVolt	Voltage drop across liquid
		VBS	55.824138	mVolt	Voltage drop across busbar
		VLW	1.7920963	mVolt	Voltage drop across wall
L		VL	147.56602	mVolt	Load voltage of TEG and EMP
L		EEH	7.6944946	%	Electrical to hydraulic efficiency
L		POH	174.00631	W	Output power (hydraulic)

	VOLND	427911.07	mm^3	Volume of nozzle and diffuser
	VOLNDI	.00014098	mm^3	Volume of nozzle
	VOLNDO	.00028693	mm^3	Volume of diffuser
	S	36993.776	mm^2	Surface area of nozzle and diffuser
	LNDI	.07459222	mm	Length of nozzle
	LNDO	.15181576	mm	Length of diffuser
	LND	226.40797	mm	Length of nozzle and of diffuser
	DENRML		Mg/m^3	Density of liquid at room temperature
295	TRML		K	Room Temperature of Liquid
	LB	2.5606383	cm	Length of armature busbars
5	TB		mm	Thickness of connecting busbars
	RBS	3.6427E-6	Ohm	Resistance of armature busbar
.5	TI		mm	Thickness of electrical insulation
1200	TL		K	Temperature of fluid
	TWC	927	C	Temperature of the walls
	MND	.15858172	kg	Mass of nozzles and diffusers
	ML	.42491782	kg	Mass of fluid
	MT	.23013267	kg	Mass of pump throat
	MB	.88162774	kg	Mass of connecting busbars
L	MASS	21.277136	kg	Total mass of EMP

MATERIALS PROPERTIES

295	TRM		K	Room temperature
	TWK	1200	K	Temperaure of wall material
	DENRTW	8.5734271	Mg/m^3	RT density of wall material
	DENW	8.385288	Mg/m^3	Density of wall material
	RHOW	50.949923	uOhm-cm	Resistivity of throat wall material
	RHOL	45.2998	uOhm-cm	Resistivity of fluid
	MU	.150844	cp	Viscosity of fluid
	DENL	.446092	Mg/m^3	Density of fluid
	DENRTL	.5272515	Mg/m^3	RT density of fluid
	RHOB	28.451506	uOhm-cm	Resistivity of busbar
	DENSB	10.084328	Mg/m^3	Density of busbar

MAGNETIC FIELD CALCULATIONS 7-22-91

	I	1899.052	A	Field Current
.5	fW		-	Fraction of WFB
	WFB	10.6	cm	Center-center span between field buses
	fL1	.22222222	-	Fractional location of L1
	fL2	.77777778	-	Fractional location of L2
	L1	16	cm	Inlet end of Field busbars
	L2	56	cm	Discharge end of Field busbars
.5	fX		-	Fraction of total pump length
72	X		cm	Total pump length
	UP	0	-	Upstream region indicator
	PUMP	1	-	Pumping section region indicator
	DOWN	0	-	Downstream region indicator
	PHI1	1.3117506	rad	Angular integration limit
	PHI2	1.3117506		Angular integration limit
	PHI3	1.3117506		Angular integration limit
	PHI4	1.3117506		Angular integration limit
	HF1	.96663486		Integrated flux fraction
	HF2	.96663486		Integrated flux fraction
	HF3	.96663486		Integrated flux fraction
	HF4	.96663486		Integrated flux fraction

		R1	5.6956024	cm	Radial distance - busbar 1 to P
		R2	5.6956024	cm	Radial distance - busbar 2 to P
		HFPR1	1.9332697		Total integrated fractions, bar 1
		HFPR2	1.9332697		Total integrated fractions, bar 2
		HFP1	3.3352055	mT	Magnetic Flux from bar 1
		HFP2	3.3352055	mT	Magnetic Flux from bar 2
	1.257E-6	MU0		T-m/A	Absolute permeability
		HAXV1	.93054248		Axial flux vector for HFP1
		HAXV2	.93054248		Axial flux vector for HFP2
		HFP	12.895704	mT	Total magnetic flux
		HFPAX	12	mT	Total axial magnetic flux
	1	fH		-	Fraction of height between busbars
L		HFB	2.0856383	cm	Height of the busbars
L	4.6	ETA		cm	Cross-section side of large BBs
		ABB	9.5939362	cm^2	Cross-sectional area of large busbars
L		CD	197.94294	A/cm^2	Current Density
LG	1899.052	IBB		A	Field Current
		RHOBB	28.451506	uOhm-cm	Resistivity of Busbars
		RHOMo	28.451506	uOhm-cm	Resistivity of Mo
		VBB	970.90634	cm^3	Volume of the LM busbars
		DENBB	10.084328	Mg/m^3	Density of Busbars
		DENMo	10.084328	Mg/m^3	Density of Mo
		DENZrB2	5.89152	Mg/m^3	Density of ZrB2
L		MLM	19.581876	kg	Mass of the Linear Magnet (busbars)
		RBB	.00030012	Ohm	Resistance of the busbars (magnet)
		LBB	101.2	cm	Length of LM coil turn
	2	NLM		-	Number of Linear magnets
	1	NCELL		-	Number of pump cells
L		VLBBP	569.93562	mV	LM load voltage - parallel connected
		RBBP	.00030012	Ohm	LM resistance - parallel connected
		VLBBS		mV	LM load voltage - series connected
		RBBS		Ohm	LM resistance - series connected
L		PLMP	2164.6747	W	LM power - parallel connected
		PLMS		W	LM power - series connected
		KMo	1.0579206	W/cm-K	Thermal conductivity of Mo
		SELECTW	0		Selects nozzle equations 1=H>W , 0=W>H
		RHOZrB2	37.03	uOhm-cm	Resistivity of ZrB2
L		PIT	4426.1138	W	Total EMP power input
L		SPMEMP	4.8071823	g/W	Specific mass of the EMP
L	45	SPMTEG		g/W	Specific mass of TEGs
L		MEMPTEG	101.76476	kg	Estimated mass of the TEG for armature
L		MLMTEG	97.410363	kg	Estimated mass of the TEG for LM
L		EMASS	220.45226	kg	Estimated mass of the LM-TEMP

```
MMMMMMMMMMMMMMMMMMMMM RULE SHEET MMMMMMMMMMMMMMMMMMMMMMMMMMMMMMMMMMMMMMMMMMMMMMM
S RuleDDDDDDDDDDDDDDDDDDDDDDDDDDDDDDDDDDDDDDDDDDDDDDDDDDDDDDDDDDDDDDDDDDDDDDDDD
  "CORELESS LINEAR CONDUCTION EMP - 07-24-91 - DESIGN AND PERFORMANCE

  DPDV=M1*B*IT
  DPMB=M2*B^2*Q
  DPMF=M3*B^2*Q
  DPHY=(DPT+DPNAD)*1000
  DPDL=DPDV-DPMB-DPMF-DPHY
  "TDPDL=DPDV-DPMB-DPMF-DPHY
  CEMF=B*W*Q/AF
  IC=CEMF/(RB+RL)
  IL=IT*RB/(RB+RL)
  AF=W*H
  RL=RHOL*10^-8*W/(H*LT)
  RB=RF*RW/(RF+RW)
  RF=2.6E-8*FX*RHOL/H
  RW=RHOW*10^-8*(W+2*TW)/(TW*2*LT)
  QE=15850*Q
  M1=RB/(RB+RL)*1/H
  M2=1/(RB+RL)*1/H^2
  M3=1/(H^2*RF)
  M4=1
  NRE=DENL*V*4*RH/(MU*10^-6)
  RH=W*H/(2*(W+H))
  V=Q/AF
  DPCV=DENL*VMAX^2/2
  f=.043/NRE^.2                                  "For 5000<NRE<200000
  HYHD=DENL*V^2/2
  DPT=f*LT/(4*RH)*HYHD
  DPNAD=(CN+(1-E)*(1-AR^2))*HYHD
  AR=4*W*H/(PI()*D^2)
  RTW=RHOW*10^-8*2*TW/(H*LT)
  PIE=VL*IT
  BMIN=M1*IT/(2*(M2+M3)*Q)
  "B=BMIN
  EEH=POH/PIE*100
  MT=NCELL*2*(H+W)*TW*LT*DENRTW
  ML=NCELL*(H*W*LT+VOLND)*DENRTL
  "ML=2*(H*W*LT+4*VOLND)*DENRTL
  S=PI()*(H^2+W^2)^(1/2)*(LNDI/COS(PI()/12)+LNDO/COS(PI()/24))
  "S=(PI()*D+2*(W+H))*(LNDI+LNDO)/2
  "S=PI()*(D/2+R2)*(LND^2+(D/2-R2)^2)^(1/2)
  SELECTW=STEP(H,W)
  (1-SELECTW)*LNDI=(D-H)/(2*TAN(PI()/12))*(1-SELECTW)
  (1-SELECTW)*LNDO=(D-H)/(2*TAN(PI()/24))*(1-SELECTW)
  SELECTW*LNDI=(D-W)/(2*TAN(PI()/12))*SELECTW
  SELECTW*LNDO=(D-W)/(2*TAN(PI()/24))*SELECTW
  LND=LNDI+LNDO
  "LND=(D/2-R2)/TAN(PI()/12)
  MND=NCELL*S*TW*DENRTW
  "MND=4*S*TW*DENRTW
  VOLNDI=(PI()*D^2/4+(W*H))*LNDI/2
  VOLNDO=(PI()*D^2/4+(W*H))*LNDO/2
  VOLND=VOLNDI+VOLNDO
  "VOLND=PI()*LND/3*((D/2)^2+D/2*R2+R2^2)
  "R2=(W^2+H^2)^(1/2)/2
```

```
"MATERIALS PROPERTIES

TWC=TL-273
TWK=TL
DENW=8.6304-1.895E-4*TWK-1.23E-8*TWK^2
DENRTW=8.6304-1.895E-4*TRM-1.23E-8*TRM^2
RHOW=16.337+4.224E-2*TWC-4.922E-6*TWC^2-3.941E-10*TWC^3 "For Nb-Zr in uOhm-cm


"DENW=7.68+0.E-2*TWK+0.E-6*TWK^2                        "For SS in MicroOhm-cm
"DENRTW=7.68+0.E-2*TRM+0.E-6*TRM^2                      "For SS in MicroOhm-cm
"RHOW=69.6+8.78E-2*TWC+1.0-6*TWC^2                         "For SS in MicroOhm-cm


RHOL=13.735+2.9256E-2*TL-2.46E-6*TL^2                   "For Li in micro-Ohm-cm
DENL=.5593-1.133E-4*TL+1.58E-8*TL^2                     "For Li in Mg/m^3
DENRTL=.5593-1.133E-4*TRM+1.58E-8*TRM^2                 "For Li in Mg/m^3
MU=1.8739-4.667E-3*TL+4.933E-6*TL^2-1.867E-9*TL^3       "For Li in centipoise
"RHOMo=-0.183+2.0321E-2*TL                               "For Mo in microOhm-cm
RHOMo=(-8.144267+.21863752*TL-6.88E-10*TL^2+2.3868E-8*TL^3-5.28E-12*TL^4)/10
                                                        "For Mo in microOhm-cm
DENMo=10.2698-1.056E-4*TL-4.08E-8*TL^2                  "For Mo in Mg/m^3
KMo=(0.3602-1.142E-4*TL+2.050E-8*TL^2)*4.1868           "For Mo in W/cm-K

"RHOL=36.768-1.6212E-2*TL+7.1741E-5*TL^2               "For NaK in micro-Ohm-cm
"DENL=.9390-2.426E-4*TL                                "For NaK in Mg/m^3
"DENRML=.9390-2.426E-4*TRML                            "For NaK in Mg/m^3
"MU=1.1914-2.7431E-3*TL+2.5463E-6*TL^2-8.492E-10*TL^3 "For NaK in centipoise

* RHOCU=16.73+0.068*(TEMPB-293)                         "For Cu in nOhm-m
RHOZrB2=-5.81+.0357*TL                                 "For ZrB2 in uOhm-cm
DENZrB2=6.08*.969                                      "For ZrB2 in Mg/m^3

"SINGLE-PASS PUMP SECTION

"DPDL=DPDLE                           "SP
"LL=IT*RB/(RB+RL)*RL                  "SP
"VLW=IT*RB/(RB+RL)*RTW                "SP
"VL=VLL+VLW+CEMF+VBS                  "SP
"POH=DPDL*Q                           "SP
"LB=2*(2*HFB)                         "SP
"MB=2*(TB*HFB)*LT*DENSB               "SP

RHOB=RHOMo
RBS= RHOB*LB/(LT*TB)*10^-8
VBS=IT*RBS
PIT=PIE+PLMP
MASS=MLM+MB+MT+ML+MND
SPMEMP=MASS/PIT
MEMPTEG=SPMTEG*PIE
MLMTEG=SPMTEG*PLMP
EMASS=MASS+MEMPTEG+MLMTEG



"DOUBLE-PASS PUMP SECTION
```

```
DPDL=DPDLE/2                                "DP
VLL=2*IT*RB/(RB+RL)*RL                      "DP
VLW=2*IT*RB/(RB+RL)*RTW                     "DP
VL=VLL+VLW+VC+VBS                           "DP
VC=2*CEMF                                   "DP"
POH=2*DPDL*Q                                "DP
LB=TB+TI+H                                  "DP

DENSB=DENMo
MB=(2*H+3*TI+4*TW)*TB*LT*DENSB              "DP


"LINEAR CORELESS MAGNET CALCULATIONS - 7/22/91


UP=(1-STEP(fX,fL1))                      "STEP=1 if fX=, >fL1 and 0 otherwise
PUMP=STEP(fX,fL1)*STEP(fL2,fX)           "CASE=1 for fL1<fX<fL2
DOWN=(1-STEP(fL2,fX))                    "STEP=1 if fX<fl2
L1=X/2-LT/2
L2=X/2+LT/2
L1=fL1*X
L2=fL2*X

"UPSTREAM OF PUMPING SECTION

UP*PHI1=ATAN((fL1-fX)*X/(fW*WFB))*UP
UP*PHI2=ATAN((fL2-fX)*X/(fW*WFB))*UP
UP*PHI3=ATAN((fL1-fX)*X/((1-fW)*WFB))*UP
UP*PHI4=ATAN((fL2-fX)*X/((1-fW)*WFB))*UP
UP*HFPR1=(HF2-HF1)*UP
UP*HFPR2=(HF4-HF3)*UP

"PUMPING SECTION REGION

PUMP*PHI1=ATAN((fX-fL1)*X/(fW*WFB))*PUMP
PUMP*PHI2=ATAN((fL2-fX)*X/(fW*WFB))*PUMP
PUMP*PHI3=ATAN((fX-fL1)*X/((1-fW)*WFB))*PUMP
PUMP*PHI4=ATAN((fL2-fX)*X/((1-fW)*WFB))*PUMP
PUMP*HFPR1=(HF1+HF2)*PUMP
PUMP*HFPR2=(HF3+HF4)*PUMP
HF1=SIN(PHI1)
HF2=SIN(PHI2)
HF3=SIN(PHI3)
HF4=SIN(PHI4)
R1=((fW*WFB)^2+(fH*HFB)^2)^.5
R2=(((1-fW)*WFB)^2+(fH*HFB)^2)^.5
HFP1=MU0*I/(4*pi()*R1)
HFP2=MU0*I/(4*pi()*R2)
HAXV1=fW*WFB/R1
HAXV2=fW*WFB/R2
HFP=HFP1*HFPR1+HFP2*HFPR2
HFPAX=HFP1*HFPR1*HAXV1+HFP2*HFPR2*HAXV2
B=NLM*HFPAX

"DOWNTSTREAM OF PUMPING SECTION

DOWN*PHI1=ATAN((fX-fL1)*X/(fW*WFB))*DOWN
DOWN*PHI2=ATAN((fX-fL2)*X/(fW*WFB))*DOWN
```

```
DOWN*PHI3=ATAN((fX-fL1)*X/((1-fW)*WFB))*DOWN
DOWN*PHI4=ATAN((fX-fL2)*X/((1-fW)*WFB))*DOWN
DOWN*HFPR1=(HF1-HF2)*DOWN
DOWN*HFPR2=(HF3-HF4)*DOWN

I=IBB
RHOBB=RHOMo
CD=IBB/ABB
WFB=W+ETA+2*(TW+TB+2*TI)
HFB=TI/2+H+TI
ABB=ETA*HFB
DENBB=DENMo
RBB=RHOBB*10^-8*LBB/ABB
LBB= 2*(LT+WFB)
VBB=LBB*ABB
MLM=NLM*VBB*DENBB
VLBBP=IBB*RBBP
RBBP=RBB
"VLBBS=IBB*RBBS
"RBBS=2*RBB
PLMP=NLM*IBB^2*RBBP
"PLMS=IBB^2*RBBS
```

```
MMMMMMMMMMMMMMMMMMMMMM UNIT SHEET MMMMMMMMMMMMMMMMMMMMMMMMMMMMMMMMMMMMMMMMMMMMMMMMMM
FromDDDDD ToDDDDDDD Multiply ByDD Add OffsetDDD
T         mT        1000
psi       Pa        6895
m         mm        1000
m^2       mm^2      1000000
m^3       mm^3      1E9
m^3/s     litre/s   1000
T-m^2/s   mVolt     1000
litre/s   gpm       15.85
T-A-m     N
N/m^2     Pa
Volt      Ohm-A
Mg/m-s    cp        1000000
Mg/m-s^2  Pa        1000
T-m^2/s   Ohm-A
Pa-m^3/s  W
kPa       T-A-m/m^2
Mg        kg        1000
Ohm-A     mVolt     1000
kA        A         1000
Volt      mVolt     1000
m^2/s^2   Pa-m^3/Mg 1000
m^2       cm^2      10000
m         cm        100
m^2/s^2   Pa-m^3/Mg 1000
Volt-A    W
cm        mm        10
V         mV        1000
kW        Volt-A    1000
kPa       Pa        1000
m         cm        100
m^3       cm^3      1000000
T         mT        1000
A/cm^2    A/m^2     10000
Mg/W      g/W       1000000
```

APPENDIX D

LINEAR MAGNET MODEL FOR CONDUCTORS OF LARGE CROSS-SECTION SIZE

MAGFLDDT.TK

MMMMMMMMMMMMMMMMMMMMM VARIABLE SHEET MMMMMMMMMMMMMMMMMMMMMMMMMMMMMMMMMMMMMMMMMMMMM

St	InputDDDD	NameDDD	OutputDDD	UnitDDDDD	CommentDDDDDDDDDDDDDDDDDDDDDDDDDDDDDDD
					FILE: MAGFLDDT.TK 52 kB
					MAGNETIC FIELD CALCULATIONS
					7-22-91
		I	3250	A	Field Current
	.5	fW		-	Fraction of WFB
L	4.2	WFB		m	Center-center span between field buses
	.2	fL1		-	Fractional location of L1
	.8	fL2		-	Fractional location of L2
	.048	L1		m	Inlet end of Field busbars
		L2	.192	m	Discharge end of Field busbars
	.5	fX		-	Fraction of total pump length
	.24	X		m	Total pump length
		UP	0	-	Upstream region indicator
		PUMP	1	-	Pumping section region indicator
		DOWN	0	-	Downstream region indicator
		PHI1	.03427229	rad	Angular integration limit
		PHI2	.03427229		Angular integration limit
		PHI3	.03427229		Angular integration limit
		PHI4	.03427229		Angular integration limit
		HF1	.03426558		Integrated flux fraction
		HF2	.03426558		Integrated flux fraction
		HF3	.03426558		Integrated flux fraction
		HF4	.03426558		Integrated flux fraction
		HFPR1	.06853116		Total integrated fractions, bar 2
		HFPR2	.06853116		Total integrated fractions, bar 1
		HFP1	.1548066	mT	Magnetic Flux from bar 1
		HFP2	.1548066	mT	Magnetic Flux from bar 2
	1.257E-6	MU0		T-m/A	Absolute permeability
		HAXV1	1		Axial flux vector for HFP1
		HAXV2	1		Axial flux vector for HFP2
		HFP	.02121815	mT	Total magnetic flux
L		HFPAX	.02121815	mT	Total axial magnetic flux
	0	fH		-	Fraction of height between busbars
		HFB	.05	m	Height of the busbars
					EQUIPOTENTIAL CIRCLE CALCULATIONS
		ho	3		Height of Po above busbar line at w/2
	10	w			Length of busbar line
	3	h			Height of P above busbar line at fw*w
	.5	fw			Fraction of the busbar line length
		ThetaA	.5404195		Angle-radial vector A to busbar line
		ThetaB	.5404195		Angle-radial vector B to busbar line
		Beta	2.0607537		Angle between radial vectors A & B
		Ro	5.6666667		Radius of the equipotential circle
		FOM	.3		This is the ratio of h/w
		Bf1	.14705882		Off bisector factor for busbar 1
		Bf2	.14705882		Off bisector factor for busbar 2
		BB	.29411765		Sum of off-bisector factors above
		dd	5.8309519		distance from busbar 1
		ddd	5.8309519		distance from busbar 2
		nn1	.85749293		Cosine factor for busbar 1
		nn2	.85749293		Cosine factor for busbar 2

L	25	IPB	130	A	Current per busbar pairs
		ETA	5	cm	Cross-section side of large BBs
L	25	ABB		cm^2	Cross-sectional area of large busbars
L	4	Wo		cm	W of inner most busbar pairs
L	130	CD		A/cm^2	Current density
L		IBB	3250	A	
		RHOBB			
		RHOMo			
		VBB			
		LT			
		DENBB			
		DENMo			
		MBB			
		RBB			
		LBB			
		NCELL			
		VLBBP			
		RBBP			
		VLBBS			
		RBBS			
		PBBP			
		PBBS			
	.5	fW1			Fraction of WFB
		fH11	2	cm	Fraction of height between busbars
		fH12	1	cm	Fraction of height between busbars
		fH13	0	cm	Fraction of height between busbars
		fH14	1	cm	Fraction of height between busbars
		fH15	2	cm	Fraction of height between busbars
	2	NF1			Height displacement unit from busbar
	1	NF2			Height displacement unit from busbar
	0	NF3			Height displacement unit from busbar
	1	NF4			Height displacement unit from busbar
	2	NF5			Height displacement unit from busbar
L		WFB1	5	cm	Center-center span between field buses
L		WFB2	7	cm	Center-center span between field buses
L		WFB3	9	cm	Center-center span between field buses
L		WFB4	11	cm	Center-center span between field buses
L		WFB5	13	cm	Center-center span between field buses
		PHI11	1.2365983		Angular integration limit
		PHI21	1.2365983		Angular integration limit
		PHI31	1.2365983		Angular integration limit
		PHI41	1.2365983		Angular integration limit
		HF11	.94467366		Integrated flux fraction
		HF21	.94467366		Integrated flux fraction
		HF31	.94467366		Integrated flux fraction
		HF41	.94467366		Integrated flux fraction
		HFPR11	1.8893473		Total integrated fractions, bar 1
		HFPR21	1.8893473		Total integrated fractions, bar 2
		HFP111	.51973456	mT	Magnetic Flux from bar 1
		HFP211	.51973456	mT	Magnetic Flux from bar 2
		HAXV111	.99920096		Axial flux vector for HFP1
		HAXV211	.99920096		Axial flux vector for HFP2

HFPAX11	1.962349	mT	Total axial magnetic flux
HFP112	.52004619	mT	Magnetic Flux from bar 1
HFP212	.52004619	mT	Magnetic Flux from bar 2
HAXV112	.99980006		Axial flux vector for HFP1
HAXV212	.99980006		Axial flux vector for HFP2
HFPAX12	1.9647028	mT	Total axial magnetic flux
HFP113	.52015019	mT	Magnetic Flux from bar 1
HFP213	.52015019	mT	Magnetic Flux from bar 2
HAXV113	1		Axial flux vector for HFP1
HAXV213	1		Axial flux vector for HFP2
HFPAX13	1.9654887	mT	Total axial magnetic flux
HFP114	.52004619	mT	Magnetic Flux from bar 1
HFP214	.52004619	mT	Magnetic Flux from bar 2
HAXV114	.99980006		Axial flux vector for HFP1
HAXV214	.99980006		Axial flux vector for HFP2
HFPAX14	1.9647028	mT	Total axial magnetic flux
HFP115	.51973456	mT	Magnetic Flux from bar 1
HFP215	.51973456	mT	Magnetic Flux from bar 2
HAXV115	.99920096		Axial flux vector for HFP1
HAXV215	.99920096		Axial flux vector for HFP2
HFPAX15	1.962349	mT	Total axial magnetic flux
HFPAX1	9.8195923	mT	Total axial magnetic flux of layer 1
			LAYER 2
PHI12	1.1183214	rad	Angular integration limit
PHI22	1.1183214		Angular integration limit
PHI32	1.1183214		Angular integration limit
PHI42	1.1183214		Angular integration limit
HF12	.89936785		Integrated flux fraction
HF22	.89936785		Integrated flux fraction
HF32	.89936785		Integrated flux fraction
HF42	.89936785		Integrated flux fraction
HFPR12	1.7987357		Total integrated fractions, bar 1
HFPR22	1.7987357		Total integrated fractions, bar 2
HFP121	.37138429	mT	Magnetic Flux from bar 1
HFP221	.37138429	mT	Magnetic Flux from bar 2
HAXV121	.99959209		Axial flux vector for HFP1
HAXV221	.99959209		Axial flux vector for HFP2
HFPAX21	1.3354994	mT	Total axial magnetic flux
HFP122	.37149794	mT	Magnetic Flux from bar 1
HFP222	.37149794	mT	Magnetic Flux from bar 2
HAXV122	.99989797		Axial flux vector for HFP1
HAXV222	.99989797		Axial flux vector for HFP2
HFPAX22	1.3363169	mT	Total axial magnetic flux
HFP123	.37153585	mT	Magnetic Flux from bar 1
HFP223	.37153585	mT	Magnetic Flux from bar 2
HAXV123	1		Axial flux vector for HFP1
HAXV223	1		Axial flux vector for HFP2
HFPAX23	1.3365896	mT	Total axial magnetic flux

HFP124	.37149794	mT	Magnetic Flux from bar 1
HFP224	.37149794	mT	Magnetic Flux from bar 2
HAXV124	.99989797		Axial flux vector for HFP1
HAXV224	.99989797		Axial flux vector for HFP2
HFPAX24	1.3363169	mT	Total axial magnetic flux
HFP125	.37138429	mT	Magnetic Flux from bar 1
HFP225	.37138429	mT	Magnetic Flux from bar 2
HAXV125	.99959209		Axial flux vector for HFP1
HAXV225	.99959209		Axial flux vector for HFP2
HFPAX25	1.3354994	mT	Total axial magnetic flux
HFPAX2	6.6802221	mT	Total axial magnetic flux of layer 2
			LAYER 3
PHI13	1.012197	rad	Angular integration limit
PHI23	1.012197		Angular integration limit
PHI33	1.012197		Angular integration limit
PHI43	1.012197		Angular integration limit
HF13	.8479983		Integrated flux fraction
HF23	.8479983		Integrated flux fraction
HF33	.8479983		Integrated flux fraction
HF43	.8479983		Integrated flux fraction
HFPR13	1.6959966		Total integrated fractions, bar 1
HFPR23	1.6959966		Total integrated fractions, bar 2
HFP131	.288901	mT	Magnetic Flux from bar 1
HFP231	.288901	mT	Magnetic Flux from bar 2
HAXV131	.99975318		Axial flux vector for HFP1
HAXV231	.99975318		Axial flux vector for HFP2
HFPAX31	.97970836	mT	Total axial magnetic flux
HFP132	.28895449	mT	Magnetic Flux from bar 1
HFP232	.28895449	mT	Magnetic Flux from bar 2
HAXV132	.99993828		Axial flux vector for HFP1
HAXV232	.99993828		Axial flux vector for HFP2
HFPAX32	.98007117	mT	Total axial magnetic flux
HFP133	.28897233	mT	Magnetic Flux from bar 1
HFP233	.28897233	mT	Magnetic Flux from bar 2
HAXV133	1		Axial flux vector for HFP1
HAXV233	1		Axial flux vector for HFP2
HFPAX33	1.1202196	mT	Total axial magnetic flux
HFP134	.28895449	mT	Magnetic Flux from bar 1
HFP234	.28895449	mT	Magnetic Flux from bar 2
HAXV134	.99993828		Axial flux vector for HFP1
HAXV234	.99993828		Axial flux vector for HFP2
HFPAX34	.98007117	mT	Total axial magnetic flux
HFP135	.288901	mT	Magnetic Flux from bar 1
HFP235	.288901	mT	Magnetic Flux from bar 2
HAXV135	.99975318		Axial flux vector for HFP1
HAXV235	.99975318		Axial flux vector for HFP2
HFPAX35	.97970836	mT	Total axial magnetic flux

HFPAX3	5.0397787 mT	Total axial magnetic flux of layer 3
		LAYER 4
PHI14	.91846543 rad	Angular integration limit
PHI24	.91846543	Angular integration limit
PHI34	.91846543	Angular integration limit
PHI44	.91846543	Angular integration limit
HF14	.79467101	Integrated flux fraction
HF24	.79467101	Integrated flux fraction
HF34	.79467101	Integrated flux fraction
HF44	.79467101	Integrated flux fraction
HFPR14	1.589342	Total integrated fractions, bar 1
HFPR24	1.589342	Total integrated fractions, bar 2
HFP141	.23639283 mT	Magnetic Flux from bar 1
HFP241	.23639283 mT	Magnetic Flux from bar 2
HAXV141	.99983475	Axial flux vector for HFP1
HAXV241	.99983475	Axial flux vector for HFP2
HFPAX41	.75129395 mT	Total axial magnetic flux
HFP142	.23642213 mT	Magnetic Flux from bar 1
HFP242	.23642213 mT	Magnetic Flux from bar 2
HAXV142	.99995868	Axial flux vector for HFP1
HAXV242	.99995868	Axial flux vector for HFP2
HFPAX42	.75148021 mT	Total axial magnetic flux
HFP143	.2364319 mT	Magnetic Flux from bar 1
HFP243	.2364319 mT	Magnetic Flux from bar 2
HAXV143	1	Axial flux vector for HFP1
HAXV243	1	Axial flux vector for HFP2
HFPAX43	.75154231 mT	Total axial magnetic flux
HFP144	.23642213 mT	Magnetic Flux from bar 1
HFP244	.23642213 mT	Magnetic Flux from bar 2
HAXV144	.99995868	Axial flux vector for HFP1
HAXV244	.99995868	Axial flux vector for HFP2
HFPAX44	.75148021 mT	Total axial magnetic flux
HFP145	.23639283 mT	Magnetic Flux from bar 1
HFP245	.23639283 mT	Magnetic Flux from bar 2
HAXV145	.99983475	Axial flux vector for HFP1
HAXV245	.99983475	Axial flux vector for HFP2
HFPAX45	.75129395 mT	Total axial magnetic flux
HFPAX4	3.7570906 mT	Total axial magnetic flux of layer 4
		LAYER 5
PHI15	.83644866 rad	Angular integration limit
PHI25	.83644866	Angular integration limit
PHI35	.83644866	Angular integration limit
PHI45	.83644866	Angular integration limit
HF15	.74226804	Integrated flux fraction
HF25	.74226804	Integrated flux fraction
HF35	.74226804	Integrated flux fraction
HF45	.74226804	Integrated flux fraction
HFPR15	1.4845361	Total integrated fractions, bar 1

HFPR25	1.4845361	Total integrated fractions, bar 2
HFP151	.20003409 mT	Magnetic Flux from bar 1
HFP251	.20003409 mT	Magnetic Flux from bar 2
HAXV151	.99988168	Axial flux vector for HFP1
HAXV251	.99988168	Axial flux vector for HFP2
HFPAX51	.59384538 mT	Total axial magnetic flux
HFP152	.20005184 mT	Magnetic Flux from bar 1
HFP252	.20005184 mT	Magnetic Flux from bar 2
HAXV152	.99997042	Axial flux vector for HFP1
HAXV252	.99997042	Axial flux vector for HFP2
HFPAX52	.59395079 mT	Total axial magnetic flux
HFP153	.20005776 mT	Magnetic Flux from bar 1
HFP253	.20005776 mT	Magnetic Flux from bar 2
HAXV153	1	Axial flux vector for HFP1
HAXV253	1	Axial flux vector for HFP2
HFPAX53	.59398594 mT	Total axial magnetic flux
HFP154	.20005184 mT	Magnetic Flux from bar 1
HFP254	.20005184 mT	Magnetic Flux from bar 2
HAXV154	.99997042	Axial flux vector for HFP1
HAXV254	.99997042	Axial flux vector for HFP2
HFPAX54	.59395079 mT	Total axial magnetic flux
HFP155	.20003409 mT	Magnetic Flux from bar 1
HFP255	.20003409 mT	Magnetic Flux from bar 2
HAXV155	.99988168	Axial flux vector for HFP1
HAXV255	.99988168	Axial flux vector for HFP2
HFPAX55	.59384538 mT	Total axial magnetic flux
HFPAX5	2.9695783 mT	Total axial magnetic flux of layer 5
HFPAXT	28.266262 mT	Total axial magnetic flux - all layers
BAX11	9.8195923 mT	Axial magnetic flux - Layer 1
BAX12	16.499814 mT	Axial magnetic flux - Layers 1 and 2
BAX13	21.539593 mT	Axial magnetic flux, Layers 1 thru 3
BAX14	25.296684 mT	Axial magnetic flux, Layers 1 thru 4
BAX15	28.266262 mT	Axial magnetic flux, Layers 1 thru 5
LAY1CON	34.739621	
LAY2CON	23.6332	
LAY3CON	17.829661	
LAY4CON	13.291784	
LAY5CON	10.505734	

L

```
MMMMMMMMMMMMMMMMMMMM RULE SHEET MMMMMMMMMMMMMMMMMMMMMMMMMMMMMMMMMMMMMMMMMMMMMMM
S RuleDDDDDDDDDDDDDDDDDDDDDDDDDDDDDDDDDDDDDDDDDDDDDDDDDDDDDDDDDDDDDDDDDDDDDDD
  "MAGNETIC FLUX CALCULATIONS FOR A LINEAR CORELESS MAGNET
  "7/22/91

  "MAGNETIC FIELD CALCULATIONS

* UP=(1-STEP(fX,fL1))                       "STEP=1 if fX=, >fL1 and 0 otherwise
* PUMP=STEP(fX,fL1)*STEP(fL2,fX)            "CASE=1 for fL1<fX<fL2
* DOWN=(1-STEP(fL2,fX))                     "STEP=1 if fX<fl2
* L1=fL1*X
* L2=fL2*X

  "UPSTREAM OF PUMPING SECTION

* UP*PHI1=ATAN((fL1-fX)*X/(fW*WFB))*UP
* UP*PHI2=ATAN((fL2-fX)*X/(fW*WFB))*UP
* UP*PHI3=ATAN((fL1-fX)*X/((1-fW)*WFB))*UP
* UP*PHI4=ATAN((fL2-fX)*X/((1-fW)*WFB))*UP
* UP*HFPR1=(HF2-HF1)*UP
* UP*HFPR2=(HF4-HF3)*UP

  "PUMPING SECTION REGION

* PUMP*PHI1=ATAN((fX-fL1)*X/(fW*WFB))*PUMP
* PUMP*PHI2=ATAN((fL2-fX)*X/(fW*WFB))*PUMP
* PUMP*PHI3=ATAN((fX-fL1)*X/((1-fW)*WFB))*PUMP
* PUMP*PHI4=ATAN((fL2-fX)*X/((1-fW)*WFB))*PUMP
* PUMP*HFPR1=(HF1+HF2)*PUMP
* PUMP*HFPR2=(HF3+HF4)*PUMP
* HF1=SIN(PHI1)
* HF2=SIN(PHI2)
* HF3=SIN(PHI3)
* HF4=SIN(PHI4)
* HFP1=MU0*I/(4*pi()*((fW*WFB)^2+(fH*HFB)^2)^.5)
* HFP2=MU0*I/(4*pi()*(((1-fW)*WFB)^2+(fH*HFB)^2)^.5)
* HAXV1=COS(ATAN(fH*HFB/(fW*WFB)))
* HAXV2=COS(ATAN(fH*HFB/((1-fW)*WFB)))
* HFPAX=HFP1*HFPR1*HAXV1+HFP2*HFPR2*HAXV2
* HFP=HFP1*HFPR1+HFP2*HFPR2

  "DOWNTSTREAM OF PUMPING SECTION

* DOWN*PHI1=ATAN((fX-fL1)*X/(fW*WFB))*DOWN
* DOWN*PHI2=ATAN((fX-fL2)*X/(fW*WFB))*DOWN
* DOWN*PHI3=ATAN((fX-fL1)*X/((1-fW)*WFB))*DOWN
* DOWN*PHI4=ATAN((fX-fL2)*X/((1-fW)*WFB))*DOWN
* DOWN*HFPR1=(HF1-HF2)*DOWN
* DOWN*HFPR2=(HF3-HF4)*DOWN

  "EQUIPOTENTIAL ELECTRIC FIELD AND MAGNETIC VECTOR CALCULATIONS

* 2*atan(ho/(w/2))=atan(h/(fw*w))+atan(h/((1-fw)*w))
* ThetaA=atan(h/(fw*w))
* ThetaB=atan(h/((1-fw)*w))
* Beta=pi()-(ThetaA+ThetaB)
* Ro=w^2/(8*ho)+ho/2
* FOM=h/w
```

```
* Bf1=cos(atan(h/(fw*w)))/((h^2+(fw*w)^2)^(1/2))
* Bf2=cos(atan(h/((1-fw)*w)))/((h^2+((1-fw)*w)^2)^(1/2))
* BB=Bf1+Bf2
* dd=(h^2+(fw*w)^2)^(1/2)
* ddd=(h^2+((1-fw)*w)^2)^(1/2)
* nn1=cos(ThetaA)
* nn2=cos(ThetaB)

  "LARGE CONDUCTOR CALCULATIONS

* IPB=IBB/25
* I=IBB
* RHOBB=RHOMo
* CD=IBB/ABB
* ABB=ETA^2
* HFB=ETA
* DENBB=DENMo
* RBB=RHOBB*10^-8*LBB/ABB
* LBB= 2*(LT+WFB)
* VBB=2*LBB*ABB
* MBB=NCELL*VBB*DENBB
* VLBBP=IBB*RBBP
* RBBP=RBB
  "VLBBS=IBB*RBBS
  "RBBS=2*RBB
* PBBP=2*IBB^2*RBBP
  "PBBS=IBB^2*RBBS

* fH11=NF1*ETA/5
* fH12=NF2*ETA/5
* fH13=NF3*ETA/5
* fH14=NF4*ETA/5
* fH15=NF5*ETA/5

  "WFB=Wo+0.2
* WFB1=Wo+1*ETA/5
* WFB2=Wo+3*ETA/5
* WFB3=Wo+5*ETA/5
* WFB4=Wo+7*ETA/5
* WFB5=Wo+9*ETA/5

  "LAYER 1

* PUMP*PHI11=ATAN((fX-fL1)*X/(fW1*WFB1))*PUMP
* PUMP*PHI21=ATAN((fL2-fX)*X/(fW1*WFB1))*PUMP
* PUMP*PHI31=ATAN((fX-fL1)*X/((1-fW1)*WFB1))*PUMP
* PUMP*PHI41=ATAN((fL2-fX)*X/((1-fW1)*WFB1))*PUMP
* PUMP*HFPR11=(HF11+HF21)*PUMP
* PUMP*HFPR21=(HF31+HF41)*PUMP
* HF11=SIN(PHI11)
* HF21=SIN(PHI21)
* HF31=SIN(PHI31)
* HF41=SIN(PHI41)

* HFP111=MU0*IPB/(4*pi()*((fW1*WFB1)^2+(fH11*HFB)^2)^.5)
* HFP211=MU0*IPB/(4*pi()*(((1-fW1)*WFB1)^2+(fH11*HFB)^2)^.5)
* HAXV111=COS(ATAN(fH11*HFB/(fW1*WFB1)))
* HAXV211=COS(ATAN(fH11*HFB/((1-fW1)*WFB1)))
```

```
* HFPAX11=HFP111*HFPR11*HAXV111+HFP211*HFPR21*HAXV211

* HFP112=MU0*IPB/(4*pi()*((fW1*WFB1)^2+(fH12*HFB)^2)^.5)
* HFP212=MU0*IPB/(4*pi()*(((1-fW1)*WFB1)^2+(fH12*HFB)^2)^.5)
* HAXV112=COS(ATAN(fH12*HFB/(fW1*WFB1)))
* HAXV212=COS(ATAN(fH12*HFB/((1-fW1)*WFB1)))
* HFPAX12=HFP112*HFPR11*HAXV112+HFP212*HFPR21*HAXV212

* HFP113=MU0*IPB/(4*pi()*((fW1*WFB1)^2+(fH13*HFB)^2)^.5)
* HFP213=MU0*IPB/(4*pi()*(((1-fW1)*WFB1)^2+(fH13*HFB)^2)^.5)
* HAXV113=COS(ATAN(fH13*HFB/(fW1*WFB1)))
* HAXV213=COS(ATAN(fH13*HFB/((1-fW1)*WFB1)))
* HFPAX13=HFP113*HFPR11*HAXV113+HFP213*HFPR21*HAXV213

* HFP114=MU0*IPB/(4*pi()*((fW1*WFB1)^2+(fH14*HFB)^2)^.5)
* HFP214=MU0*IPB/(4*pi()*(((1-fW1)*WFB1)^2+(fH14*HFB)^2)^.5)
* HAXV114=COS(ATAN(fH14*HFB/(fW1*WFB1)))
* HAXV214=COS(ATAN(fH14*HFB/((1-fW1)*WFB1)))
* HFPAX14=HFP114*HFPR11*HAXV114+HFP214*HFPR21*HAXV214

* HFP115=MU0*IPB/(4*pi()*((fW1*WFB1)^2+(fH15*HFB)^2)^.5)
* HFP215=MU0*IPB/(4*pi()*(((1-fW1)*WFB1)^2+(fH15*HFB)^2)^.5)
* HAXV115=COS(ATAN(fH15*HFB/(fW1*WFB1)))
* HAXV215=COS(ATAN(fH15*HFB/((1-fW1)*WFB1)))
* HFPAX15=HFP115*HFPR11*HAXV115+HFP215*HFPR21*HAXV215

* HFPAX1=HFPAX11+HFPAX12+HFPAX13+HFPAX14+HFPAX15

  "LAYER 2

* PUMP*PHI12=ATAN((fX-fL1)*X/(fW1*WFB2))*PUMP
* PUMP*PHI22=ATAN((fL2-fX)*X/(fW1*WFB2))*PUMP
* PUMP*PHI32=ATAN((fX-fL1)*X/((1-fW1)*WFB2))*PUMP
* PUMP*PHI42=ATAN((fL2-fX)*X/((1-fW1)*WFB2))*PUMP
* PUMP*HFPR12=(HF12+HF22)*PUMP
* PUMP*HFPR22=(HF32+HF42)*PUMP
* HF12=SIN(PHI12)
* HF22=SIN(PHI22)
* HF32=SIN(PHI32)
* HF42=SIN(PHI42)

* HFP121=MU0*IPB/(4*pi()*((fW1*WFB2)^2+(fH11*HFB)^2)^.5)
* HFP221=MU0*IPB/(4*pi()*(((1-fW1)*WFB2)^2+(fH11*HFB)^2)^.5)
* HAXV121=COS(ATAN(fH11*HFB/(fW1*WFB2)))
* HAXV221=COS(ATAN(fH11*HFB/((1-fW1)*WFB2)))
* HFPAX21=HFP121*HFPR12*HAXV121+HFP221*HFPR22*HAXV221

* HFP122=MU0*IPB/(4*pi()*((fW1*WFB2)^2+(fH12*HFB)^2)^.5)
* HFP222=MU0*IPB/(4*pi()*(((1-fW1)*WFB2)^2+(fH12*HFB)^2)^.5)
* HAXV122=COS(ATAN(fH12*HFB/(fW1*WFB2)))
* HAXV222=COS(ATAN(fH12*HFB/((1-fW1)*WFB2)))
* HFPAX22=HFP122*HFPR12*HAXV122+HFP222*HFPR22*HAXV222

* HFP123=MU0*IPB/(4*pi()*((fW1*WFB2)^2+(fH13*HFB)^2)^.5)
* HFP223=MU0*IPB/(4*pi()*(((1-fW1)*WFB2)^2+(fH13*HFB)^2)^.5)
* HAXV123=COS(ATAN(fH13*HFB/(fW1*WFB2)))
* HAXV223=COS(ATAN(fH13*HFB/((1-fW1)*WFB2)))
* HFPAX23=HFP123*HFPR12*HAXV123+HFP223*HFPR22*HAXV223
```

```
* HFP124=MU0*IPB/(4*pi()*((fW1*WFB2)^2+(fH14*HFB)^2)^.5)
* HFP224=MU0*IPB/(4*pi()*(((1-fW1)*WFB2)^2+(fH14*HFB)^2)^.5)
* HAXV124=COS(ATAN(fH14*HFB/(fW1*WFB2)))
* HAXV224=COS(ATAN(fH14*HFB/((1-fW1)*WFB2)))
* HFPAX24=HFP124*HFPR12*HAXV124+HFP224*HFPR22*HAXV224

* HFP125=MU0*IPB/(4*pi()*((fW1*WFB2)^2+(fH15*HFB)^2)^.5)
* HFP225=MU0*IPB/(4*pi()*(((1-fW1)*WFB2)^2+(fH15*HFB)^2)^.5)
* HAXV125=COS(ATAN(fH15*HFB/(fW1*WFB2)))
* HAXV225=COS(ATAN(fH15*HFB/((1-fW1)*WFB2)))
* HFPAX25=HFP125*HFPR12*HAXV125+HFP225*HFPR22*HAXV225

* HFPAX2=HFPAX21+HFPAX22+HFPAX23+HFPAX24+HFPAX25

  "LAYER 3

* PUMP*PHI13=ATAN((fX-fL1)*X/(fW1*WFB3))*PUMP
* PUMP*PHI23=ATAN((fL2-fX)*X/(fW1*WFB3))*PUMP
* PUMP*PHI33=ATAN((fX-fL1)*X/((1-fW1)*WFB3))*PUMP
* PUMP*PHI43=ATAN((fL2-fX)*X/((1-fW1)*WFB3))*PUMP
* PUMP*HFPR13=(HF13+HF23)*PUMP
* PUMP*HFPR23=(HF33+HF43)*PUMP
* HF13=SIN(PHI13)
* HF23=SIN(PHI23)
* HF33=SIN(PHI33)
* HF43=SIN(PHI43)

* HFP131=MU0*IPB/(4*pi()*((fW1*WFB3)^2+(fH11*HFB)^2)^.5)
* HFP231=MU0*IPB/(4*pi()*(((1-fW1)*WFB3)^2+(fH11*HFB)^2)^.5)
* HAXV131=COS(ATAN(fH11*HFB/(fW1*WFB3)))
* HAXV231=COS(ATAN(fH11*HFB/((1-fW1)*WFB3)))
* HFPAX31=HFP131*HFPR13*HAXV131+HFP231*HFPR23*HAXV231

* HFP132=MU0*IPB/(4*pi()*((fW1*WFB3)^2+(fH12*HFB)^2)^.5)
* HFP232=MU0*IPB/(4*pi()*(((1-fW1)*WFB3)^2+(fH12*HFB)^2)^.5)
* HAXV132=COS(ATAN(fH12*HFB/(fW1*WFB3)))
* HAXV232=COS(ATAN(fH12*HFB/((1-fW1)*WFB3)))
* HFPAX32=HFP132*HFPR13*HAXV132+HFP232*HFPR23*HAXV232

* HFP133=MU0*IPB/(4*pi()*((fW1*WFB3)^2+(fH13*HFB)^2)^.5)
* HFP233=MU0*IPB/(4*pi()*(((1-fW1)*WFB3)^2+(fH13*HFB)^2)^.5)
* HAXV133=COS(ATAN(fH13*HFB/(fW1*WFB3)))
* HAXV233=COS(ATAN(fH13*HFB/((1-fW1)*WFB3)))
* HFPAX33=HFP133*HFPR13*HAXV133+HFP223*HFPR23*HAXV233

* HFP134=MU0*IPB/(4*pi()*((fW1*WFB3)^2+(fH14*HFB)^2)^.5)
* HFP234=MU0*IPB/(4*pi()*(((1-fW1)*WFB3)^2+(fH14*HFB)^2)^.5)
* HAXV134=COS(ATAN(fH14*HFB/(fW1*WFB3)))
* HAXV234=COS(ATAN(fH14*HFB/((1-fW1)*WFB3)))
* HFPAX34=HFP134*HFPR13*HAXV134+HFP234*HFPR23*HAXV234

* HFP135=MU0*IPB/(4*pi()*((fW1*WFB3)^2+(fH15*HFB)^2)^.5)
* HFP235=MU0*IPB/(4*pi()*(((1-fW1)*WFB3)^2+(fH15*HFB)^2)^.5)
* HAXV135=COS(ATAN(fH15*HFB/(fW1*WFB3)))
* HAXV235=COS(ATAN(fH15*HFB/((1-fW1)*WFB3)))
* HFPAX35=HFP135*HFPR13*HAXV135+HFP235*HFPR23*HAXV235
```

```
* HFPAX3=HFPAX31+HFPAX32+HFPAX33+HFPAX34+HFPAX35

 "LAYER 4

* PUMP*PHI14=ATAN((fX-fL1)*X/(fW1*WFB4))*PUMP
* PUMP*PHI24=ATAN((fL2-fX)*X/(fW1*WFB4))*PUMP
* PUMP*PHI34=ATAN((fX-fL1)*X/((1-fW1)*WFB4))*PUMP
* PUMP*PHI44=ATAN((fL2-fX)*X/((1-fW1)*WFB4))*PUMP
* PUMP*HFPR14=(HF14+HF24)*PUMP
* PUMP*HFPR24=(HF34+HF44)*PUMP
* HF14=SIN(PHI14)
* HF24=SIN(PHI24)
* HF34=SIN(PHI34)
* HF44=SIN(PHI44)

* HFP141=MU0*IPB/(4*pi()*((fW1*WFB4)^2+(fH11*HFB)^2)^.5)
* HFP241=MU0*IPB/(4*pi()*(((1-fW1)*WFB4)^2+(fH11*HFB)^2)^.5)
* HAXV141=COS(ATAN(fH11*HFB/(fW1*WFB4)))
* HAXV241=COS(ATAN(fH11*HFB/((1-fW1)*WFB4)))
* HFPAX41=HFP141*HFPR14*HAXV141+HFP241*HFPR24*HAXV241

* HFP142=MU0*IPB/(4*pi()*((fW1*WFB4)^2+(fH12*HFB)^2)^.5)
* HFP242=MU0*IPB/(4*pi()*(((1-fW1)*WFB4)^2+(fH12*HFB)^2)^.5)
* HAXV142=COS(ATAN(fH12*HFB/(fW1*WFB4)))
* HAXV242=COS(ATAN(fH12*HFB/((1-fW1)*WFB4)))
* HFPAX42=HFP142*HFPR14*HAXV142+HFP242*HFPR24*HAXV242

* HFP143=MU0*IPB/(4*pi()*((fW1*WFB4)^2+(fH13*HFB)^2)^.5)
* HFP243=MU0*IPB/(4*pi()*(((1-fW1)*WFB4)^2+(fH13*HFB)^2)^.5)
* HAXV143=COS(ATAN(fH13*HFB/(fW1*WFB4)))
* HAXV243=COS(ATAN(fH13*HFB/((1-fW1)*WFB4)))
* HFPAX43=HFP143*HFPR14*HAXV143+HFP243*HFPR24*HAXV243

* HFP144=MU0*IPB/(4*pi()*((fW1*WFB4)^2+(fH14*HFB)^2)^.5)
* HFP244=MU0*IPB/(4*pi()*(((1-fW1)*WFB4)^2+(fH14*HFB)^2)^.5)
* HAXV144=COS(ATAN(fH14*HFB/(fW1*WFB4)))
* HAXV244=COS(ATAN(fH14*HFB/((1-fW1)*WFB4)))
* HFPAX44=HFP144*HFPR14*HAXV144+HFP244*HFPR24*HAXV244

* HFP145=MU0*IPB/(4*pi()*((fW1*WFB4)^2+(fH15*HFB)^2)^.5)
* HFP245=MU0*IPB/(4*pi()*(((1-fW1)*WFB4)^2+(fH15*HFB)^2)^.5)
* HAXV145=COS(ATAN(fH15*HFB/(fW1*WFB4)))
* HAXV245=COS(ATAN(fH15*HFB/((1-fW1)*WFB4)))
* HFPAX45=HFP145*HFPR14*HAXV145+HFP245*HFPR24*HAXV245

* HFPAX4=HFPAX41+HFPAX42+HFPAX43+HFPAX44+HFPAX45

 "LAYER 5

* PUMP*PHI15=ATAN((fX-fL1)*X/(fW1*WFB5))*PUMP
* PUMP*PHI25=ATAN((fL2-fX)*X/(fW1*WFB5))*PUMP
* PUMP*PHI35=ATAN((fX-fL1)*X/((1-fW1)*WFB5))*PUMP
* PUMP*PHI45=ATAN((fL2-fX)*X/((1-fW1)*WFB5))*PUMP
* PUMP*HFPR15=(HF15+HF25)*PUMP
* PUMP*HFPR25=(HF35+HF45)*PUMP
* HF15=SIN(PHI15)
* HF25=SIN(PHI25)
* HF35=SIN(PHI35)
```

```
* HF45=SIN(PHI45)

* HFP151=MU0*IPB/(4*pi()*((fW1*WFB5)^2+(fH11*HFB)^2)^.5)
* HFP251=MU0*IPB/(4*pi()*(((1-fW1)*WFB5)^2+(fH11*HFB)^2)^.5)
* HAXV151=COS(ATAN(fH11*HFB/(fW1*WFB5)))
* HAXV251=COS(ATAN(fH11*HFB/((1-fW1)*WFB5)))
* HFPAX51=HFP151*HFPR15*HAXV151+HFP251*HFPR25*HAXV251

* HFP152=MU0*IPB/(4*pi()*((fW1*WFB5)^2+(fH12*HFB)^2)^.5)
* HFP252=MU0*IPB/(4*pi()*(((1-fW1)*WFB5)^2+(fH12*HFB)^2)^.5)
* HAXV152=COS(ATAN(fH12*HFB/(fW1*WFB5)))
* HAXV252=COS(ATAN(fH12*HFB/((1-fW1)*WFB5)))
* HFPAX52=HFP152*HFPR15*HAXV152+HFP252*HFPR25*HAXV252

* HFP153=MU0*IPB/(4*pi()*((fW1*WFB5)^2+(fH13*HFB)^2)^.5)
* HFP253=MU0*IPB/(4*pi()*(((1-fW1)*WFB5)^2+(fH13*HFB)^2)^.5)
* HAXV153=COS(ATAN(fH13*HFB/(fW1*WFB5)))
* HAXV253=COS(ATAN(fH13*HFB/((1-fW1)*WFB5)))
* HFPAX53=HFP153*HFPR15*HAXV153+HFP253*HFPR25*HAXV253

* HFP154=MU0*IPB/(4*pi()*((fW1*WFB5)^2+(fH14*HFB)^2)^.5)
* HFP254=MU0*IPB/(4*pi()*(((1-fW1)*WFB5)^2+(fH14*HFB)^2)^.5)
* HAXV154=COS(ATAN(fH14*HFB/(fW1*WFB5)))
* HAXV254=COS(ATAN(fH14*HFB/((1-fW1)*WFB5)))
* HFPAX54=HFP154*HFPR15*HAXV154+HFP254*HFPR25*HAXV254

* HFP155=MU0*IPB/(4*pi()*((fW1*WFB5)^2+(fH15*HFB)^2)^.5)
* HFP255=MU0*IPB/(4*pi()*(((1-fW1)*WFB5)^2+(fH15*HFB)^2)^.5)
* HAXV155=COS(ATAN(fH15*HFB/(fW1*WFB5)))
* HAXV255=COS(ATAN(fH15*HFB/((1-fW1)*WFB5)))
* HFPAX55=HFP155*HFPR15*HAXV155+HFP255*HFPR25*HAXV255

* HFPAX5=HFPAX51+HFPAX52+HFPAX53+HFPAX54+HFPAX55

* BAX11=HFPAX1
* BAX12=BAX11+HFPAX2
* BAX13=BAX12+HFPAX3
* BAX14=BAX13+HFPAX4
* BAX15=BAX14+HFPAX5

* LAY1CONTR=HFPAX1/HFPAXT*100
* LAY2CONTR=HFPAX2/HFPAXT*100
* LAY3CONTR=HFPAX3/HFPAXT*100
* LAY4CONTR=HFPAX4/HFPAXT*100
* LAY5CONTR=HFPAX5/HFPAXT*100

* HFPAXT=HFPAX1+HFPAX2+HFPAX3+HFPAX4+HFPAX5
```

MMMMMMMMMMMMMMMMMMMMM TABLE SHEET MMMMMMMMMMMMMMMMMMMMMMMMMMMMMMMMMMMMMMMMMMMMMMMMMM

NameDDDDDDDDDD	TitleDDDDDDDDDDDDDDDDDDDDDDDDDDDDDDDDDDDDDDDDDDDDDDDDDDD
HFP_2_8_91	HL, L=12, W=.6 DISTRIBUTION OF MAGNETIC FIELD
H_ANGLE_2_8_91	HL, L=12, W=.6 MAGNETIC FIELD INTEGRATION ANGLES
H_SIN_2_8_91	HL, L=12, W=.6 MAGNETIC FIELD INTEGRATION FRACTIONS
HL_2_8_91	HL, MAGNETIC FIELD ALONG DUCT (fW=.5)
HW_2_8_91	HW, MAGNETIC FIELD ACROSS DUCT (fL=.5)
BH_2_11_91	BH, MAGNETIC FIELD VS HEIGHT BETWEEN BUSBARS
CIRCCALC	EQUIPOTENTIAL CIRCLE CALCULATIONS
HW_7_15_91	HW, MAGNETIC FIELD ACROSS DUCT (fL=.21)
LARGE_LM	AXIAL FLUX OF LAYERS VS HEIGHT
LARGE_LM1	AXIAL FLUX VS CROSS-SECTIONAL AREA OF BUSBARS
LARGE_LM2	CONTRIBUTIONS OF LAYERS TO MAGNETIC FLUX

APPENDIX E

DESIGN MODEL
VCLCP

MMMMMMMMMMMMMMMMMMMM VARIABLE SHEET MMMMMMMMMMMMMMMMMMMMMMMMMMMMMMMMMMMMMMMMMMMMM

St	Input	Name	Output	Unit	Comment
					FILE:VCLCP.TK 37 kB VERIFICATION CORELESS LINEAR CONDUCTION PUMP (VCLCP) PROGRAM DESIGN AND PERFORMANCE PROGRAM 3/28/91
	.125	DPDLE		psi	Delivered pressure from cell
	2	QE		gpm	Volumetric flowrate
		DPDL	.861875	kPa	Delivered pressure from cell
		TDPDL		kPa	Trial DPDL
		Q	.12618297	litre/s	Volumetric flowrate
		DPDV	395.28887	kPa	Differential pressure rise developed
		DPMB	220.43099	kPa	Pressure loss from magnetic braking
		DPMF	173.82796	kPa	Pressure loss from magnetic fringe
		DPHY	.16804477	kPa	Pressure loss from fluid friction
		DPT	.02522894	Pa	Pressure loss in throat flow
		DPNAD	.14281583	Pa	Pressure loss in nozzle and diffuser
		B	3041.8864	mT	Magnetic flux noraml to Q and I
		BOPT	1902.7648	mT	Optimum magnetic flux
		IT	1.2510426	kA	Total pump current
		IL	1.0026123	kA	Electric current in fluid
		IA	1.2510426	kA	Armature busbar current
	2	IF		kA	Field busbar current
	6.35	H		mm	Inside height of throat duct
	12.7	W		mm	Inside width of throat duct
	35	LT		mm	Length of throat
		V	1.5646719	m/s	Velocity of liquid in throat
		VMAX		m/s	Velocity limited by cavitation
		M1	129.61002	1/m	First term coefficient
		M2	188793020	1/Ohm-m^2	Second term coefficient
		M3	148878825	1/Ohm-m^2	Third term coefficient
		M4	1	-	Fourth term coefficient
		AF	80.645	mm^2	Throat cross-sectional flow area
		IC	.46015419	kA	Counter current from CEMF
		RB	108113.25	nOhm	Electrical resistance bypassing fluid
		RL	23247.805	nOhm	Electrical resistance across W
		RHOL	406.83658	nOhm-m	Resistivity of fluid
		RA	26788.63	nOhm	Electrical resistance armature current
		RWP	308034.09	nOhm	Parallel Resistance of throat walls
		RHOW	786.94841	nOhm-m	Resistivity of duct wall
		RWS	3540.8252	nOhm	Series Resistance of throat wall
		RFR	166578.76	nOhm	Resistance of fringe path
		RFB	.12903451	Ohm	Resistance of field busbar(coil)
		RHOFB	24.5	nOhm-m	Resistivity of field busbar material
	.000006	AFB		m^2	Cross-section area of coil wires
		RAB	38582.677	nOhm	Resistance of armature busbar
		RHOAB	24.5	nOhm-m	Resistivity - armature busbar material
		RCELL	111273.31	nOhm	FBB to FBB Resistance of pump cell
		RTP	45902.002	nOhm	Resistance of tap pin
		RHOTP	786.94841	nOhm-m	Resisitivity of Tap Pin
	1	FX		_	Empirical factor from MSA calcs
	.5	TW		mm	Thickness of throat walls
		NRE	20989.073	-	Reynolds Number in the throat
		RH	2.1166667	mm	Hydraulic radius in the throat
		DPCV		Pa	Pressure margin for cavitation limit
	.0000001	EPSOD			Ratio e/D

	LAMINAR	0		1 = the flow IS laminar, 0 = IS NOT
	TURBLNT	1		1 = the flow IS transient or turbulen
	f	.00587584	-	Fluid friction factor in throat
	HYHD	1038.6606	Pa	Hydraulic velocity head in throat
.05	CN		-	Discharge coefficient of nozzles
.8	E		-	Diffuser recovery coefficient
.75	AR		-	Area ratio throat to pipe
	D	11.700735	mm	Diameter of circuit piping
	PIE	202194.35	W	Input power to EMP (electrical)
	VC	60.446338	mVolt	Counter EMF of fluid moving across B
	VLL	23.308535	mVolt	Voltage drop across liquid
	VWS	3.5500749	mVolt	Voltage drop across wall
	VA	26.85861	mVolt	Voltage drop outside of duct
	VAB	48.268574	mVolt	Voltage drop across armature buses
	VTP	57.425361	mVolt	Voltage drop across tap pin
	VFB	161.42768	Volt	Voltage drop across field buses
	VCELL	192.99888	mVolt	Voltage drop across pump cell
	VL	161.62067	Volt	"Load or terminal voltage of TEG or EMP
	EEH	5.3787E-5	%	Electrical to hydraulic efficiency
	POH	.10875394	W	Output power (hydraulic)
	VOLND		mm^3	Volume of nozzle and diffuser
	VOLNDI		mm^3	Volume of nozzle
	VOLNDO		mm^3	Volume of diffuser
	S		mm^2	Surface area of nozzle and diffuser
	R2		mm	Equivalent radius of throat area
	LNDI		mm	Length of nozzle
	LNDO		mm	Length of diffuser
	LND		mm	Length of nozzle and of diffuser
373	TL		K	Temperature of fluid
373	TDW		K	Temperature of the walls
	MND		kg	Mass of nozzles and diffusers
	ML		kg	Mass of fluid
	MT		kg	Mass of pump throat
	MB		kg	Mass of busbar
	MASS		kg	Total mass of EMP
	TI		mm	Thickness of electrical insulation
295	TRML		K	
295	TRM		K	Room temperature
	TWK	373	K	Temperaure of wall material
	CEMF	60.446338	mV	
				MAGNETIC FIELD CALCULATIONS
				2-13-91
	I	2000	A	Field Current
.5	fW		-	Fraction of WFB
.02	WFB		m	Center-center span between field buses
.25	fL1		-	Fractional location of L1
.75	fL2		-	Fractional location of L2
	L1	.06	m	Inlet end of Field busbars
	L2	.18	m	Discharge end of Field busbars
.5	fX		-	Fraction of total pump length
.24	X		m	Total pump length
	UP	0	-	Upstream region indicator
	PUMP	1	-	Pumping section region indicator
	DOWN	0	-	Downstream region indicator
	PHI1	1.4056476	rad	Angular integration limit
	PHI2	1.4056476		Angular integration limit

		PHI3	1.4056476		Angular integration limit
		PHI4	1.4056476		Angular integration limit
		HF1	.98639392		Integrated flux fraction
		HF2	.98639392		Integrated flux fraction
		HF3	.98639392		Integrated flux fraction
		HF4	.98639392		Integrated flux fraction
		HFPR1	1.9727878		Total integrated fractions, bar 2
		HFPR2	1.9727878		Total integrated fractions, bar 1
L		HFP1	20.005776	mT	Magnetic Flux from bar 1
L		HFP2	20.005776	mT	Magnetic Flux from bar 2
	1.257E-6	MU0		T-m/A	Absolute Permeability
		N	38.536938	turns	Number of coil turns
	.01	d		m	Midpoint between long sides of coils
L		HFP	78.934305	mT	Total magnetic flux
	.35	LFB		m	Length of field busbar
	.00635	FBW		m	Thickness of field busbar
	.0635	LAB		m	Length of amature busbar
	.00635	TAB		m	Thickness of armature busbar
	.000508	LTP		m	Length of Tap Pin
		ATP	8.709E-10	m^2	Cross-sectional area of Tap Pin
	.00333	DOTP		m	Outside diameter of Tap Pin
	0	DITP		m	Inside diameter of Tap Pin
L	0	fH		-	Fraction of height between busbars
	.0127	HFB		m	Height of the busbars
	373	TCU		K	Temperature
					MATERIALS PROPERTIES
					STAINLESS STEEL
		DENRTW		Mg/m^3	RT density of wall material
		RHOSS	786.94841	nOhm-m	Resistivity of 300 series
		DENW	7.68	Mg/m^3	Density of wall material
					NAK-78 ALLOY
		PV		Pa	Vapor Pressure
		K		W/m-K	Thermal Conductivity
		RHO			
		DEN		Mg/m^3	Density
		RHO78	406.83658	nOhm-m	Resisitivity of NAK-78
		MU	.53554943	cp	Viscosity of fluid
		DENL	.8485102	Mg/m^3	Density of fluid
		DENRTL		Mg/m^3	RT density of fluid
		DENRML		Mg/m^3	RT density of fluid
					COPPER
		DENSB		Mg/m^3	Density of busbar
		RHOCU	24.5	nOhm-m	Resistivity

```
MMMMMMMMMMMMMMMMMMMM RULE SHEET MMMMMMMMMMMMMMMMMMMMMMMMMMMMMMMMMMMMMMMMMMMMMMMM
S RuleDDDDDDDDDDDDDDDDDDDDDDDDDDDDDDDDDDDDDDDDDDDDDDDDDDDDDDDDDDDDDDDDDDDDDD
  "VCLCP DESIGN AND PERFORMANCE PROGRAM
  "04-1-91

* QE=15850*Q
* DPDV=M1*B*IL
* DPMB=M2*B^2*Q
* DPMF=M3*B^2*Q
* DPHY=(DPT+DPNAD)*1000
* DPDL=DPDV-DPMB-DPMF-DPHY
  "TDPDL=DPDV-DPMB-DPMF-DPHY
* CEMF=B*W*Q/AF
* AF=W*H
* IC=CEMF/(RB+RL)
* IL=IA*RB/(RB+RA)
  "IA=IT*RFB/(RFB+RCELL)
* IA=IT
* RL=RHOL*W/(H*LT)
* RHOL=RHO78
* RA=RL+RWS
* RWS=RHOW*2*TW/(H*LT)
* RHOW=RHOSS
* RB=RFR*RWP/(RFR+RWP)
* RFR=2.6*FX*RHOL/H
* RWP=RHOW*(W+2*TW)/(TW*2*LT)
* RFB=RHOFB*N/(AFB)*(2*LFB+6*WFB)
* RHOFB=RHOCU
* RCELL=RTP+RAB+RA
* RAB=RHOAB*LAB/(H*TAB)
* RHOAB=RHOCU
* RTP=RHOTP*LTP/ATP
* RHOTP=RHOSS
* ATP=PI()*(DOTP^2-DITP^2)/4
* M1=RB/(RB+RL)*1/H
* M2=1/(RB+RL)*1/H^2
* M3=1/(H^2*RFR)
* M4=1
* NRE=DENL*V*4*RH/(MU*10^-6)
* RH=W*H/(2*(W+H))
* V=Q/AF
* DPCV=DENL*VMAX^2/2
* LAMINAR=STEP(2000,NRE)
* TURBLNT=1-LAMINAR
* LAMINAR*f=64/NRE*LAMINAR
  "(1-LAMINAR)*1/sqrt(f)=-2*log(EPSOD/3.7+2.51/(NRE*sqrt(f)))*(1-LAMINAR)
* (TURBLNT)*f=.043/NRE^.2*(TURBLNT)                              "For 5000<NRE<20000
* HYHD=DENL*V^2/2
* DPT=f*LT/(4*RH)*HYHD
* DPNAD=(CN+(1-E)*(1-AR^2))*HYHD
* AR=4*W*H/(PI()*D^2)
* PIE=VL*IA
* BOPT=M1*IA/(2*(M2+M3)*Q)
  "B=BOPT
* EEH=POH/PIE*100
  "MT=2*(H+W)*TW*LT*DENRTW
  "ML=2*(H*W*LT+VOLND)*DENRTL
  "ML=2*(H*W*LT+4*VOLND)*DENRTL
```

```
  "S=(PI()*D+2*(W+H))*(LNDI+LNDO)/2
  "S=PI()*(D/2+R2)*(LND^2+(D/2-R2)^2)^(1/2)
  "LNDI=(H-D)/(2*TAN(PI()/12))
  "LNDO=(H-D)/(2*TAN(PI()/24))
  "LND=LNDI+LNDO
  "LND=(D/2-R2)/TAN(PI()/12)
  "MND=2*S*TW*DENRTW
  "MND=4*S*TW*DENRTW
  "VOLNDI=(PI()*D^2/4+W*H)*LNDI/2
  "VOLNDO=(PI()*D^2/4+W*H)*LNDO/2
  "VOLND=VOLNDI+VOLNDO
  "VOLND=PI()*LND/3*((D/2)^2+D/2*R2+R2^2)
  "R2=(W^2+H^2)^(1/2)/2
* TWC=TL-273
* TWK=TL

  "MATERIALS PROPERTIES

  "NB-ZR ALLOY

  "DENW=8.6304-1.895E-4*TWK-1.23E-8*TWK^2
  "DENRTW=8.6304-1.895E-4*TRM-1.23E-8*TRM^2
  "RHOW=16.337+4.224E-2*TWC-4.922E-6*TWC^2-3.941E-10*TWC^3 "microOhm-cm

  "316 STAINLESS STEEL

* DENW=7.68+0.E-2*TWK+0.E-6*TWK^2                  "Mg/m^3
* RHOSS=(47.874+7.1365*10^-2*TDW+3.02*10^-5*TDW^2)*10^-8 "Ohm-m

  "LITHIUM

  "RHOL=13.735+2.9256E-2*TL-2.46E-6*TL^2           "micro-Ohm-cm
  "DENL=.5593-1.133E-4*TL+1.58E-8*TL^2             "Mg/m^3
  "DENRTL=.5593-1.133E-4*TRM+1.58E-8*TRM^2         "Mg/m^3
  "MU=1.8739-4.667E-3*TL+4.933E-6*TL^2-1.867E-9*TL^3    "centipoise

  "MOLYBDENUM

  "RHOMo=-0.183+2.0321E-2*TL                            "microOhm-cm
  "DENMo=10.2698-1.056E-4*TL-4.08E-8*TL^2               "Mg/m^3
  "KMo=(0.3602-1.142E-4*TL+2.050E-8*TL^2)*4.1868        "W/cm-K

  "NAK-78

  "RHOL=36.768-1.6212E-2*TL+7.1741E-5*TL^2                   "micro-Ohm-cm
* RHO78=(36.75-1.631*10^-2*TL+7.2*10^-5*TL^2)*10^-8          "Ohm-m
* DENL=.9390-2.426E-4*TL                                    "Mg/m^3
  "DENRML=.9390-2.426E-4*TRML                               "Mg/m^3
  "MU=1.1914-2.7431E-3*TL+2.5463E-6*TL^2-8.492E-10*TL^3 "centipoise
* MU=3.437-1.62*10^-2*TL+3.184*10^-5*TL^2-2.833*10^-8*TL^3+9.375*10^-12*TL^4
                                                                              "mPa-s
  "K=-6.917+1.872*10^-1*TL-4.377*10^-4*TL^2+4.858*10^-7*TL^3-2.08*10^-10*TL^4
                                                                              "W/m-K
  "PV=3.1622*10^9/(EXP(10686/T))                              "Pa

  "COPPER

* RHOCU=(-.96471+6.454*10^-2*TCU+1*10^-5*TCU^2)*1e-9              "Ohm-m
```

```
  "SINGLE-PASS PUMP SECTION
* DPDL=DPDLE                                  "SP
* VLL=IL*RL                                   "SP
* VWS=IL*RWS                                  "SP
* VA=IL*RA                                    "SP
* VC=CEMF                                     "SP
* VCELL=VC+VLL+VWS+VAB+VTP                    "SP
* VL=VCELL+VFB                                    "SP
* VTP=IA*RTP                                  "SP
* VFB=IA*RFB                                  "SP
* VAB=IA*RAB                                  "SP
* POH=DPDL*Q                                  "SP
  "LB=H/2+TI+3/2*TB+W                          "SP
  "MB=(LB-TB/2+H/2)*TB*LT*DENSB                "SP

* RHOB=RHOCU
  "RBS= RHOB*LB/(LT*TB)*10^-8
  "VBS=IT*RBS
  "MASS=MM+MB+MT+ML+MND

  "DOUBLE-PASS PUMP SECTION

  "DPDL=DPDLE/2                                   "DP
  "VLL=2*IT*RB/(RB+RL)*RL                         "DP
  "VLW=2*IT*RB/(RB+RL)*RTW                        "DP
  "VL=VLL+VLW+VC+VBS                              "DP
  "VC=2*CEMF                                      "DP"
  "POH=2*DPDL*Q                                   "DP
  "LB=TB+TI+H                                     "DP
  "MB=(2*H+3*TI+4*TW)*TB*LT*DENSB                 "DP
  "DENSB=DENMo

  "MAGNETIC FLUX CALCULATIONS FOR A RECTANGULAR COIL ELECTROMAGNETIC PUMP
  "2/7/91

* UP=(1-STEP(fX,fL1))                        "STEP=1 if fX=, >fL1 and 0 otherwise
* PUMP=STEP(fX,fL1)*STEP(fL2,fX)             "CASE=1 for fL1<fX<fL2
* DOWN=(1-STEP(fL2,fX))                      "STEP=1 if fX<fl2
* L1=fL1*X
* L2=fL2*X

  "UPSTREAM OF PUMPING SECTION

* UP*PHI1=ATAN((fL1-fX)*X/(fW*WFB))*UP
* UP*PHI2=ATAN((fL2-fX)*X/(fW*WFB))*UP
* UP*PHI3=ATAN((fL1-fX)*X/((1-fW)*WFB))*UP
* UP*PHI4=ATAN((fL2-fX)*X/((1-fW)*WFB))*UP
* UP*HFPR1=(HF2-HF1)*UP
* UP*HFPR2=(HF4-HF3)*UP

  "PUMPING SECTION REGION

* PUMP*PHI1=ATAN((fX-fL1)*X/(fW*WFB))*PUMP
* PUMP*PHI2=ATAN((fL2-fX)*X/(fW*WFB))*PUMP
* PUMP*PHI3=ATAN((fX-fL1)*X/((1-fW)*WFB))*PUMP
* PUMP*PHI4=ATAN((fL2-fX)*X/((1-fW)*WFB))*PUMP
```

```
* PUMP*HFPR1=(HF1+HF2)*PUMP
* PUMP*HFPR2=(HF3+HF4)*PUMP

* HF1=SIN(PHI1)
* HF2=SIN(PHI2)
* HF3=SIN(PHI3)
* HF4=SIN(PHI4)
* I=IF
* HFP1=MU0*I/(4*PI()*((fW*WFB)^2+(fH*HFB)^2)^.5)
* HFP2=MU0*I/(4*PI()*(((1-fW)*WFB)^2+(fH*HFB)^2)^.5)
* HFP=HFP1*HFPR1+HFP2*HFPR2
* B=N*HFP

  "DOWNTSTREAM OF PUMPING SECTION

* DOWN*PHI1=ATAN((fX-fL1)*X/(fW*WFB))*DOWN
* DOWN*PHI2=ATAN((fX-fL2)*X/(fW*WFB))*DOWN
* DOWN*PHI3=ATAN((fX-fL1)*X/((1-fW)*WFB))*DOWN
* DOWN*PHI4=ATAN((fX-fL2)*X/((1-fW)*WFB))*DOWN
* DOWN*HFPR1=(HF1-HF2)*DOWN
* DOWN*HFPR2=(HF3-HF4)*DOWN


* N=4/(HFPR1+HFPR2)*(M1/(2*(M2+M3))*PI()*d/(MU0*Q))
```

MMMMMMMMMMMMMMMMMMMMM UNIT SHEET MMMMMMMMMMMMMMMMMMMMMMMMMMMMMMMMMMMMMMMMMMMMMMMMMM

FromDDDDD	ToDDDDDDD	Multiply ByDD	Add OffsetDDD
T	mT	1000	
psi	Pa	6895	
N/m^2	Pa		
Mg/m-s^2	Pa	1000	
Pa-m^3/s	W		
kPa	T-A-m/m^2		
kPa	Pa	1000	
m^2/s^2	Pa-m^3/Mg	1000	
kPa	T-A-m/m^2		
cm	mm	10	
m^2	cm^2	10000	
m	cm	100	
m	mm	1000	
m^2	mm^2	1000000	
m^3	mm^3	1E9	
m^3/s	litre/s	1000	
litre/s	gpm	15.85	
T-m^2/s	mVolt	1000	
T-A-m	N		
Volt	Ohm-A		
T-m^2/s	Ohm-A		
T-m^2/s	Ohm-A		
Ohm-A	mVolt	1000	
Volt	mVolt	1000	
Mg/m-s	cp	1000000	
Mg	kg	1000	
kg	hg	10	
Mg	kg	1000	
kA	A	1000	
kA	hA	10	
Volt-A	kW	.001	
V	mV	1000	
Pa-m^3/s	W		
kW	Volt-A	1000	
W	Volt-A		
Ohm-m	nOhm-m	1E9	
Ohm-m	uOhm-m	1000000	
Ohm-m	mOhm-m	1000	
Ohm	uOhm	1000000	
Ohm	mOhm	1000	
Ohm	nOhm	1E9	

FLUX VS VARIABLES

FLUX	10	15	20	25	30	35
EFF	13.3833872	25.1620972	36.2249292	45.2431519	51.9858677	56.7062036
LOADV	623.767694	493.226541	451.170387	444.508234	455.543081	476.690499
AMPS	1750.5502	1177.52522	894.160246	726.659284	617.090326	540.625369
MASS	?9890.905	?11249.162	?12606.82	?13969.364	?15341.09	?16725.398
POWER	1091.93666	580.786689	403.418625	323.006035	281.111228	257.710977
WIDTH	664.6	664.6	664.6	664.6	664.6	664.6
LENGTH	11750	11750	11750	11750	11750	11750
HIEGHT	221.5	221.5	221.5	221.5	221.5	221.5
MAGNET	2748.8978	4107.15498	5464.81244	6827.3565	8199.08262	9583.39045
BUSBAR	4246.71221	4246.71221	4246.71221	4246.71221	4246.71221	4246.71221
DIFFUSER	52.9553838	52.9553838	52.9553838	52.9553838	52.9553838	52.9553838
LIQUID	2753.07589	2753.07589	2753.07589	2753.07589	2753.07589	2753.07589
THROAT	89.2637365	89.2637365	89.2637365	89.2637365	89.2637365	89.2637365

FLUX VS VARIABLES

FLUX	40	45	50	55	60	65
EFF	59.7845301	61.5819715	62.3982191	62.4696543	61.9794225	61.0689519
LOADV	504.158274	535.839621	570.470467	607.246405	645.631161	685.253469
AMPS	484.850414	442.868793	410.542506	385.23828	365.2006	349.214108
MASS	?18125.004	?19542.098	?20978.458	?22435.54	?23914.539	?25416.448
POWER	244.441348	237.306646	234.202375	233.934561	235.784887	239.300179
WIDTH	664.6	664.6	664.6	664.6	664.6	664.6
LENGTH	11750	11750	11750	11750	11750	11750
HIEGHT	221.5	221.5	221.5	221.5	221.5	221.5
MAGNET	10982.9966	12400.0907	13836.4511	15293.5324	16772.5319	18274.441
BUSBAR	4246.71221	4246.71221	4246.71221	4246.71221	4246.71221	4246.71221
DIFFUSER	52.9553838	52.9553838	52.9553838	52.9553838	52.9553838	52.9553838
LIQUID	2753.07589	2753.07589	2753.07589	2753.07589	2753.07589	2753.07589
THROAT	89.2637365	89.2637365	89.2637365	89.2637365	89.2637365	89.2637365

FLUX VS VARIABLES

FLUX	70
EFF	59.8477639
LOADV	725.84814
AMPS	336.410694
MASS	?26942.092
POWER	244.183077
WIDTH	664.6
LENGTH	11750
HIEGHT	221.5
MAGNET	19800.0849
BUSBAR	4246.71221
DIFFUSER	52.9553838
LIQUID	2753.07589
THROAT	89.2637365

```
(s) Screen or Printer: Printer                                         25+/1
Display options: Screen  Printer
MMMMMMMMMMMMMMMMMMMM TABLE: FLUX MMMMMMMMMMMMMMMMMMMMMMMMMMMMMMMMMMMMMMMMMMMMMM
Screen or Printer:            Printer
Title:                        FLUX VS VARIABLES
Vertical or Horizontal:       Horizontal
Row Separator:
Column Separator:
First Element:                1
Last Element:                 13
ListDDDDD Numeric FormatDD WidthDD HeadingDDDDDDDDDDDDDDDDDDDDDDDDDDDDDDDDDDDDD
B                          10      FLUX
EEH                        10      EFF
VL                         10      LOADV
IT                         10      AMPS
MASS                       10      MASS
PIE                        10      POWER
W                          10      WIDTH
LT                         10      LENGTH
H                          10      HIEGHT
MM                         10      MAGNET
MB                         10      BUSBAR
MND                        10      DIFFUSER
ML                         10      LIQUID
  F1 Help  F2 Cancel  F5 Edit  F9 Solve  / Commands  = Sheets  ; Window switch
```

APPENDIX F

RESISTANCE NETWORK ANALYTICAL MODEL
OF CLCP
RESCALCS.TK

MMMMMMMMMMMMMMMMMMMMM VARIABLE SHEET MMMMMMMMMMMMMMMMMMMMMMMMMMMMMMMMMMMMMMMMMMMMM

St	InputDDDD	NameDDD	OutputDDD	UnitDDDDD	CommentDDDDDDDDDDDDDDDDDDDDDDDDDDDDD
					RESISTANCE CALCULATIONS FOR CLCP
					FILE:RESCALCS.TK
		RFB	5.3568E-5	Ohm	Resistance of field busbar
	.0000018	RHOCU		Ohm-cm	Resistivity of field busbar
	12	LT		cm	length of busbar
	1.27	FBH		cm	Field bubar height
	.635	FBW		cm	Field bubar width
		RAB	.00013392	Ohm	Resistance of armature busbar
	1.27	ABH		cm	Armature busbar height
	.254	ABW		cm	Armature busbar width
		RSDW	.00000048	Ohm	Resistance of series duct wall
	.000072	RHOSS		Ohm-cm	Resistivity if duct wall
	.0508	TW		cm	Thkn of series duct wall
		RPDW	.0000375	Ohm	Resistance of 2-parallel duct walls
	.635	W			Width of duct
		RNAK	1.6959E-6		Resistance of the fluid (NaK)
		RHONAK	4.0702E-5		Resistivity of NaK
	1.27	H		CM	Inside duct height
	373	TL			
		RCEMFEQ	.0000127	Ohm	Equivalent resistance of CEMF
		CEMF	.00635	V	Counter EMF of fluid in magnetic field
	1000	B		G	Magnetic field density
	500	IA		A	Armature current
	1000	V		cm/s	Velocity of fluid in duct
L		RTP	.00025	Ohm	Resistance of tap pins
	.0508	LTP		cm	Length of tap pins
	.34559261	DOTP		cm	Outside diameter of tap pins
	.3175	DITP		cm	Inside diameter of tap pins
		ATP		cm^2	Cross-sectional area of tap pins
L		DOTPE	.13606008	in.	
L		DITPE	.125	in.	
		R7	1		Resistance ratio RSDW/RSDW
		R4	3.5331751		Resistance ratio NaK/RSDW
		R5	26.458333		Resistance ratio RCEMFEQ/RSDW
		R3	78.125		Resistance ratio RPDW/RSDW
		R1	111.60022		Resistance ratio RFB/RSDW
		R2	279.00056		Resistance ratio RAB/RSDW
		R6	520.83333		Resistance ratio RTP/RSDW
					RTP can be varied to a ratio of 104 or less.

```
MMMMMMMMMMMMMMMMMMMM RULE SHEET MMMMMMMMMMMMMMMMMMMMMMMMMMMMMMMMMMMMMMMMMMMMMMMM
S RuleDDDDDDDDDDDDDDDDDDDDDDDDDDDDDDDDDDDDDDDDDDDDDDDDDDDDDDDDDDDDDDDDDDDDDDDDD
  "RESISTANCE OF CLCP MATERIALS

* RFB=RHOCU*2*LT/(FBH*FBW)
* RAB=RHOCU*2*LT/(ABH*ABW)
* RSDW=2*RHOSS*TW/(ABH*LT)
* RPDW=RHOSS*W/(2*TW*LT)
* RNAK=RHONAK*W/(H*LT)
* RHONAK=(36.768-1.6212*10^-2*TL+7.1741*10^-5*TL^2)*10^-6
* CEMF=B*V*W*10^-8
* RCEMFEQ=CEMF/IA
  "ATP=PI()*(DOTP^2-DITP^2)/4
  "RTP=RHOSS*LTP/ATP
  "ATP=PI()*DOTP^2/4
* RTP=RHOSS*LTP/(PI()*(DOTP^2-DITP^2)/4)
* DOTPE=DOTP/2.54
* DITPE=DITP/2.54
* R1=RFB/RSDW
* R2=RAB/RSDW
* R3=RPDW/RSDW
* R4=RNAK/RSDW
* R5=RCEMFEQ/RSDW
* R6=RTP/RSDW
* R7=RSDW/RSDW


MMMMMMMMMMMMMMMMMMMM TABLE SHEET MMMMMMMMMMMMMMMMMMMMMMMMMMMMMMMMMMMMMMMMMMMMMMM
NameDDDDDDDDD TitleDDDDDDDDDDDDDDDDDDDDDDDDDDDDDDDDDDDDDDDDDDDDDDDDDDDDDDDDDDD
DIAMS         DIAMETERS OF THE TAP PINS
DIAMS2        ALTERNATE DIAMETERS FOR TAP PINS
```

DIAMETERS OF THE TAP PINS

RES	OD	ID
.00005	.173383194	.125
.0001	.151140219	.125
.00015	.142958889	.125
.0002	.138687357	.125
.00025	.136060084	.125

APPENDIX G

NaK-78 PHYSICAL PROPERTIES VERSUS TEMPERATURE
NaKPRO.PTY

DENSITY (mg/m^3)

ELECTRICAL RESISTIVITY (mOhm-m)

THERMAL CONDUCTIVITY (W/m-k)

VISCOSITY (mPa-s)

VAPOR P. EQN

VAPOR PRESSURE (Pa)

MMMMMMMMMMMMMMMMMMMMM VARIABLE SHEET MMMMMMMMMMMMMMMMMMMMMMMMMMMMMMMMMMMMMMMMMMMMM

St	InputDDDD	NameDDD	OutputDDD	UnitDDDDD	CommentDDDDDDDDDDDDDDDDDDDDDDDDDDDDDDDDDD
					FILE:NAK78PRO.PTY
					PHYSICAL PROPERTIES OF NAK-78
					VISCOSITY
	3.436541	AMU			Polynomial Equation Coefficicent
	-.0162033	BMU			Polynomial Equation Coefficicent
	3.1836E-5	CMU			Polynomial Equation Coefficicent
	-2.833E-8	DMU			Polynomial Equation Coefficicent
	9.375E-12	EMU			Polynomial Equation Coefficicent
	.5333	MU781		cp	MU78 in 1st Polynomial Equation
	.3663	MU782		cp	MU78 in 2nd Polynomial Equation
	.2856	MU783		cp	MU78 in 3rd Polynomial Equation
	.2389	MU784		cp	MU78 in 4th Polynomial Equation
	.1964	MU785		cp	MU78 in 5th Polynomial Equation
	373	TNAK1		K	Temperature of NaK in 1st Equation
	773	TNAK2		K	Temperature of NaK in 2nd Equation
		TNAK3		K	Temperature of NaK in 3rd Equation
		TNAK4		K	Temperature of NaK in 4th Equation
		TNAK5		K	Temperature of NaK in 5th Equation
		MU78		mPa-s	Viscosity of NaK-78 at TNAK
L	373	TNAK		K	Temperature of NaK
					THERMAL CONDUCTIVITY
	-.0691676	AK			Polynomial Equation Coefficicent
	.00187204	BK			Polynomial Equation Coefficicent
	-4.377E-6	CK			Polynomial Equation Coefficicent
	4.8583E-9	DK			Polynomial Equation Coefficicent
	-2.08E-12	EK			Polynomial Equation Coefficicent
	.232	KNAK781		W/cm-K	KNAK78 in 1st Polynomial Equation
	.247	KNAK782		W/cm-K	KNAK78 in 2nd Polynomial Equation
	.256	KNAK783		W/cm-K	KNAK78 in 3rd Polynomial Equation
	.262	KNAK784		W/cm-K	KNAK78 in 4th Polynomial Equation
	.263	KNAK785		W/cm-K	KNAK78 in 5th Polynomial Equation
		KNAK78	23.2	W/m-K	Thermal Conductivity at TNAK
					ELECTRICAL RESISTIVITY OF NAK-78
	36.747088	ARHO			Polynomial Equation Coefficicent
	-.016312	BRHO			Polynomial Equation Coefficicent
	.000072	CRHO			Polynomial Equation Coefficicent
	4.34E-20	DRHO			Polynomial Equation Coefficicent
	-1.97E-23	ERHO			Polynomial Equation Coefficicent
	40.68	RHO781		fOhm-cm	RHO78 in 1st Polynomial Equation
	45.14	RHO782		fOhm-cm	RHO78 in 2nd Polynomial Equation
	51.04	RHO783		fOhm-cm	RHO78 in 3rd Polynomial Equation
	58.38	RHO784		fOhm-cm	RHO78 in 4th Polynomial Equation
	67.16	RHO785		fOhm-cm	RHO78 in 5th Polynomial Equation
		RHO78	406.8	nOhm-m	Electrical Resistivity at TNAK
					DENSITY

.847	DEN1	Mg/m^3	Density in eqn 1
.751	DEN2	Mg/m^3	Density in eqn 2
.93652	ADEN		Polynomial Coefficient
-.00024	BDEN		Polynomial Coefficient
L	DEN	Mg/m^3	Density of NaK-78

.847	DEN1	Mg/m^3	Density in eqn 1
.751	DEN2	Mg/m^3	Density in eqn 2
.93652	ADEN		Polynomial Coefficient
-.00024	BDEN		Polynomial Coefficient
L	DEN	Mg/m^3	Density of NaK-78

```
MMMMMMMMMMMMMMMMMMMM RULE SHEET MMMMMMMMMMMMMMMMMMMMMMMMMMMMMMMMMMMMMMMMMMMMMMMMMM
S RuleDDDDDDDDDDDDDDDDDDDDDDDDDDDDDDDDDDDDDDDDDDDDDDDDDDDDDDDDDDDDDDDDDDDDDDDDDD
  "PHYSICAL PROPERTIES OF NAK-78

  "VISCOSITY

  "MU781=AMU+BMU*TNAK1+CMU*TNAK1^2+DMU*TNAK1^3+EMU*TNAK1^4
  "MU782=AMU+BMU*TNAK2+CMU*TNAK2^2+DMU*TNAK2^3+EMU*TNAK2^4
  "MU783=AMU+BMU*TNAK3+CMU*TNAK3^2+DMU*TNAK3^3+EMU*TNAK3^4
  "MU784=AMU+BMU*TNAK4+CMU*TNAK4^2+DMU*TNAK4^3+EMU*TNAK4^4
  "MU785=AMU+BMU*TNAK5+CMU*TNAK5^2+DMU*TNAK5^3+EMU*TNAK5^4

  "MU78=AMU+BMU*TNAK+CMU*TNAK^2+DMU*TNAK^3+EMU*TNAK^4

  "THERMAL CODUCTIVITY

  "KNAK781=AK+BK*TNAK1+CK*TNAK1^2+DK*TNAK1^3+EK*TNAK1^4
  "KNAK782=AK+BK*TNAK2+CK*TNAK2^2+DK*TNAK2^3+EK*TNAK2^4
  "KNAK783=AK+BK*TNAK3+CK*TNAK3^2+DK*TNAK3^3+EK*TNAK3^4
  "KNAK784=AK+BK*TNAK4+CK*TNAK4^2+DK*TNAK4^3+EK*TNAK4^4
  "KNAK785=AK+BK*TNAK5+CK*TNAK5^2+DK*TNAK5^3+EK*TNAK5^4

* KNAK78=(AK+BK*TNAK+CK*TNAK^2+DK*TNAK^3+EK*TNAK^4)*100

  "ELECTRICAL RESISTIVITY

* RHO78=(ARHO+BRHO*TNAK+CRHO*TNAK^2+DRHO*TNAK^3+ERHO*TNAK^4)*10

  "DENSITY

  "DEN1=ADEN+BDEN*TNAK1
  "DEN2=ADEN+BDEN*TNAK2
* DEN=ADEN+BDEN*TNAK
```

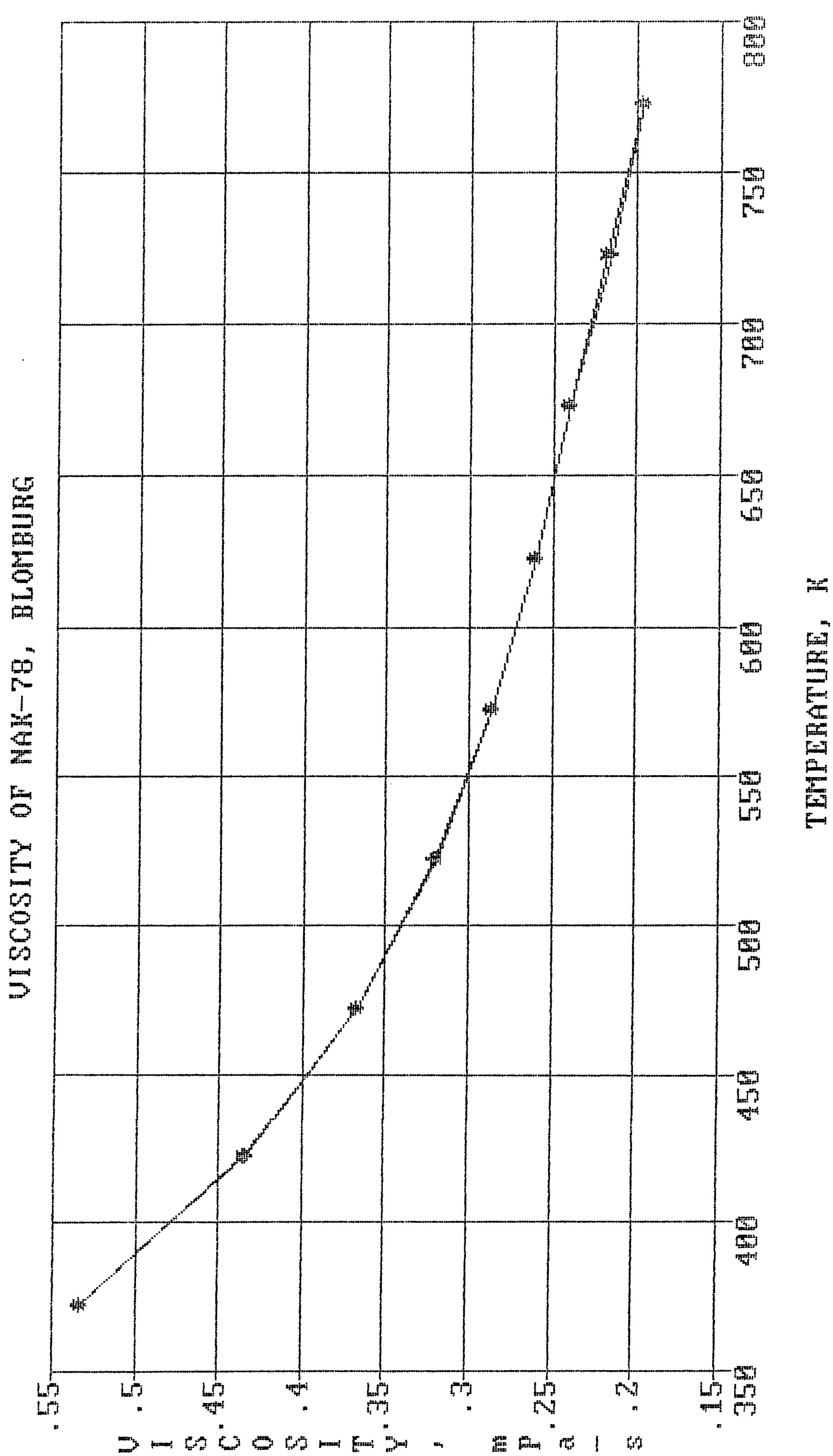
VISCOSITY OF NAK-78, BLOMBURG
VISCOSITY, mPa-s
TEMPERATURE, K
.55
.5
.45
.4
.35
.3
.25
.2
.15
350
400
450
500
550
600
650
700
750
800

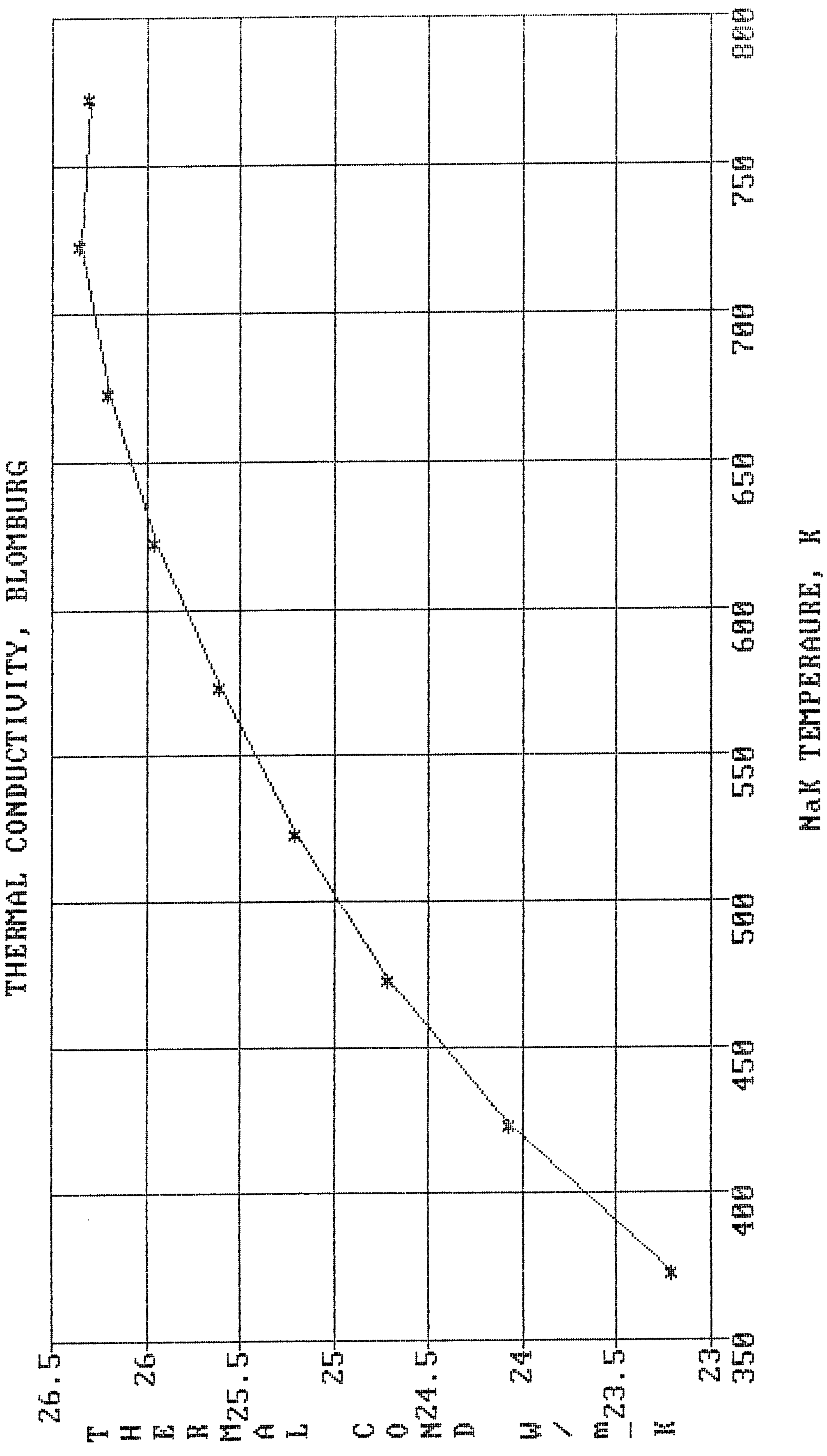

THEMMAL CONDUCTIVITY, BLOMBURG
NaK TEMPERAURE, K
THERMAL COND W/M_K
26.5
26
25.5
25
24.5
24
23.5
23
350
400
450
500
550
600
650
700
750
800

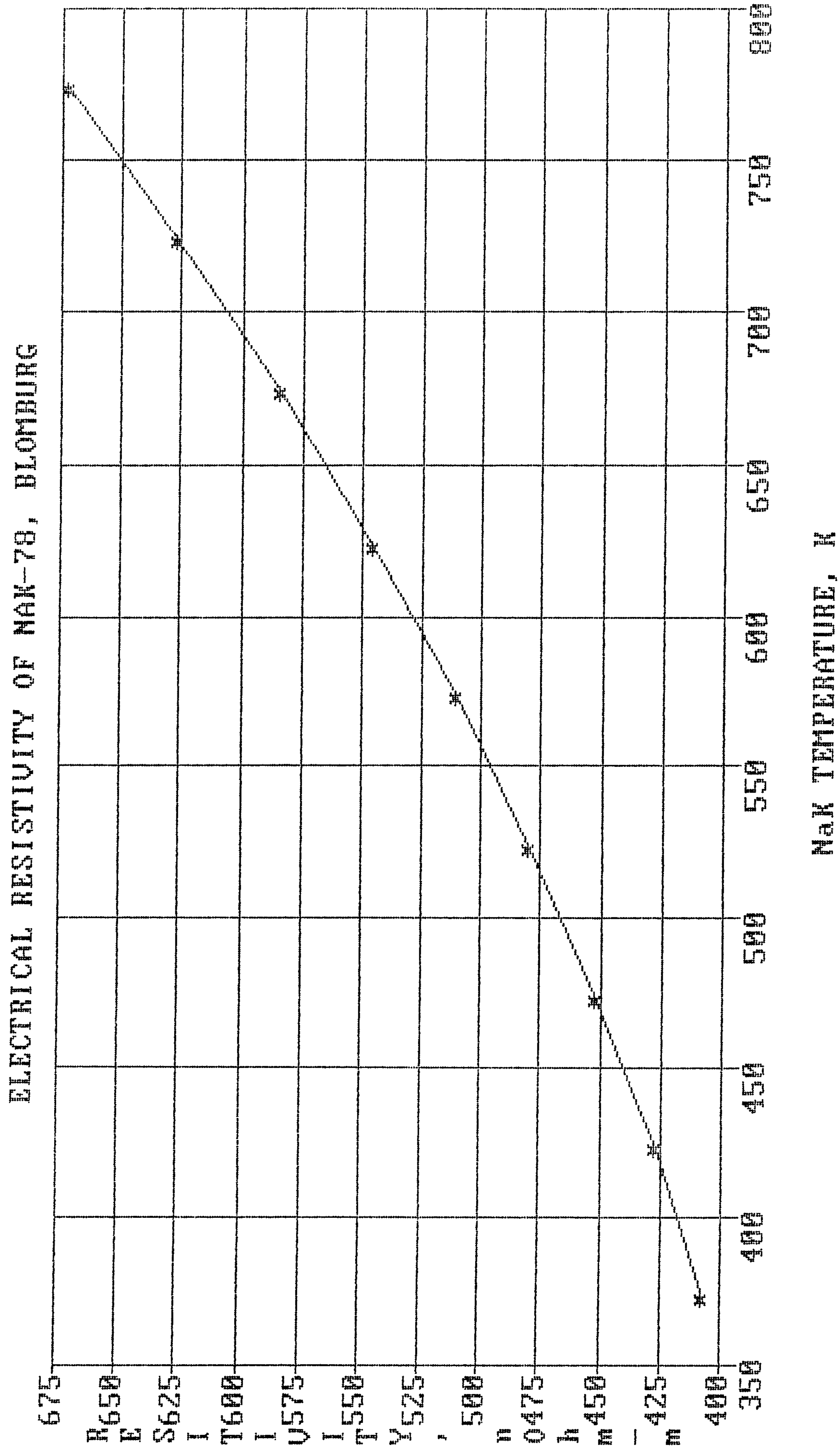
ELECTRICAL RESISTIVITY OF NAK-78, BLOMBURG
NaK TEMPERATURE, K
350
400
450
500
550
600
650
700
750
800
675
650
625
600
575
550
525
500
475
450
425
400

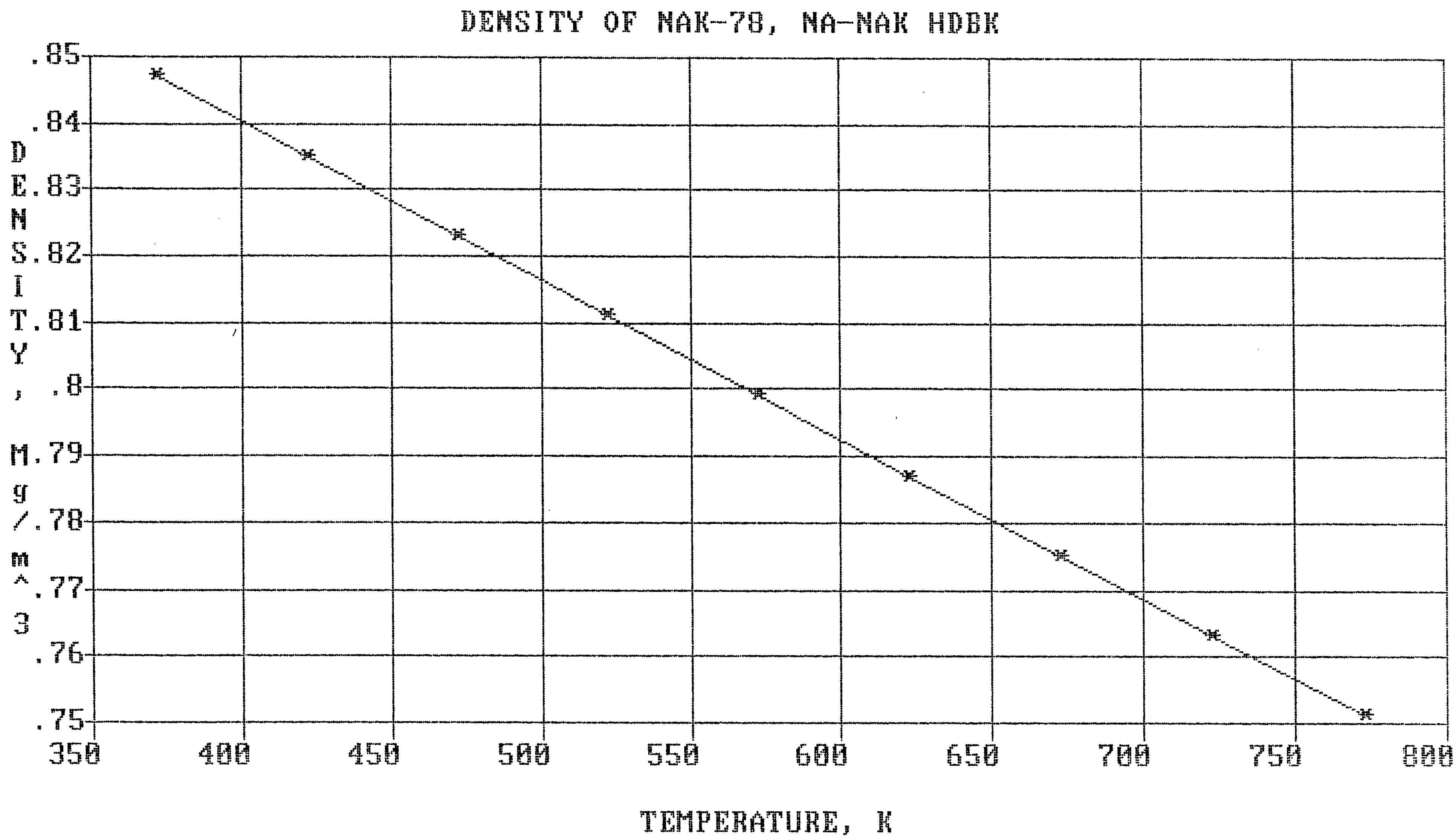
DENSITY OF NAK-78, NA-NAK HDBK
DENSITY, M g/m^3
.85
.84
.83
.82
.81
.8
.79
.78
.77
.76
.75
350
400
450
500
550
600
650
700
750
800
TEMPERATURE, K

MMMMMMMMMMMMMMMMMMMMM VARIABLE SHEET MMMMMMMMMMMMMMMMMMMMMMMMMMMMMMMMMMMMMMMMMMM

St	Input	Name	Output	Unit	Comment
					FILE: VAPORP.EQN
					DISKETTE: CLCP-TECH
					Vapor Pressure vs Temperature
L		P	1000	Pa	Pressure
		P0	.01	atm	Pressure
L	714	T		K	Temperature
		TP	1.4005602	1/K	Inverse Temperature
L		T0	441	deg C	Temperature
L		T0P	2.2675737	1/C	Inverse Temperature
	3.16228E9	A			Coefficient
	10686.297	B			Coefficient
		C			Coefficient
	1000	P1		Pa	Pressure in 1st eqn
		P10		atm	Pressure in 1st eqn
	714	T1		K	Temperature in 1st eqn
		T10	441	deg C	Temperature in 1st eqn
	100	P2		Pa	Pressure in 2nd eqn
		P20		atm	Pressure in 2nd eqn
	617	T2		K	Temperature in 2nd eqn
		T20	344	deg C	Temperature in 2nd eqn
	10	P3		Pa	Pressure in 3rd eqn
		P30		atm	Pressure in 3rd eqn
	546	T3		K	Temperature in 3rd eqn
		T30	273	deg C	Temperature in 3rd eqn
	10.151865	ASb			
	11121.563	BSb			
	659.379	CSb			
	32.570051	ABi			
	231760.16	BBi			Coefficients for Bi equation
	6891.4834	CBi			
	11.512364	ACd			
	6189.6255	BCd			Coefficients for Cd equation
	86.026332	CCd			
	9.2825295	APb			
	4614.2737	BPb			Coefficients for Pb equation
	-607.3846	CPb			
	10.959671	AP			
	2756.5896	BP			Coefficients for P equation
	.44140838	CP			
	10.959671	AS			
	3675.4528	BS			Coefficients for S equation
	23.921878	CS			
	98.307981	ATl			
	2538860.4	BTl			Coefficients for Tl equation
	25762.936	CTl			
	11.699187	ASn			
	20397.825	BSn			Coefficients for Sn equation
	559.66503	CSn			

34.814147	AZn	
171873.22	BZn	Coefficients for Zn equation
4786.0722	CZn	
16.613534	AMg	
29055.626	BMg	Coefficients for Mg equation
1356.0747	CMg	
3.16228E9	ANaK78	Coefficients for NaK-78 equation
10686.297	BNaK78	

```
  "Fluid Properties
  "Vapor pressure curve coefficients

* T=T0+273
* TP=(1/T)*10^3
* TOP=(1/T0)*10^3

* T1=T10+273
* T2=T20+273
* T3=T30+273

* P=P0*10^5                        "10^5 Pa/atm
  "P1=P10*10^5
  "P2=P20*10^5
  "P3=P30*10^5

  "P=P0*10^6
  "P1=P10*10^6
  "P2=P20*10^6
  "P3=P30*10^6

  "LOG(P)=ASb-BSb/(T+CSb)
  "LOG(P1)=ASb-BSb/(T1+CSb)
  "LOG(P2)=ASb-BSb/(T2+CSb)
  "LOG(P3)=ASb-BSb/(T3+CSb)

  "LOG(P)=ABi-BBi/(T+CBi)
  "LOG(P1)=ABi-BBi/(T1+CBi)
  "LOG(P2)=ABi-BBi/(T2+CBi)
  "LOG(P3)=ABi-BBi/(T3+CBi)

  "LOG(P)=ACd-BCd/(T+CCd)
  "LOG(P1)=ACd-BCd/(T1+CCd)
  "LOG(P2)=ACd-BCd/(T2+CCd)
  "LOG(P3)=ACd-BCd/(T3+CCd)

  "LOG(P)=APb-BPb/(T+CPb)
  "LOG(P1)=APb-BPb/(T1+CPb)
  "LOG(P2)=APb-BPb/(T2+CPb)
  "LOG(P3)=APb-BPb/(T3+CPb)

  "LOG(P)=AP-BP/(T+CP)
  "LOG(P1)=AP-BP/(T1+CP)
  "LOG(P2)=AP-BP/(T2+CP)
  "LOG(P3)=AP-BP/(T3+CP)

  "LOG(P)=AS-BS/(T+CS)
  "LOG(P1)=AS-BS/(T1+CS)
  "LOG(P2)=AS-BS/(T2+CS)
  "LOG(P3)=AS-BS/(T3+CS)

  "LOG(P)=ATl-BTl/(T+CTl)
  "LOG(P1)=ATl-BTl/(T1+CTl)
  "LOG(P2)=ATl-BTl/(T2+CTl)
```

```
  "LOG(P3)=ATl-BTl/(T3+CTl)

  "LOG(P)=ASn-BSn/(T+CSn)
  "LOG(P1)=ASn-BSn/(T1+CSn)
  "LOG(P2)=ASn-BSn/(T2+CSn)
  "LOG(P3)=ASn-BSn/(T3+CSn)

  "LOG(P)=AZn-BZn/(T+CZn)
  "LOG(P1)=AZn-BZn/(T1+CZn)
  "LOG(P2)=AZn-BZn/(T2+CZn)
  "LOG(P3)=AZn-BZn/(T3+CZn)

  "LOG(P)=AMg-BMg/(T+CMg)
  "LOG(P1)=AMg-BMg/(T1+CMg)
  "LOG(P2)=AMg-BMg/(T2+CMg)
  "LOG(P3)=AMg-BMg/(T3+CMg)
* P=A/EXP(B/T)
  "P1=A/EXP(B/T1)
  "P2=A/EXP(B/T2)
  "P3=A/EXP(B/T3)

  "T=B/LN(A/P)
```

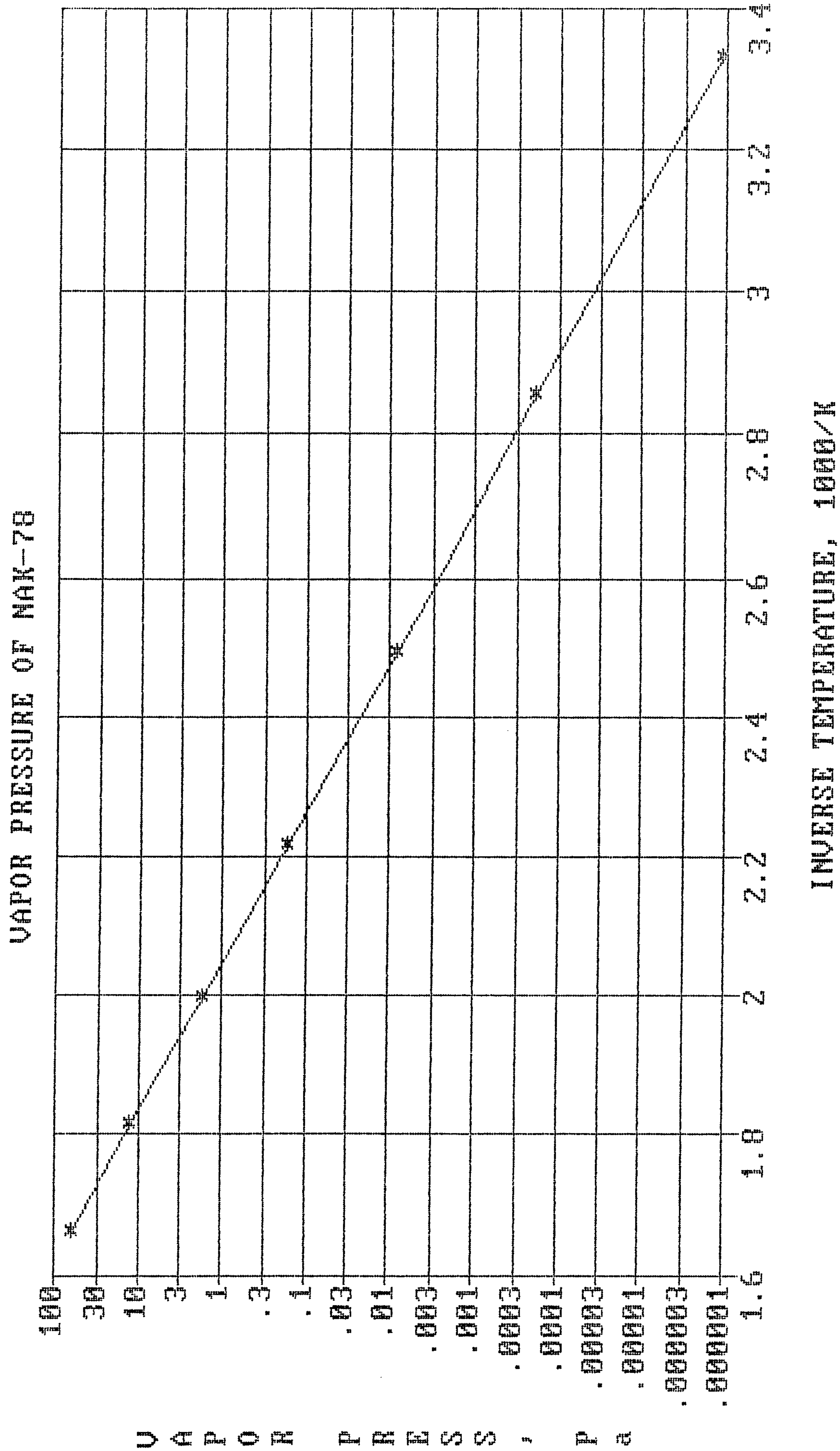
VAPOR PRESSURE OF NAK-78
VAPOR PRESS, Pa
100
30
10
3
1
.3
.1
.03
.01
.003
.001
.0003
.0001
.00003
.00001
.000003
.000001
1.6
1.8
2
2.2
2.4
2.6
2.8
3
3.2
3.4
INVERSE TEMPERATURE, 1000/K